1997

New chemical sources of energy: a theoretical study

Galina Chaban
Iowa State University

INFORMATION TO USERS

This manuscript has been reproduced from the microfilm master. UMI films the text directly from the original or copy submitted. Thus, some thesis and dissertation copies are in typewriter face, while others may be from any type of computer printer.

The quality of this reproduction is dependent upon the quality of the copy submitted. Broken or indistinct print, colored or poor quality illustrations and photographs, print bleedthrough, substandard margins, and improper alignment can adversely affect reproduction.

In the unlikely event that the author did not send UMI a complete manuscript and there are missing pages, these will be noted. Also, if unauthorized copyright material had to be removed, a note will indicate the deletion.

Oversize materials (e.g., maps, drawings, charts) are reproduced by sectioning the original, beginning at the upper left-hand corner and continuing from left to right in equal sections with small overlaps. Each original is also photographed in one exposure and is included in reduced form at the back of the book.

Photographs included in the original manuscript have been reproduced xerographically in this copy. Higher quality 6" x 9" black and white photographic prints are available for any photographs or illustrations appearing in this copy for an additional charge. Contact UMI directly to order.

UMI

A Bell & Howell Information Company
300 North Zeeb Road, Ann Arbor MI 48106-1346 USA
313/761-4700 800/521-0600

New chemical sources of energy: A theoretical study

by

Galina Chaban

A dissertation submitted to the graduate faculty

in partial fulfillment of the requirements for the degree of

DOCTOR OF PHILOSOPHY

Major: Physical Chemistry

Major Professor: Mark S. Gordon

Iowa State University

Ames, Iowa

1997

Graduate College
Iowa State University

This is to certify that the Doctoral dissertation of

Galina Chaban

has met the dissertation requirements of Iowa State University

Signature was redacted for privacy.

Major Professor

Signature was redacted for privacy.

For the Major Program

Signature was redacted for privacy.

For the Graduate College

TABLE OF CONTENTS

ACKNOWLEDGMENTS

I would like to thank my advisor, Prof. Mark Gordon for his guidance, help, and support during my graduate work at ISU. It is mostly due to his care and encouragement that I was able to make progress with the research presented in this dissertation and to gain as much knowledge and skills in theory and programming as I have now.

I would also like to thank all other members of Gordon's group. I am particularly grateful to Dr. Michael Schmidt from whom I learned a great deal of electronic structure theory. I have benefited a lot from his incredible knowledge and ability to explain even very difficult things in a simple and very organized way.

I would like to acknowledge several former members of Gordon's group, Dr. Kiet Nguyen, Dr. Tetsuya Taketsugu, and Dr. Nikita Matsunaga for very helpful discussions and inspirations. I would also like to thank Prof. David Yarkony for fruitful collaboration.

ABSTRACT

The research presented in this dissertation employs methods of quantum chemistry for the search of highly energetic chemical compounds that can have applications as possible energy sources. The areas of research include: 1) improvement of orbital optimization methods for different types of wavefunctions which leads to substantial savings of computer time and memory; 2) predicting new high energy isomers for singlet and triplet states of N_3F and their kinetic stability with respect to isomerisation and dissociation reactions; 3) estimation of minimum energy reaction paths for dissociation reactions of high energy isomers of N_2O_2 including potential energy barriers and minimum energy crossing points between the closest singlet and triplet states; 4) investigation of thermodynamic and kinetic stability of Van der Waals complexes M-H_2 (M = Li, Be, B, C, Na, Mg, Al, Si) that can play an important role in improvement of energetic properties of hydrogen based rocket fuels; 4) mapping of the potential energy surface for AlH_2 compound in the region of crossing between $^2B_2$ and $^2A_1$ electronic states and predicting the kinetic stability of Al complex, which suggests that Al may be among the promising candidates for inclusion into solid hydrogen for the purpose of energy storage.

CHAPTER 1. GENERAL INTRODUCTION

The role of computational quantum chemistry in the prediction of structure and properties of chemical compounds has become very important in recent years. The main principle that makes quantum mechanics useful in chemistry is that many important physical and chemical properties of molecules are defined by the properties of the nuclei and electrons that constitute molecules. The basic interactions between nuclei and electrons can be described by the laws of quantum mechanics. However, solving the Schrödinger equation even for an average size molecular system involves hundreds of variables and is a very challenging task. Recent progress in computer hardware, as well as development of new efficient methods and algorithms, has brought quantum-chemical methods into new areas of chemistry. However, computational chemistry is still a state-of-the-art field and cannot be approached only by blind use of numerical algorithms and computational software. Chemical knowledge and intuition are essential, and a proper balance is necessary in using quantum chemical methods and prior chemical knowledge, so that, on one hand, one can distinguish unphysical results of a numerical method, but on the other hand, one does not bias the results of calculations to support incorrect prior knowledge.

In this work, methods of quantum chemistry are applied to the search for new chemical compounds that are highly energetic and can possibly be used as fuels in the future. Theory can play an important role in predicting such compounds and their stability. In order for a chemical compound to be a possible candidate for highly energetic material, it must have high energy metastable isomers that can transform to lower energy products via some chemical process that can be either isomerisation to other stable isomers of this compound or dissociation, combustion or other chemical reaction. Another important requirement is kinetic stability which makes it possible to synthesize and store such metastable compounds. These issues can be assessed by theoretical studies of potential energy surfaces of possible candidate compounds

and calculating potential barriers that separate metastable structures from lower lying products. There are, of course, other requirements for successful synthesis of highly energetic chemical compounds, as well as environmental considerations for their use as sources of energy. Therefore, the two conditions mentioned above are only first steps in prediction of possible high energy compounds. If theoretical calculations show that a compound is highly energetic and kinetically stable, it does not necessarily mean it can be useful in practice, and additional experimental work must be performed. But if theoretical study predicts that a compound is not stable, it is likely that it cannot be synthesized and used for energy storage purposes. Therefore, the main purpose of theoretical works is to eliminate those suggested chemical compounds that do not satisfy the above conditions, and recommend other compounds as likely candidates for which experimental work may be attempted to synthesize them. Theory can also suggest possible synthetic routes to such promising compounds.

Reliable prediction of kinetic stability of high energy species requires estimation of reaction paths and potential energy barriers for reactions that often involve bond breaking and formation. The proper description of such reactions requires very accurate multi-configurational wavefunctions. Calculations of such wavefunctions can take substantial amounts of computer time. That is why development of time-saving computational algorithms is very important. Efficient techniques has been developed recently that include the quasi-Newton method for the optimization of closed shell SCF wavefunctions[1] and the first order method for optimization of multi-configurational SCF (MCSCF) wavefunctions[2]. These methods are combined in this work (chapter 2) to achieve faster convergence of the MCSCF procedure. The resulting method saves both computer time and memory required for optimizations of multi-configurational wavefunctions. This is especially important when a large number of points on potential energy surfaces is needed, and large basis set expansions are required to obtain accurate wavefunctions along reaction paths.

MCSCF wavefunctions are also required for computation of nonadiabatic interactions between intersecting electronic states. The evaluation of such interactions becomes very important when the stability of high energy species is considered. It is very likely that low-lying excited electronic states are close in energy to the regions of ground electronic states that contain metastable high energy minima. Therefore, surface crossings are possible and may decrease or destroy the stability of high energy isomers. This means that besides evaluation of potential barriers on the adiabatic surfaces, one also must determine minimum energy crossing points between different electronic states[3] and estimate nonadiabatic interactions between these states. This work also includes implementation of MCSCF techniques that can help the evaluation of nonadiabatic interactions.

Dissertation Organization

This dissertation includes both theory development (Chapter 2) and applications related to the search for highly energetic materials (Chapters 3 - 6). Chapter 2 discusses the approximate second order method which is applied to the optimization of molecular orbitals of different wavefunctions and is implemented in the GAMESS electronic structure program[4]. In Chapter 3, new high energy isomers for the N_3F molecule are studied, including their structure and stability with respect to isomerisation and dissociation reactions. Dynamic reaction path (DRP) calculations that describe dynamics of the dissociation of the N_3F singlet cyclic isomer are presented in the Appendix. Chapter 4 considers potential energy surfaces for dissociation reactions of high energy isomers of (NO) dimer, which can be possible candidates for high energy density materials. An investigation of thermodynamic and kinetic stabilities of Van der Waals complexes M-H_2 (M = Li, Be, B, C, Na, Mg, Al, Si) is presented in Chapter 5. Inclusion of small amounts of light metal atoms in solid hydrogen may improve energetic properties of hydrogen based rocket fuels if these atoms form only weakly bound complexes and do not react with H_2 to form stable hydrides. The Al complex is predicted to be kinetically

stable and, therefore, a good candidate for energy storage. The Al-H_2 potential energy surface is further investigated in Chapter 6.

Chapters 2 - 6 are papers either published or submitted to refereed journals. These chapters are preceded by the theoretical background section given below in this chapter. Finally, general conclusions are given in Chapter 7.

Theoretical background

In this section, a brief review of basic concepts and selected methods of quantum chemistry is given as a background to the following chapters. Some of these methods are used in the discussion of the new theoretical developments that improve existing SCF and MCSCF methods (chapter 2). The rest of the methods described here are used as tools for studies of high energy compounds (chapters 3-6).

Adiabatic (Born-Oppenheimer) approximation

The Hamiltonian for a molecule with N nuclei and n electrons includes terms that correspond to the kinetic energy of the nuclei, the kinetic energy of the electrons, the potential energy due to the electrostatic repulsions between the nuclei, the potential energy due to the attractions between the electrons and the nuclei, and the potential energy due to the repulsions between the electrons:

$$\hat{H} = -\frac{\hbar^2}{2}\sum_{\alpha=1}^{N}\frac{1}{M_\alpha}\nabla_\alpha^2 - \frac{\hbar^2}{2m_e}\sum_{i=1}^{n}\nabla_i^2 + \sum_{\alpha}^{N}\sum_{\beta>\alpha}^{N}\frac{Z_\alpha Z_\beta e^2}{R_{\alpha\beta}} - \sum_{\alpha}^{N}\sum_{i}^{n}\frac{Z_\alpha e^2}{R_{i\alpha}} + \sum_{j}^{n}\sum_{i>j}^{n}\frac{e^2}{r_{ij}} \qquad (1.1)$$

$$= K_{nucl} + K_{el} + V_{nucl-nucl} + V_{nucl-el} + V_{el-el}$$

where indices α and β belong to nuclei and i and j refer to electrons, $R_{\alpha\beta}$ is the distance between α th and β th nuclei, $R_{i\alpha}$ is the distance between the ith electron and the αth nucleus, r_{ij} is the distance between the ith and jth electron.

The Hamiltonian (1.1) depends both on electron (r) and nuclear coordinates (R); therefore the molecular wavefunction also depends on r and R which makes solving the Schrödinger equation for such a function very complicated.

A key simplification to the solution of the molecular Schrödinger equation is the Born-Oppenheimer approximation. It is based on the fact that nuclei are much heavier than electrons (the mass of the lightest nucleus (proton) is 1836 times greater than the mass of an electron). Accordingly, the electrons move much faster than the nuclei. Therefore, as a first approximation, the electron motion can be separated from the nuclear motion[5]:

$$\Psi(r,R) = \Psi_{el}(r;R)\Psi_{nucl}(R) \tag{1.2}$$

where Ψ_{el} depends on nuclear coordinates R as parameters.

Substitution of (1.2) into the time-independent Schrödinger equation $H\Psi = E\Psi$ gives:

$$(K_{nucl} + K_{el} + V_{nucl-nucl} + V_{nucl-el} + V_{el-el})\Psi_{el}(r,R)\Psi_{nucl}(R) = E\Psi_{el}(r,R)\Psi_{nucl}(R) \tag{1.3}$$

Terms that are included in the kinetic energy part (first two terms of (1.3)) and involve differentiation, can be expressed as

$$\nabla_\alpha^2\Psi_{el}\Psi_{nucl} = \Psi_{el}\nabla_\alpha^2\Psi_{nucl} + 2\nabla_\alpha\Psi_{el}\nabla_\alpha\Psi_{nucl} + \Psi_{nucl}\nabla_\alpha^2\Psi_{el} \tag{1.4a}$$

$$\nabla_i^2\Psi_{el}\Psi_{nucl} = \Psi_{nucl}\nabla_i^2\Psi_{el} \tag{1.4b}$$

Then equation (1.3) becomes

$$\begin{aligned} &-\frac{\hbar^2}{2}\Psi_{el}\sum_{\alpha=1}^{N}\frac{1}{M_\alpha}\nabla_\alpha^2\Psi_{nucl} - \left[\hbar^2\sum_{\alpha=1}^{N}\frac{1}{M_\alpha}\nabla_\alpha\Psi_{el}\nabla_\alpha\Psi_{nucl} + \frac{\hbar^2}{2}\sum_{\alpha=1}^{N}\frac{1}{M_\alpha}\Psi_{nucl}\nabla_\alpha^2\Psi_{el}\right] \\ &-\frac{\hbar^2}{2m_e}\Psi_{nucl}\sum_{i=1}^{n}\nabla_i^2\Psi_{el} + (V_{nucl-nucl} + V_{nucl-el} + V_{el-el})\Psi_{el}\Psi_{nucl} = E\Psi_{el}\Psi_{nucl} \end{aligned} \tag{1.5}$$

In the standard Born-Oppenheimer approximation, the terms included in square brackets (that is, the first and second derivatives of Ψ_{el} with respect to nuclear coordinates) are neglected.

We can define electronic and nuclear Hamiltonians as:

$$H_{el} = -\frac{\hbar^2}{2m_e}\sum_{i=1}^{n}\nabla_i^2 + V_{nucl-nucl} + V_{nucl-el} + V_{el-el} \tag{1.6}$$

$$H_{nucl} = -\frac{\hbar^2}{2}\sum_{\alpha=1}^{N}\frac{1}{M_\alpha}\nabla_\alpha^2 \tag{1.7}$$

and define Ψ_{el} as an eigenfunction of H_{el}:

$$H_{el}\Psi_{el} = E_{el}\Psi_{el} \ , \tag{1.8}$$

Then, substituting (1.8) into (1.5), ignoring the derivative terms in square brackets and dividing (1.5) by Ψ_{el} gives the nuclear Schrödinger equation for Ψ_{nucl}:

$$(H_{nucl} + E_{el})\Psi_{nucl} = E\Psi_{nucl} \tag{1.9}$$

In order for the above separation to work, the electronic wavefunction Ψ_{el} must change very slowly as a function of nuclear coordinates R, so that its first and second derivatives with respect to R can be neglected.

The adiabatic approximation is essential for quantum chemistry. It is extremely useful for the majority of applications, especially those that deal with ground electronic states of molecules in the regions close to equilibrium. The error introduced by the Born-Oppenheimer approximation for such systems is negligible compared with the total energy of the system. However, this approximation breaks down for degenerate or quasi-degenerate electronic states, e.g., Jahn-Teller effect [6]. Nonadiabatic effects become very important in the regions of intersections of electronic states, and must be taken into account when studying such processes as photodissociation, electronic quenching, and charge-transfer reactions[7]. As was mentioned earlier, consideration of nonadiabatic interactions is very important for predicting the stability of high energy species. One of the theoretical approaches that can be used to account for nonadiabatic effects is discussed later in this chapter.

Potential energy surfaces

In the framework of the Born-Oppenheimer approximation, most problems in quantum chemistry are reduced to solving the electronic Schrödinger equation (1.8). There have been developed a number of methods that allow one to find approximate solutions of this equation. Some of the methods that have been used for the projects discussed in this dissertation, will be briefly described in the next section. In a typical quantum chemistry calculation, equation (1.8) is solved for a given set of fixed nuclear coordinates R^1, and the energy E^1 is obtained that

consists of electronic energy terms plus the nuclear-nuclear repulsion energy. This procedure is then repeated for other sets of nuclear coordinates R. The resulting function E(R) is called a *potential energy surface* (PES). Because of the large number of nuclear coordinates for polyatomic molecules, E(R) is typically a multidimensional surface in the space of 3N-6 dimensions. As a result, an enormous amount of calculations is needed to obtain such a surface for a molecule with more than 3 atoms. In practice, however, the knowledge of the entire PES is not necessary for understanding of chemical reactions in which a given molecular system is involved. It is often sufficient to obtain only key parts of the PES that give important information about the way the reactants transform into products.

The most common calculation in the practice of quantum chemistry is locating *stationary points* on potential energy surfaces, that is points for which the gradient of the energy with respect to nuclear coordinates is zero. These points include minima (equilibrium structures), where the hessian (matrix of second derivatives of the energy with respect to nuclear coordinates) has all positive eigenvalues, and *transition states*, where the hessian has one (and only one) negative eigenvalue. Transition states are maximum points on minimum energy paths that connect two minima corresponding to reactants and products. The energy difference between the transition state and the reactants (products) is called the *barrier height* for the forward (reverse) reaction. A *reaction path* is a path that connects reactants and products via the transition state. The *intrinsic reaction coordinate* (IRC)[8] is often used as a model for the reaction path. The IRC is defined as the steepest descent path (or minimum energy path) from the transition state to each of the minima obtained in mass weighted Cartesian coordinates $m_\alpha^{1/2}x_\alpha$, $m_\alpha^{1/2}y_\alpha$, $m_\alpha^{1/2}z_\alpha$ (m_α is the mass of nucleus α).

In many cases, knowledge of the locations of the minima, transition states, and IRC gives enough information to understand mechanisms of chemical reactions. The actual path of reacting molecules that possess kinetic energy is, of course, different from the minimum energy path. One way to study reaction dynamics of molecules with translational or vibrational

kinetic energy is the dynamic reaction path (DRP) method[9], in which the negative of the potential energy gradient is used to obtain atomic accelerations, and then numerical integration methods are used to obtain velocities and positions of nuclei. This method is also called the classical "trajectory on-the-fly" method and may be started at any convenient point on a PES.

Approximate solutions of the electronic Schrödinger equation

Exact solutions of equation (1.8) can be found only in very limited cases (for example, one-electron systems like the hydrogen molecule ion H_2^+). For the majority of molecular systems of interest, however, it is impossible to solve (1.8) exactly, because the electron-electron repulsion term of the electronic Hamiltonian (1.6), $\sum_{j}^{n}\sum_{i>j}^{n}\frac{e^2}{r_{ij}}$, does not allow separation of variables. Therefore, the greatest challenge of quantum chemistry is to develop approximate methods that allow one to obtain wavefunctions and molecular properties that are accurate enough for chemical applications.

One of the most commonly used approximate wavefunctions is the *Hartree-Fock wavefunction*. The idea of the Hartree-Fock approximation is to replace the exact electron-electron repulsion term by the sum of the repulsion potentials between each electron and the average field of all other electrons. This allows one to reduce the n-electron Schrödinger equation (1.8) to the system of n one-electron equations, called Hartree-Fock equations:

$$F_i\psi_i = \varepsilon_i\psi_i \qquad (i = 1, 2, ..., n) \tag{1.10}$$

where F_i is the one-electron Fock operator; ψ_i is the one-electron wavefunction (orbital); ε_i is the one-electron (orbital) energy.

The total wavefunction of a molecule that has n electrons in n/2 doubly occupied orbitals ψ_i can be represented as a Slater determinant :

$$\Phi = \frac{1}{\sqrt{n!}}\begin{vmatrix} \psi_1(1)\alpha & \psi_1(2)\alpha & \dots & \psi_1(n/2)\alpha \\ \psi_1(1)\beta & \psi_1(2)\beta & \dots & \psi_1(n/2)\beta \\ \dots & \dots & \dots & \dots \\ \psi_n(1)\beta & \psi_n(2)\beta & \dots & \psi_n(n/2)\beta \end{vmatrix} \tag{1.11}$$

Molecular orbitals ψ_i are usually expanded as linear combinations of atomic orbitals χ_μ (MO-LCAO approximation):

$$\psi_i = \sum_\mu C_{i\mu}\chi_\mu \tag{1.12}$$

which leads to Hartree-Fock-Roothaan equations[10]:

$$\mathbf{FC} = \mathbf{SC}\varepsilon \tag{1.13}$$

where **F** is the Fock matrix, **S** is the overlap matrix between basis functions, **C** is the matrix of expansion coefficients, ε is the diagonal matrix of orbital energies. Since **F** depends on **C**, these equations are non-linear and are solved iteratively by means of a self consistent field (SCF) procedure. A second order method for solving the Hartree-Fock equations, involving Newton-Raphson optimization of orbital coefficients, will be discussed in chapter 2.

The Hartree-Fock method, though a reasonable approximation in many cases, often is not able to properly describe energetic properties of molecules, such as, for example, dissociation energies. Since the true electron-electron repulsion potential is replaced by an average potential, the Hartree-Fock method does not account for the correlation of electron motions at any given instant of time, and therefore, underestimates energies of chemical bonds. The *electron correlation error* is usually defined as the difference between the exact (nonrelativistic) energy and the Hartree-Fock energy. However, this definition makes sense only when the Hartree-Fock description is qualitatively correct, that is when the single determinant (1.11) dominates the molecular wavefunction. This is not always the case.

The single-determinant Hartree-Fock model usually works for equilibrium structures, but it breaks down in situations where several electronic configurations are close in energy. This is usually the case for reaction paths that involve bond breaking and formation, such as, for example, dissociation reactions and symmetry-forbidden reactions.

The simplest example of the breakdown of the Hartree-Fock method is the dissociation of the H_2 molecule. It works reasonably well around the H_2 equilibrium geometry (~0.74 Å),

with electron correlation improving the total energy only slightly, but results in very high energies at large separations (about 160 kcal/mol higher than the correct dissociation products). The explanation of this is that the Hartree-Fock model includes terms with both electrons located at the same H atom. These terms correspond to the dissociation to $H^+ + H^-$, which is much higher in energy than $H^{\cdot} + H^{\cdot}$. Therefore, the Hartree-Fock method is not the appropriate model when one needs to describe dissociation reactions that result in products with unpaired electrons. The improved wavefunction for H_2 that gives qualitatively correct description of the dissociation process can be constructed as the linear combination of two configurations:

$$\Psi_{MCSCF} = C_1 (\psi_1)^2 + C_2 (\psi_2)^2$$

where ψ_1 and ψ_2 are the bonding and antibonding molecular orbitals:

$$\psi_1 = 1s_A + 1s_B; \quad \psi_2 = 1s_A - 1s_B;$$

$1s_A$ and $1s_B$ are the atomic orbitals that belong to atoms A and B, respectively.

This wavefunction describes the entire potential energy surface correctly, with $C_1 \sim 1$, $C_2 \sim 0$ in the regions close to equilibrium, and $C_1 \sim - C_2$ at large separations. The wavefunction above is the simplest example of a *multiconfigurational self consistent field (MCSCF)*[11] wavefunction, which in the general case can be written as a superposition of several electronic configurations Φ_K:

$$\Psi_{MCSCF} = \sum_K A_K \Phi_K \ , \qquad (1.14)$$

where coefficients A_K are called *configuration interaction (CI) coefficients.* In general, each Φ_K may be a linear combination of Slater determinants to assure the appropriate spin and symmetry. MCSCF wavefunctions are obtained by optimization of both CI coefficients (A) and orbital expansion coefficients (C). CI and orbital coefficients can be optimized either separately by a two-step procedure or simultaneously. Different methods of optimization of MCSCF orbital coefficients in a two-step procedure are discussed in Chapter 2. These methods are implemented in GAMESS, as well as the full second order method that optimizes CI and orbital coefficients simultaneously[12].

The corrections introduced by replacing single-configurational wavefunctions (1.11) by multi-configurational wavefunctions (1.14) are sometimes called *static correlation* effects, in contrast with *dynamic correlation*[13] which corrects for interactions between electrons at very short inter-electronic distances. Static correlation must be taken into account in order to obtain a correct qualitative description of molecular systems, while dynamic correlation is needed to obtain energetics that are in quantitative agreement with experimental data. Dynamic correlation can be defined as the difference between the exact (nonrelativistic) energy and the energy given by the qualitatively correct wavefunction (which can be either Hartree-Fock, generalized valence bond (GVB)[14], or MCSCF wavefunction).

There are several approaches to account for dynamic correlation. One of these is the *configuration interaction (CI)* method. The idea of this method is to correct the initial (reference) wavefunction by mixing in contributions from excited configurations.

A CI wavefunction based on a single-determinant Hartree-Fock reference constitutes a linear combination of a large number of configurations, $\Psi_{CI} = \sum_K A_K \Phi_K$, in which the coefficients A_K are variationally optimized. The configurations are determined as different ways of replacing electrons from occupied orbitals to virtual orbitals. Φ_0 usually corresponds to the ground state configuration, and all other Φ_K's - to excited state configurations. Including all possible configurations gives the *full CI wavefunction*, the exact wavefunction for a given basis set. For most molecules, however, the number of all possible configurations is extremely large and a full CI is not possible to achieve. Therefore, one normally needs to select the most important configurations. One of the most practical selections is to include configurations that correspond only to single and double excitations out of reference configuration Φ_0. This scheme gives a *CISD wavefunction* (CI singles and doubles). An improved CISD method was developed by Pople and coworkers and is called the *quadratic configuration interaction (QCI)* method[15]. This method is intermediate between the CISD method and the coupled-cluster singles and doubles (CCSD) method[16]. One of the variations of this method, *QCISD(T)*, also

includes triple excitations in an approximate way. This method gives very reliable correlation corrections to single determinant energies and is used for some applications included in this dissertation.

CI methods based on multi-configurational (MCSCF) wavefunctions are called *multi-reference CI (MRCI).* In these methods, the configuration list includes single and double excitations from several configurations used in the MCSCF expansion rather than from a single reference. The resulting wavefunction therefore includes some triple and quadruple excitations depending on the size of MCSCF reference wavefunction. MRCI wavefunctions include a very large number of configurations and are very time consuming calculations.

Another commonly used method for finding dynamic correlation energy is perturbation theory. The *Møller-Plesset (MP)* method[17] is based on Rayleigh-Schrödinger perturbation theory, in which the unperturbed wavefunction is the Hartree-Fock wavefunction Φ_0. The perturbation $\hat{H}'$ is the difference between the true electronic Hamiltonian $\hat{H}$ and the unperturbed Hamiltonian $\hat{H}_0$ taken as the sum of one-electron Fock operators: $\hat{H}' = \hat{H} - \hat{H}_0 = \hat{H} - \sum_{i=1}^{n} \hat{F}(i)$. The energy is expressed as a sum of contributions of increasing order from the matrix elements of $\hat{H}'$ between the eigenfunctions of $\hat{H}_0$. This expansion is usually truncated to include corrections up to second (MP2), third (MP3), or fourth (MP4) order.

There are several different ways to define *multireference perturbation theory* (where the zeroth order unperturbed wavefunction is the multiconfigurational MCSCF wavefunction). The one used in this work is the second order *CASPT2* method developed by Roos and coworkers[18].

Nonadiabatic interactions between potential energy surfaces

One way to provide a theoretical treatment of chemical reactions that involve nonadiabatic processes is to start from the adiabatic potential energy surfaces[19]. After adiabatic surfaces $E^I(R)$ for several electronic states $\Psi_{el}^I(r;R)$ are obtained, one determines first and

second derivative nonadiabatic couplings between these states in the regions where these surfaces cross or come close to each other[20]. Although this approach still assumes that electronic and nuclear motions can be separated, nuclear motion is no longer restricted to a single potential energy surface, but can occur on two or several surfaces. The number of intersecting surfaces must however be small for this approach to work[3]. The total wavefunction is expanded as[20]

$$\Psi_T(r,R) = \sum_I \Psi_{el}^I(r;R)\chi^I(R) \tag{1.15}$$

where $\Psi_{el}^I(r;R)$ is the adiabatic electronic wavefunction and $\chi^I(R)$ is the nuclear wavefunction corresponding to the Ith electronic state. Substitution of (1.15) into the Schrödinger equation gives the system of coupled equations for nuclear functions $\chi^I(R)$:

$$(H_{nucl} + E_{el}^I - K^{II} - E)\chi^I = \sum_{J(\neq I)} \left(\hbar^2 \sum_\alpha \frac{1}{M_\alpha} f_\alpha^{IJ} \frac{\partial}{\partial R_\alpha} + \frac{\hbar^2}{2} \sum_\alpha \frac{1}{M_\alpha} h_{\alpha\alpha}^{IJ} \right) \chi^J \tag{1.16}$$

where K^{II} is the adiabatic correction (or the Born-Oppenheimer diagonal correction)[20] which modifies the potential energy surface E_{el}^I :

$$K^{II} = -\frac{\hbar^2}{2} \sum_\alpha \frac{1}{M_\alpha} k_{\alpha\alpha}^{II} = -\frac{\hbar^2}{2} \sum_\alpha \frac{1}{M_\alpha} \left\langle \frac{\partial}{\partial R_\alpha} \Psi^I \middle| \frac{\partial}{\partial R_\alpha} \Psi^I \right\rangle_r \tag{1.17}$$

f_α^{IJ} is the first derivative coupling matrix element:

$$f_\alpha^{IJ} = \left\langle \Psi^I \middle| \frac{\partial}{\partial R_\alpha} \Psi^J \right\rangle_r \tag{1.18}$$

$h_{\alpha\alpha}^{IJ}$ is the second derivative coupling matrix element:

$$h_{\alpha\alpha}^{IJ} = \left\langle \Psi^I \middle| \frac{\partial^2}{\partial R_\alpha^2} \Psi^J \right\rangle_r \tag{1.19}$$

The subscript r in the above expressions stands for integration over all electronic coordinates. The first and second derivative couplings are related as:

$$\frac{\partial}{\partial R_\alpha} f_\alpha^{IJ} = k_{\alpha\alpha}^{IJ} + h_{\alpha\alpha}^{IJ} \tag{1.20}$$

Therefore, the first step is to calculate the first derivative coupling f_α^{IJ}, and then (1.20) can be used to evaluate second derivative coupling matrix elements.

It has been shown[21] that derivative couplings can be evaluated using analytic derivative techniques that are routinely used in calculations of adiabatic energy derivatives $\frac{\partial E_{el}^{I}}{\partial R}$. The adiabatic wavefunctions can be expanded as MCSCF wavefunctions (1.14). Differentiating the MCSCF variational conditions with respect to nuclear coordinates R results in a set of equations referred to as the coupled-perturbed MCSCF equations. These equations are necessary to solve in order to obtain derivatives of the MO coefficients which contribute to the nonadiabatic coupling matrix elements f_{α}^{JI}. Forming and solving the coupled-perturbed MCSCF equations is the most difficult and time-consuming part of the evaluation of f_{α}^{JI} and requires calculation of the full hessian matrix that includes second derivatives of the MCSCF energy with respect to orbital and CI coefficients. This matrix is also formed during full second order MCSCF[12]. Therefore, the full second order MCSCF method implemented in GAMESS is not only a convenient way to optimize MCSCF wavefunctions, but also a first step towards evaluation of nonadiabatic coupling matrix elements.

References

1. Fischer, T. H.; Almlöf, J. *J. Phys. Chem.* **1992**, *96*, 9768.
2. Dupuis, M.; Chin, S.; Marquez, A. In *Relativistic and Electron Correlation Effects in Molecules and Solids*. Edited by G. L. Malli, Plenum Press, New York, **1994**, p.315.
3. (a) Yarkony, D. R. *J. Am. Chem. Soc.* **1992**, 114, 5406; (b) Yarkony, D. R. *J. Chem. Phys.* **1990**, 92, 2457.
4. Schmidt, M. W.; Baldridge, K. K.; Boatz, J. A.; Elbert, S. T.; Gordon, M. S.; Jensen, J. H.; Koseki, S.; Matsunaga, N.; Nguyen, K. A.; Su, S.; Windus, T. L.; Dupuis, M.; Montgomery, J. A. *J. Comp. Chem.* **1993**, 14, 1347.
5. Born M.; Oppenheimer, J. R. *Ann. Phys.*, **1927**, 84, 457.
6. (a) Jahn H. A.; Teller E. Proc. Roy. Soc. **1937**, 161, 220. (b) Bersuker, I. B. *The Jahn-Teller Effect and Vibronic Interactions in Modern Chemistry*. New York, 1984.

(c) Bersuker, I. B.; Polinger V. Z. *Vibronic Interactions in Molecules and Crystals.* Berlin, 1989.

7. (a) Yarkony D. R. *J. Phys. Chem.* **1996**, 100, 18612. (b) Yarkony D. R. *Rev. Mod. Phys.* **1996**, 68, 985.
8. (a) Truhlar, D. G.; Steckler, R.; Gordon, M. S.; *Chem. Rev.* **1987**, *87*, 217; (b) Baldridge, K. K.; Gordon, M. S.; Truhlar, D. G.; Steckler, R. *J. Phys. Chem.*, **1989**, *93*, 5107; (c) Truhlar, D. G.; Gordon, M. S. *Science*, **1990**, *249*, 491; (d) McKee, M. L.; Page, M. *Rev. Comput. Chem.*, **1993**, *4*, 35.
9. (a) Stewart, J. J. P.; Davis, L. P.; Burggraf, L. W. *J. Comp. Chem.* **1987**, *8*, 1117. (b) Maluendes S. A.; Dupuis, M. *J. Chem. Phys.*, **1990**, *93*, 5902.
10. Roothaan C. C. J. *Rev. Mod. Phys.* **1951**, 23, 69.
11. (a) Roos, B. O. *Lecture Notes in Quantum Chemistry*, Springer-Verlag, Berlin, **1992**, vol 58, pp. 177-254. (b) Werner, H.-J., *Advances in Chemical Physics*, Wiley Interscience, New York, **1987**, vol. 69, pp. 1-62. (c) Shepard, R. *Advances in Chemical Physics*, Wiley Interscience, New York, **1987**, vol. 69, pp. 63-200.
12. (a) Werner, H.-J.; Meyer, W. *J. Chem. Phys.* **1980**, 73, 2342; (b) Werner, H.-J.; Meyer, W. *J. Chem. Phys.* **1981**, 74, 5794; (c) Lengsfield, B. H. *J. Chem. Phys.* **1982**, 77, 4073. (d) Jensen, H. J.; Agren, H. *Chem. Phys.* **1986**, 104, 229.
13. Silverstone, H. J.; Sinanoglu O. *J. Chem. Phys.* **1966**, 44, 1899.
14. Bobrowicz, F. W.; Goddard III, W. A. In *Modern Theoretical Chemistry: Methods of Electronic Structure Theory.* Ed. by H. F. Schaefer III. Plenum, New York, 1977, v.3, p.79.
15. (a) Pople, J. A.; Head-Gordon, M.; Raghavachari, K. *J. Chem.*. Phys. **1987**, *87*, 5968; (b) Pople, J. A.; Head-Gordon, M.; Raghavachari, K. *J. Chem.*. Phys. **1989**, *90*, 4635.

16. (a) Noga, J.; Bartlett, R. J. *J. Chem. Phys.* **1987**, 86, 7041; (b) Bartlett, R. J. *J. Phys. Chem.* **1989**, 93, 1697.

17. (a) Møller, C.; Plesset, M. S. *Phys. Rev.* **1934**, 46, 618. (b) Pople, J. A.; Binkley, J. S.; Seeger, R. *Int. J. Quantum Chem.* **1976**, 10, 1. (c) Krishnan, R.; Frisch, M. J.; Pople, J. A. *J. Chem. Phys.* **1980**, 72, 4244.

18. (a) Anderson, K.; Malmqvist, P.-Å.; Roos, B.O. *J. Chem. Phys.* **1992**, 96, 1218. (b) Anderson, K. Malmqvist, P.-Å., Roos, B. O. *J. Phys. Chem.* **1990**, 94, 5483.

19. (a) Tully, J. C. *Modern Theoretical Chemistry*, Plenum, New York, 1976; (b) Garrett, B. C.; Truhlar, D. G. *Theoretical Chemistry Advances and Perspectives*, Academic Press, New York, 1981; (c) Baer, M. In *Theory of Chemical Reaction Dynamics*, Chemical Rubber, Boca Raton, 1985. Vol. 2, Chapter 4.

20. Lengsfield, B. H.; Yarkony, D. R. *Advances in Chemical Physics*, Vol. LXXXII, p.1-71.

21. (a) Lengsfield, B. H.; Saxe, P.; Yarkony, D. R. *J. Chem. Phys.* **1986**, 84, 348. (b) Saxe, P.; Lengsfield, B. H.; Yarkony, D. R. *Chem. Phys. Lett.* **1985**, 113, 4549. (c) Lengsfield, B. H.; Yarkony, D. R. *J. Chem. Phys.* **1986**, 84, 348. (d) Saxe, P.; Yarkony, D. R. *J. Chem. Phys.* **1987**, 86, 321. (e) Jensen, J. O.; Yarkony, D. R. *J. Chem. Phys.* **1988**, 89, 975.

CHAPTER 2. APPROXIMATE SECOND ORDER METHOD FOR ORBITAL OPTIMIZATION OF SCF AND MCSCF WAVEFUNCTIONS

A paper accepted for publication in *Theoretica Chimica Acta*

Galina Chaban, Michael W. Schmidt, Mark S. Gordon

Abstract

A quasi-Newton method involving a diagonal guess orbital Hessian with iterative updates has been proposed recently by Almlof for the optimization of closed shell SCF wavefunctions. The technique is extended in the present work to more general wavefunctions, ranging from open shell SCF through multi-configurational SCF. A number of examples are presented to show that convergence for closed and open shell SCF rivals conventional DIIS. For MCSCF wavefunctions, the method presented here requires more iterations than an exact second order program, but since each iteration is substantially faster, leads to a more efficient overall program.

Introduction

Most quantum chemistry calculations start from Hartree-Fock (HF) self consistent field (SCF), generalized valence bond (GVB), or multiconfigurational self consistent field (MCSCF) wavefunctions, which serve as starting points for obtaining more accurate wavefunctions that include electron correlation by means of configuration interaction, cluster expansions, or perturbation theory.

Optimization of molecular orbitals expanded in a basis of atomic orbitals is the common step that is required to obtain all of these wavefunctions. The standard scheme for SCF orbital optimization is based on an iterative procedure involving diagonalization of the Fock matrix [1],

normally supplemented today by a method referred to as Direct Inversion in the Iterative Subspace (DIIS) [2-4]. An alternative approach with an almost equally long history [5-16] is a second order method involving Newton-Raphson optimization. This method uses an exponential parameterization to obtain orbital rotation angles, and requires calculation of first and second derivatives of the energy with respect to these orbital coordinates (orbital gradient and orbital hessian). This method has not been very popular for optimization of HF wavefunctions, due to the high cost of computing the orbital hessian (which requires an integral transformation in the original formulations [8,9]), as well as the large size of the hessian matrices which are difficult to store even for average size molecular systems. A solution to both problems was presented by Fischer and Almlöf [12] who suggested the use of a quasi-Newton approach using an approximate hessian to avoid its accurate computation, and also devised a very efficient recursive algorithm which allows the updating of the inverse hessian multiplied by gradient vectors without actual storage of the hessian matrix. Another solution to both problems has been given by Shepard[13], but the accurate computation of the hessian requires additional builds of Fock-like matrices, and thus a considerable increase in computational cost[16].

The purpose of this paper is to demonstrate how an approximate second order method based on the hessian update procedure suggested by Fischer and Almlöf can be used to perform efficient orbital optimizations, not only for closed shell restricted Hartree-Fock (RHF) [12], but also for other types of wavefunctions, namely restricted open shell Hartree-Fock (ROHF), GVB, and MCSCF. These procedures have been implemented in the electronic structure code GAMESS [17], and are the present default convergence methods.

1. Closed shell RHF wavefunctions

Second order SCF methods for RHF wavefunctions have been described in previous papers [5-16]. Here, we outline this method and present some details of our implementation of it.

The closed shell RHF wavefunction can be represented as an anti-symmetrized product of doubly occupied orbitals ψ_i :

$$\Psi_{RHF} = \hat{A}\left[\psi_1(1)\overline{\psi}_1(2).....\psi_{N/2}(N-1)\overline{\psi}_{N/2}(N)\right] \tag{1.1}$$

where N is the number of electrons. The electronic energy is given by

$$E = \sum_{i}^{occ} 2h_{ii} + \sum_{i,j}^{occ}\left(2J_{ij} - K_{ij}\right) \tag{1.2}$$

where $h_{ii} = \int \psi_i(1)\mathbf{h}(1)\psi_i(1)dV_1$ (1.3)

$$J_{ij} = (ii \mid jj) = \int\int \psi_i(1)\psi_j(2)\frac{1}{r_{12}}\psi_i(1)\psi_j(2)\, dV_1\, dV_2 \tag{1.4}$$

$$K_{ij} = (ij \mid ij) = \int\int \psi_i(1)\psi_j(2)\frac{1}{r_{12}}\psi_j(1)\psi_i(2)\, dV_1\, dV_2 \tag{1.5}$$

The variational condition leads to the familiar Hartree-Fock equations

$$\mathbf{F}\psi_i = \varepsilon_i\psi_i \tag{1.6}$$

where **F** is the Fock operator:

$$\mathbf{F} = \mathbf{h} + \sum_{j}^{occ}(2\mathbf{J}_j - \mathbf{K}_j) \tag{1.7}$$

The standard method of solution of the Hartree-Fock equations includes constructing the Fock matrix in the atomic orbital (AO) basis, transforming it to the current molecular orbital (MO) basis, and diagonalizing. Diagonalization gives new MOs which are used for the next iteration, and this is repeated until convergence.

In the second order method based on exponential parametrization [8,9], the new set of orbitals is obtained from the old by an orthogonal transformation represented as an exponential of an antisymmetric matrix:

$$\mathbf{C}_{new} = \mathbf{C}_{old}\ \mathbf{U} = \mathbf{C}_{old}\ \exp(\mathbf{A})\,, \tag{1.8}$$

where $\exp(\mathbf{A}) = \mathbf{I} + \mathbf{A} + 1/2\ \mathbf{A}^2 + ...$ (1.9)

$$\mathbf{A} = \begin{pmatrix} \mathbf{0} & \mathbf{x} \\ -\mathbf{x} & \mathbf{0} \end{pmatrix}. \tag{1.10}$$

The x_{ia} elements are the $L=n_{occ}\times n_{virt}$ independent rotational parameters, each corresponding to a rotation between occupied orbital *i* and virtual orbital *a*. The variational condition is:

$$\frac{\partial E}{\partial x_{ia}} = g_{ia} = 0 \tag{1.11}$$

where g_{ia} are the elements of the orbital gradient of the energy. This equation can be solved using the Newton-Raphson method:

$$\boldsymbol{\delta}_n = \mathbf{x}_{n+1} - \mathbf{x}_n = -\mathbf{B}_n^{-1} \cdot \mathbf{g}_n \tag{1.12}$$

where δ_n is the displacement vector, $\mathbf{g}_n$ is the gradient vector, and $\mathbf{B}_n$ is the hessian matrix on iteration n.

Using the Newton-Raphson method in a fixed coordinate system requires very time consuming computations of the first and second derivatives of the energy with respect to the parameters x_{ia}. The first derivatives $\frac{\partial E}{\partial x_{ia}}$ can be calculated exactly (see ref.14 for exact formulae), but the calculations involve many matrix operations. Our implementation, like most others, does not use fixed coordinates. Instead, we set the parameters x_{ia} to zero at the beginning of each iteration and use the new displacement $\delta_n = \mathbf{x}_{n+1}$ to update the orbital coefficient matrix obtained on the previous iteration $\mathbf{C}_{n+1} = \mathbf{C}_n \exp(\mathbf{A}_{n+1})$. This gives much simpler expressions for the derivatives at $\mathbf{x}=\mathbf{0}$. For example, the first derivative[8] is simply:

$$g_{ia} = \left.\frac{\partial E}{\partial x_{ia}}\right|_{x_{ia}=0} = 4\langle \psi_i | \mathbf{F} | \psi_a \rangle = 4F_{ia} \tag{1.13}$$

where F_{ia} is an element of the Fock matrix transformed into the MO basis. The orthogonal transformation matrix $\mathbf{U}=\exp(\mathbf{A})$ is obtained by truncating the expansion to first order:

$$\exp(\mathbf{A}) = \mathbf{I} + \mathbf{A} \tag{1.14}$$

followed by a Schmidt orthogonalization. We have found that addition of the second order term $1/2\mathbf{A}^2$ does not lead to any decrease in the total number of iterations. Other more exact expressions for the rotation matrix, such as the Klein-Cayley formula

$$\mathbf{U} = (\mathbf{I} + \mathbf{A}/2) / (\mathbf{I} - \mathbf{A}/2) \tag{1.15}$$

have not been considered due to our desire to minimize the number of floating point operations to obtain **U**.

The second derivative expressions at **x=0** [8] include not only Fock matrix elements, but also two-electron integrals in the MO basis. To avoid the expensive integral transformation required to compute the exact hessian matrix, we follow Almlöf [12] and start with an approximate diagonal hessian, which thus can be inverted trivially. The inverse orbital hessian is then updated using the Broyden-Fletcher-Goldfarb-Shanno (BFGS) updating formula [18] via the recursive update recipe given in ref.12. The greatest advantage of this procedure is memory savings, since the Hessian matrix itself does not need to be kept in memory. The recursive algorithm requires storage of three vectors of size L (where L is the number of rotational parameters) from each previous iteration. We write these vectors to disk and read them on each iteration to update hessian related information.

Our experience shows that the choice of the approximate initial diagonal Hessian is very important to provide good convergence for this method. The use of a unit matrix for this purpose is certainly not satisfactory. Consideration of the general formula for the RHF orbital hessian [8] (i,j = occupied orbitals; a,b = virtual orbitals)

$$B_{ia,jb} = 4F_{ab}\delta_{ij} - 4F_{ij}\delta_{ab} + 4\,[4(ia\,|\,bj) - (ja\,|\,ib) - (ab\,|\,ij)] \qquad (1.16)$$

suggests that the use of orbitals which are approximately canonical will increase the diagonal dominance of the hessian. Since our Huckel guess orbitals [17] are not nearly canonical, we diagonalize the Fock matrix on the first iteration, and on the next cycle take as our approximate initial diagonal hessian

$$B_{ia,ia} = 4F_{aa} - 4F_{ii} = 4(\varepsilon_a - \varepsilon_i) \qquad (1.17)$$

since the two-electron integral terms from (1.16) are much smaller than the Fock contributions. At subsequent geometries, it suffices to use orbital energies from the previous geometry to form the initial diagonal orbital hessian.

The entire orbital update algorithm is shown in Figure 1. We begin the algorithm when the maximum orbital gradient element falls below a threshold, normally 0.25. Our Huckel guess orbitals [17] normally meet this criterion after the conventional diagonalization on the first iteration, but if the starting orbitals are very poor we rely on conventional extrapolation to bring us within the radius of convergence of our second order SCF (SOSCF) method. The SCF process is considered converged when the maximum orbital gradient component is one microhartree. This is roughly equivalent to 10^{-5} convergence of the density matrix. Since applications such as nuclear gradient and hessian computation, perturbation theory, and Koopmans' theorem require canonical orbitals, we always perform one Fock matrix diagonalization after final convergence.

The convergence of this approximate second order method is not, of course, quadratic because of the various approximations used, but it is superlinear and is comparable with that of the DIIS method [2]. However, the number of computations is less for the approximate second order method than for DIIS. The floating point operation (FLOP) count of our RHF DIIS implementation [17] is roughly 17 N^3, from seven matrix multiplies (14 N^3) and one diagonalization (10/3 N^3). Taking n_{occ} = 1/3 N as typical of RHF calculations, Figure 1 shows that the approximate SOSCF orbital improvement requires roughly $5N^3$ FLOPs.

Table 1 shows several examples of organic molecules converged with the conventional Fock diagonalization method + DIIS convergence accelerator, compared to the second order SCF method described above. The two final columns show the times needed for computation of integrals and construction of the Fock matrix in direct mode. As can be seen from the table, the number of iterations is practically the same for both methods (± 1 iteration), but the time required to solve the Hartree-Fock equations is about 3 times less for SOSCF than for DIIS. This is not very important for a serial run, since much more time is required to calculate integrals and form Fock matrices than to solve the Hartree-Fock equations. However, if integrals are calculated in parallel (assuming perfect parallelization of the integrals and Fock

build), then the smaller time of the sequential solve step gives better results for speedups. For the last example of cyclic AMP, the theoretical speedup on 32 nodes,

DIIS: (24,262 + 275) / (24,262 / 32 + 275) = 23.7

SOSCF: (23,647 + 77) / (23,647 / 32 + 77) = 29.0

is much better in the case of second order SCF.

Another advantage of using this second order SCF method is a decreased number of iterations during geometry optimizations. Table 2 presents the number of SCF iterations on each geometry optimization step for glycine. The number of iterations is consistently 1-2 iterations less for second order SCF on all subsequent geometries. This saves a total of 18 iterations during this optimization run.

2. High spin open shell ROHF wavefunctions

The high spin coupled restricted open shell HF wavefunction can be written as:

$$\Psi_{ROHF} = \hat{A}\left[\psi_1 \overline{\psi}_1 \psi_2 \overline{\psi}_2 \ldots\ldots \psi_{N-M} \overline{\psi}_{N-M} \psi_{N-M+1} \ldots\ldots \psi_N\right] = \hat{A}\left[\Psi_{core} \Psi_{open}\right] \qquad (2.1)$$

where N-M is the number of doubly occupied (closed shell) orbitals, and M is the number of singly occupied (open shell) orbitals.

Previously, high spin ROHF wavefunctions were optimized in GAMESS by diagonalizing a single Fock matrix in the MO basis, constructed as follows[17]:

$$\mathbf{F}_{ROHF} = \begin{bmatrix} F_2 & F_\beta & (F_\alpha + F_\beta)/2 \\ F_\beta & F_1 & F_\alpha \\ (F_\alpha + F_\beta)/2 & F_\alpha & F_0 \end{bmatrix} \qquad (2.2)$$

where F_α and F_β are alpha and beta Fock matrices transformed to the MO basis.

F_2, F_1, and F_0 are doubly, singly, and zero occupied diagonal blocks:

$$F_2 = A_{cc} F_\alpha + B_{cc} F_\beta \qquad (2.3a)$$

$$F_1 = A_{oo} F_\alpha + B_{oo} F_\beta \qquad (2.3b)$$

$$F_0 = A_{vv} F_\alpha + B_{vv} F_\beta \qquad (2.3c)$$

The best convergence rate is found with Roothaan's A and B canonicalization coefficients[19].

To use our quasi-Newton approach for ROHF wavefunctions, we construct the orbital gradient vector from the off-diagonal blocks of the above Fock matrix:

$$g_{ik} = F_{ik}^{\beta} \qquad \text{if } i = \text{doubly occupied, } k = \text{singly occupied orbital} \qquad (2.4a)$$

$$g_{ia} = \frac{1}{2}\left(F_{ia}^{\alpha} + F_{ia}^{\beta}\right) \qquad \text{if } i = \text{doubly occupied, } a = \text{virtual orbital} \qquad (2.4b)$$

$$g_{ka} = F_{ka}^{\alpha} \qquad \text{if } k = \text{singly occupied, } a = \text{virtual orbital} \qquad (2.4c)$$

As in the case of RHF, we diagonalize the above Fock matrix on the very first iteration and use its eigenvalues ε to approximate the initial diagonal hessian:

$$B_{ik,ik} = \varepsilon_k - \varepsilon_i \qquad (2.5a)$$

$$B_{ia,ia} = \varepsilon_a - \varepsilon_i \qquad (2.5b)$$

$$B_{ka,ka} = \varepsilon_a - \varepsilon_k \qquad (2.5c)$$

where the index i denotes doubly occupied, k singly occupied, and a virtual orbitals. The rest of our implementation is the same as for closed shell RHF wavefunctions.

3. GVB and low spin ROHF wavefunctions

A Generalized Valence Bond (GVB) wavefunction can be represented as [20, 3]:

$$\Psi_{GVB} = \hat{A}\left[\Psi_{core}\Psi_{open}\Psi_{pair}\right] \qquad (3.1)$$

where Ψ_{core} is a product of doubly occupied orbitals, Ψ_{open} is a product of singly occupied orbitals, and

$$\Psi_{pair} = \prod_{i=1}^{n_{pair}}\left(C_{gi}\phi_{gi}(1)\phi_{gi}(2) + C_{ui}\phi_{ui}(1)\phi_{ui}(2)\right)\left(\alpha(1)\beta(2) - \beta(1)\alpha(2)\right). \qquad (3.2)$$

Here, ϕ_{gi} and ϕ_{ui} are orthogonal GVB natural orbitals, and C_{gi} and C_{ui} are GVB configuration interaction (CI) coefficients. This wavefunction leads to the energy expression[20]:

$$E = \sum_{i}^{occ} 2f_i h_{ii} + \sum_{i,j}^{occ}\left(a_{ij}J_{ij} + b_{ij}K_{ij}\right) \qquad (3.3)$$

where $h_{ii} = \langle \phi_i | \mathbf{h} | \phi_i \rangle$ (3.4)

$$J_{ij} = (ii \mid jj) = \int \phi_i(1) \mathbf{J}^j(1) \phi_i(1) dv_1 \quad (3.5)$$

$$K_{ij} = (ij \mid ij) = \int \phi_i(1) \mathbf{K}^j(1) \phi_i(1) dv_1 \quad (3.6)$$

$\mathbf{h}$, $\mathbf{J}^j(1)$, and $\mathbf{K}^j(1)$ are one- and two-electron (Coulomb and exchange) operators, and f_i, a_{ij}, b_{ij} are orbital occupation coefficients (see refs. 3 and 20 for their definitions).

The variational condition using this energy expression is:

$$\delta E = \sum_i \langle \delta \phi_i | \mathbf{F}^i | \phi_i \rangle = 0 \quad (3.7)$$

where $\mathbf{F}^i$ is the Fock operator for the orbital ϕ_i:

$$\mathbf{F}^i = f_i \mathbf{h} + \sum_j^{occ} \left(a_{ij} \mathbf{J}^j + b_{ij} \mathbf{K}^j \right) \quad (3.8)$$

Orbitals with the same occupation coefficients, and therefore the same Fock operator, form a shell.

Several methods have been used to optimize orbitals of GVB wavefunctions. The standard OCBSE (orthogonality constrained basis set expansion) procedure is based on diagonalizing the Fock matrices corresponding to each shell [20]. An orbital DIIS method has been suggested to improve convergence of this method [4]. Another approach is to diagonalize a single combined Fock matrix. Several possible generalized Fock operators are discussed in ref.3, together with the use of DIIS with this approach. Although their suggested GVB-DIIS Fock operator [3] introduces second-order mixing, we find that our quasi-Newton optimization based on the hessian update method of Fisher and Almlöf [12] works more reliably and in fewer iterations.

The general formula for the GVB orbital gradient (that has to be brought to zero at convergence) is:

$$g_{ij} = \frac{\partial E}{\partial x_{ij}} = 4F_{ij}^J - 4F_{ij}^I \quad (3.9)$$

which reduces to:

$$g_{ij} = 4F_{ij}^{J} \qquad \text{if } j = \text{occupied orbital from shell } J,\ i = \text{ virtual orbital} \qquad (3.10)$$

$$g_{ij} = 0 \qquad \text{if orbitals } i \text{ and } j \text{ belong to the same shell} \qquad (3.11)$$

$$g_{ij} = 4F_{ij}^{J} - 4F_{ij}^{I} \qquad \text{if } i \text{ and } j \text{ are occupied orbitals from different shells } I \text{ and } J \qquad (3.12)$$

The general formula [3, 8, 21] for the diagonal elements of the GVB orbital hessian in the MO basis is:

$$B_{ij,ij} = \frac{\partial^2 E}{\partial x_{ij}^2} = 4(F_{ii}^{J} - F_{ii}^{I}) - 4(F_{jj}^{J} - F_{jj}^{I}) + 8(a_{ii} + a_{jj} - 2a_{ij})(ij \mid ij) + 4(b_{ii} + b_{jj} - 2b_{ij})[(ii \mid jj) + (ij \mid ij)] \qquad (3.13)$$

In the case for which i is a virtual orbital, $F^{I} = 0$, $a_{ii} = b_{ii} = 0$, $a_{ij} = b_{ij} = 0$, and $B_{ij,ij}$ becomes:

$$B_{ij,ij} = 4F_{ii}^{J} - 4F_{jj}^{J} + 4(2a_{jj} + b_{jj})(ij \mid ij) + 4b_{jj}(ii \mid jj) \qquad (3.14)$$

Since the $(ii|jj) = J_{ij}$ and $(ij|ij) = K_{ij}$ matrices corresponding to open-shell **J** and **K** operators are already available in the MO basis as a by-product of the GVB Fock matrix formation, we can calculate all diagonal hessian elements exactly, except those that correspond to core - virtual rotations. In the case for which j is doubly occupied and i is a virtual orbital ($a_{jj} = 2$, $b_{jj} = -1$):

$$B_{ij,ij} = 4F_{ii}^{J} - 4F_{jj}^{J} + 4(3(ij \mid ij) - (ii \mid jj)) \qquad (3.15)$$

It would require additional integral transformation work to get the two-electron integrals in (3.15), and therefore we neglect these terms. Fortunately, the neglected terms are much smaller than the remaining part

$$B_{ij,ij} = 4F_{ii}^{J} - 4F_{jj}^{J} \qquad (3.16)$$

which is the same expression we use in the case of closed-shell RHF. Note that all terms are, however, important for hessian elements corresponding to core - pair , pair - pair, and pair - virtual rotations, and these are calculated exactly. As in the case of RHF, we perform one single combined Fock matrix diagonalization on the first iteration to provide a better initial orbital hessian for our approximate second order (SOSCF) method.

Several examples of GVB calculations are given in Table 3. The middle column of the table represents the original one-pair GVB-DIIS [2-c] implemented in GAMESS several years

ago, while the multi-pair results are obtained from our implementation of the GVB-DIIS multishell Fock operator method given in ref.3. GVB wavefunctions can be difficult to converge, and each of the three methods fails from time to time. We find, however, that the approximate second order method is the most successful in converging the majority of GVB cases we have tried.

The energy formula (3.3), as well as the gradient (3.9) and hessian (3.13) formulae can be also used for different kinds of low spin ROHF calculations by using the appropriate coefficients f_i, a_{ij}, and b_{ij}. GAMESS contains values of these coefficients for some cases of singly occupied orbitals, and they can be input for other cases of partial orbital occupancies. Both the DIIS method based on a single combined Fock matrix and the approximate second order method work very successfully for all kinds of low spin ROHF calculations. Two examples are shown in Table 4.

4. MCSCF wavefunctions

The approximate second order update method is also implemented for the orbital improvement step for MCSCF wavefunction optimization. Space precludes a full review of all previously proposed MCSCF optimization schemes here. Early first order methods based on the Generalized Brillouin Theorem [22-24] were abandoned by most workers with the advent of second-order Newton-Raphson methods [25-27]. Recently a Renormalized Fock Operator approach based on diagonalization of a matrix of single excitation matrix elements has been proposed by Meier and Staemmler [28]. This method exhibits first order convergence, and has recently been implemented in HONDO8 by Dupuis [29] . This code served as the basis of our approximate second order MCSCF scheme.

The MCSCF wave function Ψ is a superposition of electronic configurations Φ_K :

$$\Psi_{MCSCF} = \sum_K A_K \Phi_K \ , \qquad (4.1)$$

where A_K are the CI coefficients. Typically, many of the orbitals can be constrained to be doubly occupied in all configurations - these are *core* (or inactive) orbitals and will be denoted *i,j,k*. *Active* orbitals are allowed to have variable occupation numbers and are denoted *t,u,v,w*. *Virtual* orbitals are those that are empty in all configurations, and are denoted *a,b,c*. We use the notation *p,q,r,s* for general orbitals.

The energy expression for an MCSCF wavefunction is:

$$E = \sum_{pq} \gamma_{pq} h_{pq} + \frac{1}{2} \sum_{pqrs} \Gamma_{pqrs} (pq \mid rs) \tag{4.2}$$

where γ_{pq} and Γ_{pqrs} are the elements of one- and two-body density matrices, depending on A_K. The one- and two-electron integrals h_{pq} and $(pq \mid rs)$ depend on the orbitals. The optimization of CI coefficients and molecular orbitals may be separated, or unfolded, into two steps: solving the secular equation for A_K, followed by some sort of orbital improvement scheme.

The first order method suggested for MCSCF orbital improvement by Meier and Staemmler [28] and implemented in HONDO by Dupuis [29] has many advantages. Although it requires more iterations to converge than second order (Newton-Raphson) methods, the time needed for each iteration is much less. Each macroiteration in the first order algorithm includes several microiterations which skip the CI step and part of the integral transformation. Each microiteration [29] consists of diagonalization of an approximate Fock matrix which is formed using old density matrices and partially updated two-electron integrals. The fairly numerous microiterations in the first order scheme add a modest, but non-negligible, amount of time to each macroiteration. In contrast, the high cost of the full second order method comes from the construction of the orbital hessian matrix which requires $(pt \mid qu)$ and $(pq \mid tu)$ types of molecular integrals with two indices *p,q* running over the entire orbital space. Only a single general orbital index needs to be transformed in order to construct the Lagrangian matrix for the

first order MCSCF. Of course, another problem associated with using second order methods is storage of the orbital hessian matrix.

The method we have implemented in GAMESS is an attempt to use all the advantages of the first order MCSCF method, while also introducing some features of the second order approach. Again, we construct an approximate initial diagonal hessian and use the update procedure suggested by Fisher and Almlöf [12] . The resulting convergence behavior is not, of course, as good as that of an exact Newton-Raphson method, but is better than that of a first order method.

Our implementation of the approximate second order method in GAMESS uses part of the first order MCSCF program written by Dupuis for HONDO [29]. The Lagrangian matrix G calculated by the first order code is used to construct the orbital gradient vector. The components of the orbital gradient corresponding to core-virtual (a), active-virtual (b), and core-active (c) rotations are:

$$g_{ia} = \frac{\partial E}{\partial x_{ia}} = 4(F_{ai}^{core} + F_{ai}^{act}) = G_{ai} \tag{4.3a}$$

$$g_{ta} = \frac{\partial E}{\partial x_{ta}} = 2\sum_{u} \gamma_{tu} F_{au}^{core} + 2\sum_{u,v,w} \Gamma_{tuvw}(au \mid vw) = G_{at} \tag{4.3b}$$

$$g_{it} = \frac{\partial E}{\partial x_{it}} = 4(F_{ti}^{core} + F_{ti}^{act}) - 2\left[\sum_{u} \gamma_{tu} F_{iu}^{core} + \sum_{u,v,w} \Gamma_{tuvw}(iu \mid vw)\right] = G_{ti} - G_{it} \tag{4.3c}$$

where γ and Γ are the one- and two-body density matrices, and F^{core} and F^{act} are two Fock type matrices:

$$F_{pq}^{core} = h_{pq} + \sum_{k}^{core} [2(pq \mid kk) - (pk \mid qk)] \tag{4.4}$$

$$F_{pq}^{act} = \sum_{u,v}^{act} \gamma_{uv} [(pq \mid uv) - \tfrac{1}{2}(pu \mid qv)] \tag{4.5}$$

Explicit expressions for the MCSCF orbital hessian in terms of two-electron integrals and density matrix elements are given in ref.26 . The exact formulae for diagonal orbital hessian elements are:

$$B_{ia,ia} = \frac{\partial^2 E}{\partial x_{ia}^2} = 4(F_{aa}^{core} + F_{aa}^{act}) - 4(F_{ii}^{core} + F_{ii}^{act}) + 4[3(ai \mid ai) - (aa \mid ii)] \qquad (4.6a)$$

$$\begin{aligned} B_{ta,ta} = \frac{\partial^2 E}{\partial x_{ta}^2} &= 2\gamma_{tt} F_{aa}^{core} - 2\sum_{u} \gamma_{tu} F_{tu}^{core} - 2\sum_{u,v,w} \Gamma_{tuvw}(tu \mid vw) \\ &+ 2\sum_{u,v} \{\Gamma_{tuuv}(aa \mid uv) + 2\Gamma_{tvtu}(av \mid au)\} \end{aligned} \qquad (4.6b)$$

$$\begin{aligned} B_{it,it} = \frac{\partial^2 E}{\partial x_{it}^2} &= 4(F_{tt}^{core} + F_{tt}^{act}) - 4(F_{ii}^{core} + F_{ii}^{act}) \\ &+ 2\gamma_{tt} F_{ii}^{core} - 2\sum_{u} \gamma_{tu} F_{tu}^{core} - 2\sum_{u,v,w} \Gamma_{tuvw}(tu \mid vw) \\ &+ 2\sum_{u,v} \{\Gamma_{tuuv}(uv \mid ii) + 2\Gamma_{tvtu}(ui \mid vi)\} \\ &+ 4\sum_{u} \{(\delta_{tu} - \gamma_{tu})[3(ui \mid ti) - (tu \mid ii)]\} \end{aligned} \qquad (4.6c)$$

No active-active hessian elements are shown, as we restrict our method to complete active spaces. In the framework of the first order MCSCF approach [29], an integral transformation is performed only for F^{core}, F^{act}, and $(pu|vw)$ types of integrals with only one general index p running through all orbital space, and three other indices over active orbitals only. Accordingly, we ignore those terms of the above expressions that contain two-electron integrals with two non-active indices. The truncated diagonal hessian contains only F^{core} and F^{act} matrix elements and $(tu|vw)$ integrals with all indices in the active space. This approximation is satisfactory for $B_{ia,ia}$ hessian elements since the last term is small compared with the first two. In the case of $B_{ta,ta}$ and $B_{it,it}$ elements, the last terms may be quite substantial. Ignoring these terms may result in negative signs for some of the hessian elements. This causes severe convergence problems when starting a Newton-Raphson optimization from such an initial hessian.

To improve this situation, we add $2\gamma_{tt}F_{aa}^{act}$ to $B_{ta,ta}$ and $2\gamma_{tt}F_{ii}^{act}$ to $B_{it,it}$ hessian elements. In the limit of active orbital t becoming weakly occupied ($\gamma_{tt} \to 0$), the final term of 4.6b and $2\gamma_{tt}F_{aa}^{act}$ both vanish. In the limit of active orbital t becoming nearly filled (

$\gamma_{tt} \rightarrow 2$, $\Gamma_{tuuv} \rightarrow 2\gamma_{uv}$, $\Gamma_{tutv} \rightarrow -\frac{1}{2}\gamma_{uv}$), $2\gamma_{tt}F_{aa}^{act}$ becomes identical to the final term of 4.6b. Similarly, in the limit $t \rightarrow$ doubly occupied, the two final terms in 4.6c reduce to the same expression as $2\gamma_{tt}F_{ii}^{act}$. The $2\gamma_{tt}F^{act}$ terms prove to be a satisfactory compensation for the exact terms and provide a positive definite starting hessian for use with the quasi-Newton update procedure. The resulting diagonal hessian used to start the approximate second order MCSCF orbital improvement is therefore calculated as follows:

$$B_{ia,ia} = 4(F_{aa}^{core} + F_{aa}^{act}) - 4(F_{ii}^{core} + F_{ii}^{act}) \tag{4.7a}$$

$$B_{ta,ta} = 2\gamma_{tt}F_{aa}^{core} - 2\sum_{u}\gamma_{tu}F_{tu}^{core} - 2\sum_{u,v,w}\Gamma_{tuvw}(tu \mid vw) + 2\gamma_{tt}F_{aa}^{act} \tag{4.7b}$$

$$\begin{aligned} B_{it,it} &= 4(F_{tt}^{core} + F_{tt}^{act}) - 4(F_{ii}^{core} + F_{ii}^{act}) \\ &\quad + 2\gamma_{tt}F_{ii}^{core} - 2\sum_{u}\gamma_{tu}F_{tu}^{core} - 2\sum_{u,v,w}\Gamma_{tuvw}(tu \mid vw) + 2\gamma_{tt}F_{ii}^{act} \end{aligned} \tag{4.7c}$$

A previous attempt to reduce the amount of work in the integral transformation by approximating the orbital hessian has been made by Camp, Nicholas, and King [30]. These workers made the same approximation of dropping the final term of 4.6a, but calculated sufficient integrals with two virtual indices to evaluate the final terms of 4.6b and 4.6c. Our approach is to transform only one virtual index, requiring the additional approximations just described.

Since very little additional work is required to construct the approximate diagonal hessian and it is done only on the initial iteration, the cost of each quasi-Newton iteration is less than that of one first order macroiteration, which consists of several Fock matrix diagonalizations (microiterations) [28, 29]. The convergence rate is also better than that of the first order method. As a result, the approximate second order method is very fast and useful for MCSCF calculations of very large molecular systems.

Table 5 shows several examples of MCSCF calculations using three methods for orbital improvement: 1) an exact second order method with the full orbital hessian matrix calculated on

each iteration; 2) a first order MCSCF method based on effective Fock matrix diagonalization, supplemented by DIIS convergence acceleration [29] ; 3) the approximate second order method described above. As can be seen from the table, the approximate second order approach provides substantial savings of computer time. Note that the final example is a MCSCF(10,9) calculation of 7-azaindole ($C_7N_2H_6$, 165 AOs) which proved impossible to do with the exact second order program because insufficient memory was available. About 22,000,000 words of memory are required for the orbital update procedure with the exact Newton-Raphson scheme, but less than 1,000,000 words are needed in the case of the approximate quasi-Newton approach. The exact second order method is, however, preferable for MCSCF calculations with large numbers of configurations, but small basis sets, since in this case the CI part (solution for A_K's) is more time consuming than the orbital improvement part, and the least number of iterations is desirable.

Conclusion

We have demonstrated an efficient way to optimize molecular orbitals for different types of wavefunctions (RHF, ROHF, GVB, and MCSCF) by extending the approximate second order method with a diagonal hessian update procedure due to Fisher and Almlöf. The algorithm is quite simple, and it is remarkable that essentially the same process can be used to optimize all these classes of wavefunctions. Details relating to our implementation, and explicit formulae for the exact orbital gradient and the approximate diagonal orbital hessian have been presented for each kind of wavefunction. The method is faster than the standard diagonalization techniques used for RHF and GVB. Its convergence properties (number of iterations) are comparable to that of DIIS accelerated SCF methods, but the time needed for solving the HF equations is about three times less. In addition, the method eliminates the traditional diagonalization step (except for the final orbital canonicalization) which is not easily parallelizable. For MCSCF, the approximate second order orbital update is trivial compared to

the cost of the orbital gradient, and convergence rates are intermediate between the Renormalized Fock Operator first order method and the exact second order approach.

Acknowledgments

We thank Michel Dupuis who provided us with his first order MCSCF code from HONDO8, and both Michel Dupuis and Klaus Ruedenberg for helpful comments upon the manuscript. Funding for this work was provided by the Air Force Office of Scientific Research (grant F49620-95-1-0077).

References

1. C.C.J. Roothaan. Rev. Mod. Phys. **1951**, *23*, 69.
2. a) P. Pulay. Chem. Phys. Lett. **1980**, *73*, 393; b) P. Pulay. J. Comp. Chem. **1982**, *3*, 556; c) T. P. Hamilton, P. Pulay. J. Chem. Phys. **1986**, *84*, 5728; d) H. Sellers. Chem. Phys. Lett. **1991**, *180*, 461; e) H. Sellers. Int. J. Quantum Chem. **1993**, *45*, 31.
3. R. P. Muller, J. - M. Langlois, M. Ringnalda, R. A. Friesner, W. A. Goddard III. J. Chem. Phys. **1994**, *100*, 1226.
4. a) I. V. Ionova, E. A. Carter. J. Chem. Phys. **1995**, *102*, 1251; b) I. V. Ionova, E. A. Carter. J. Comput. Chem. **1996**, *17*, 1836.
5. D. J. Thouless. Nucl. Phys. **1960**, *21*, 225.
6. a) T. H. Brown, R. L. Taylor. J. Phys. Chem. **1965**, *69*, 2316; b) T. H. Brown. J. Chem. Phys. **1968**, *49*, 2291.
7. W. R. Wessel. J. Chem. Phys. **1967**, *47*, 3253.
8. J. Douady, Y. Ellinger, R. Subra, B. Levy. J. Chem. Phys. **1980**, *72*, 1452.
9. a) G. B. Bacskay. Chem. Phys. **1981**, *61*, 385; b) G. B. Bacskay. Chem. Phys. **1982**, *65*, 383.
10. M. Head-Gordon, J. A. Pople. J. Phys. Chem. **1988**, *92*, 3063.

11. T. Sano, Y. J. I'Haya. J. Chem. Phys. **1991**, *95*, 6607.

12. T. H. Fischer, J. Almlöf. J. Phys. Chem. **1992**, *96*, 9768.

13. R. Shepard. Theor. Chim. Acta. **1993**, *84*, 343.

14. J. Hutter, M. Parinello, S. Vogel. J. Chem. Phys. **1994**, *101*, 3862.

15. A. P. Rendell. Chem. Phys. Lett. **1994**, *229*, 204.

16. A. T. Wong, R. J. Harrison. J. Comput. Chem. **1995**, *16*, 1291.

17. M. W. Schmidt, K. K. Baldridge, J. A. Boatz, S. T. Elbert, M. S. Gordon, J. H. Jensen, S. Koseki, N. Matsunaga, K. A. Nguyen, S. Su, T. L. Windus, M. Dupuis, J. A. Montgomery. J. Comput. Chem. **1993**, *14*, 1347.

18. R. Fletcher. *Practical methods of optimization.* Wiley. New York, **1980**, Vol.1.

19. C.C.J. Roothaan. Rev. Mod. Phys. **1960**, *32*, 179.

20. F. W. Bobrowicz and W. A. Goddard III. In *Modern Theoretical Chemistry: Methods of Electronic Structure Theory.* Ed. by H. F. Schaefer III (Plenum, New York, 1977), v.3, 79.

21. L. G. Yaffe, W. A. Goddard III. Phys Rev. A, **1976**, *13*, 1682.

22. B. Levy, G. Berthier. Int. J. Quantum Chem. **1968**, *2*, 307; erratum: Int. J. Quantum Chem. **1969**, *3*, 247.

23. K. Ruedenberg, L. M. Cheung, S. T. Elbert. Int. J. Quantum Chem. **1979**, *16*, 1069.

24. B. O. Roos. Int. J. Quantum Chem. **1980**, *S14*, 175.

25. E. Dalgaard, P. Jørgensen. J. Chem. Phys. **1978**, *69*, 3833.

26. Siegbahn P., Heiberg A., Roos B., Levy B. Physica Scripta, **1980**, *21*, 323.

27. R. Shepard. Adv. Chem. Phys. **1987**, *69*, 63.

28. U. Meier and V. Staemmler. Theor. Chim. Acta. **1989**, *76*, 95.

29. M. Dupuis, S. Chin, A. Marquez. In *Relativistic and Electron Correlation Effects in Molecules and Solids.* Edited by G. L. Malli, Plenum Press, New York, **1994**, p.315.

30. N. Camp, R. Nicholas, H. F. King. J. Chem. Phys. **1982**, *77*, 3056.

STEP	COST [a]
0. Estimate $\mathbf{B}^{-1}$, on first iteration [b]	2L
1. Obtain gradient in MO basis [b]	$2n_{occ} N^2 + 2LN$
2. Apply BFGS updates to obtain the orbital rotation parameters $\mathbf{x}=\mathbf{B}^{-1}\mathbf{g}$	$16L + 20 (n_{iter} - 2) L$
3. Generate transformation $\mathbf{U}=\mathbf{I}+\mathbf{A}$ from x	negligible
4. Schmidt orthogonalize **U**	$2N^3 + N^2$
5. Rotate orbitals, $\mathbf{C}_{n+1} = \mathbf{C}_n \mathbf{U}$	$2N^3$

[a] N is the size of the AO basis, L is the number of independent orbital rotation parameters, and n_{iter} is the number of iterations since SOSCF was initiated.

[b] The costs of these steps are wavefunction dependent, and values shown are for RHF computations.

Figure 1. Summary of approximate second order SCF algorithm, with FLOP count.

Table 1. Comparison of second order SCF and DIIS methods [a].

Molecule	# basis functions	# iterations		SCF time (sec.)		Fock time (sec.)	
		DIIS	SOSCF	DIIS	SOSCF	DIIS	SOSCF
Glycine	85	12	12	3.1	0.8	355	same as DIIS
Thymine	149	13	13	17.4	5.7	2,243	same as DIIS
Nicotine	208	13	12	48.4	14.1	6,361	6,123
Luciferin	294	14	15	153.6	51.1	13,733	14,574
Cyclic AMP	356	14	13	275.4	77.4	24,262	23,647

[a] The calculations were performed on a 67 MHz IBM SP2 thin node running sequentially. The basis set is 6-31G(d), and none of the molecules possesses any symmetry. All runs used direct SCF techniques.

Table 2. Number of SCF iterations during geometry optimization of glycine molecule.

Geometry step	1	2	3	4	5	6	7	8	9	10	11	12	13	14	15	16
DIIS	13	11	11	10	10	8	8	8	8	8	9	9	7	7	7	6
SOSCF	13	10	10	9	8	7	7	7	6	7	8	8	6	6	5	5

Table 3. Comparison of different GVB orbital optimization methods (number of iterations).

Molecule	OCBSE	GVB-DIIS [a]	SOSCF
Methylene, CH_2, 1P [b]	10	11	10
Bicyclobutane, C_4H_6,1P	doesn't converge	23	18
Disilane, Si_2H_6, 1P	doesn't converge	doesn't converge	10
Ethylene, C_2H_4, 2P	12	11	11
Stannobenzene, 3P	46	doesn't converge	31
Cyclic N_2O_2, 5P	23	doesn't converge	14

[a] These results are given for Single Fock Operator + DIIS methods implemented in GAMESS (single-pair GVB-DIIS [2c] and multi-pair GVB-DIIS [3]).

[b] The notation nP indicates the number of GVB pairs used.

Table 4. Comparison of different methods for low-spin ROHF calculations.

Molecule	OCBSE	DIIS	SOSCF
H_2CO n→π* $^1A''$	doesn't converge	10	11
Y atom s^2d^1 ^2D	doesn't converge	8	9

Table 5. Comparison of three MCSCF orbital improvement methods [a].

	2nd order method		1st order method		approx. 2nd order	
Molecule [b]	iterations	time (sec)	iterations	time (sec)	iterations	time (sec)
SiH_2	7	18	23	25	12	13
N_3F	8	333	31	270	16	145
C_4H_4	7	1398	12	496	12	441
CH_3AsNCH_3	9	5608	34	2432	14	1194
7-azaindole	-	-	14	15,018	9	10,098

[a] CPU timings for these runs are taken on 42 Mhz model 350 IBM RS/6000 workstation.

[b] The MCSCF(n,m) examples are complete active spaces with n electrons in m orbitals:

1)MCSCF(6,6)/6-31G(d,p) calculation of triplet SiH_2 (29 AOs, 51 CSFs);

2)MCSCF(6,6)/6-31G(d) calculation of cyclic isomer of N_3F (60 AOs, 92 CSFs);

3)MCSCF(4,4)/6-31++G(d,p) ground state of C_4H_4 (100 AOs, 12 CSFs);

4)MCSCF(4,4)/DZP for CH_3-As=N-CH_3 compound (103 AOs, 12 CSFs);

5)MCSCF(10,9)/DZP for 7-azaindole (165 AOs, 5292 CSFs). This job is impossible to run with the exact second order program because of memory requirements.

CHAPTER 3. ON THE STRUCTURE AND STABILITY OF GEOMETRICAL ISOMERS OF N_3F

A paper published in *Journal of Chemical Physics*

Galina Chaban, David R. Yarkony, and Mark S. Gordon

Abstract

The potential energy surfaces for the N_3F molecule have been studied using multi-configurational wave functions. Two new isomers were found, one on the singlet ($^1A'$) and one on the triplet ($^3A''$) surface. Both isomers have a 3-membered cyclic structure and C_s symmetry. The singlet cyclic isomer is endoergic relative to the open fluorine azide by 15-17 kcal/mol. Its kinetic stability is close to the stability of the open isomer: the barrier separating the cyclic isomer from the dissociation products $N_2(X^1\Sigma_g^+)$+NF ($a^1\Delta$) is about 13-17 kcal/mol and is lower than the barrier to isomerization. The triplet cyclic isomer is much higher in energy (about 70 kcal/mol), with a barrier to dissociation to $N_2(X^1\Sigma_g^+)$+$NF(X^3\Sigma^-)$ on the order of 15 kcal/mol. Crossings of the $^1A'$ and the $^3A''$ surfaces may allow the cyclic singlet isomer to predissociate to the ground state products, $N_2(X^1\Sigma_g^+)$+$NF(X^3\Sigma^-)$. It is shown, however, that the singlet-triplet surface of intersection lies 'behind' the barrier to singlet decomposition, so that spin-forbidden predissociation will not preclude detection of cyclic N_3F.

I. Introduction

The very high heat of formation (about 130 kcal/mol) of fluorine azide (NNNF) makes it a candidate as an energetic material. The equilibrium structure of fluorine azide and its decomposition to $N_2(X^1\Sigma_g^+)$ + $NF(a^1\Delta)$ have been studied in a number of experimental and theoretical works.[1-6] It was found that gas phase thermal dissociation of fluorine azide yields

metastable NF($a^1\Delta$) radicals, and the experimental activation barrier for this dissociation is 15 kcal/mol.[2] Theoretical calculations of the potential energy surface(PES) for the dissociation, including electron correlation via configuration interaction (CI) and fourth order perturbation theory (MP4) with zero point energy corrections predict a barrier height of about 12-16 kcal/mol,[4,5] in good agreement with the experimental value. Both experimental and theoretical studies predict a singlet-triplet crossing to lie outside the barrier, that is, in the (product) $N_2(X^1\Sigma_g^+)$ + $NF(X^3\Sigma^-)$ channel.

The low barrier to dissociation (15 kcal/mol) is responsible for the explosiveness of fluorine azide and is the main obstacle to using this compound as an energy source. In this work other regions of the lowest singlet PES of N_3F will be explored in an attempt to identify additional isomers that might be more stable kinetically than fluorine azide. Also considered is the lowest triplet PES and the possibility of radiationless decay attributable to spin-orbit induced coupling of the singlet and triplet states.

Section II discusses the theoretical approach. Section III presents the results of our calculations and Section IV summarizes and concludes.

II. Theoretical Approach

The geometrical parameters of the stationary points on the PESs were determined at the restricted Hartree-Fock (RHF), second order perturbation theory (MP2)[7], single pair generalized valence bond (GVB-1P)[8] and multiconfigurational self-consistent field (MCSCF)[9] levels of theory using the standard 6-31G(d) basis sets[10] [denoted BASIS-1]. Minima and transition states were verified by determining the number of negative eigenvalues (0 for minima, 1 for transition states) of the energy second derivative (hessian) matrix. The hessians were determined analytically for RHF, GVB, and MP2 wavefunctions, and by divided difference of analytic gradients for general MCSCF wave functions. Relative isomer energies were recalculated at higher levels of theory: fourth order perturbation theory (MP4)[11],

quadratic configuration interaction (QCISD(T))[12], multireference perturbation theory (CASPT2)[13], and multireference configuration interaction (MRCI).[14]

Potential energy surfaces for dissociation (where one can expect considerable configurational mixing) were studied using MCSCF wave functions with (6,6) and (10,10) active spaces. Here the notation (X,Y) denotes all the configuration state functions (CSFs) obtained from distributing X electrons in Y orbitals. The character of these active spaces is discussed in Section III. The intrinsic reaction coordinate (IRC) method was used – at the MCSCF(6,6) level with BASIS-1 denoted MCSCF(6,6)/1 - to connect all transition states to their corresponding minima. The IRC algorithm used was the second order method developed by Gonzalez and Schlegel [15] with a step size of 0.3 amu$^{1/2}$ bohr. Barrier heights were reevaluated using single point calculations. These calculation were performed using 6-31G(d), 6-311G(d)[denoted BASIS-2] and 6-311G(2d) [denoted BASIS-3] basis sets[16] at the single reference perturbation theory, MP2 and MP4, and QCISD(T) levels and using MCSCF-based multiconfigurational methods including second order internally contracted CI (SOICCI - all single and double excitations from a (6,6) or (10,10) reference space), MRCI (single and double excitations from reference CSFs) and CASPT2 (second order perturbation theory with a MCSCF(6,6) or MCSCF(10,10) reference wave function). Several quantum chemistry programs were used including: GAMESS[17] for MCSCF calculations, MOLCAS-2[18] for CASPT2, MOLPRO[19] for SOICCI and (some) MRCI, and GAUSSIAN-92[20] MP2, MP4 and QCISD(T) calculations.

For reasons described below a section of the surface of intersection for the lowest singlet and triplet states was explored using methods developed by Yarkony and co-workers[21]. The states were described at the MRCI level. The nitrogen 1s and fluorine 1s and 2s orbitals were kept doubly occupied. The remaining twenty electrons were distributed among the [active1(5–11 a',2–3 a"), active2(12a', 4–5 a") ,virtual] orbitals as: [18,2,0] [17,3,0], [16,4,0], [18,1,1], [17,2,1], [18,0,2], [17,1,2] and [16,2,2]. The four molecular orbitals

with the highest orbital energies were excluded from the virtual space. All CSFs arising from these electron configurations were included in the MRCI expansion. The molecular orbitals were in turn determined from CAS state-averaged MCSCF calculations using the active2 space. The character of the active orbitals is discussed in Section III (see Table 3 and Figure 3). These calculations were performed using [4s2p1d] Dunning double zeta polarization[22], and [5s4p1d] McLean and Chandler bases[23], denoted BASIS-4 and BASIS-5 respectively. These levels of treatment will be denoted MRCI/4 and MRCI/5 respectively. Here and throughout this work the designation M/J will refer to a calculation performed at level of theory (or method) M using BASIS-J.

Additional calculations were performed at the CCSD(T) level of theory[24], with two basis sets, 6-311++G(d,p)[20] [BASIS-6] and 6-311++G(2df,2pd)[16] [BASIS-7] and at the MRCI level using 5s4p2d[25] bases [BASIS-8].

III. Results

1. Structural isomers

The key result of this work is the discovery of a new metastable cyclic isomer of N_3F that is endoergic relative to the open isomer N-N-N-F (see Table 1 and Figure 1, structure 1 ($^1A'$)). This new isomer has a three-membered cyclic structure with C_S symmetry (see Figure 1, structure 2 ($^1A'$)). Geometrical parameters for this cyclic isomer are shown in Table 1. The MP2/1 and MCSCF(10,10)/1 levels of theory predict very similar geometries, while the MRCI/4 and MRCI/5 bond distances are only sligthly shorter. The cyclic isomer 2 ($^1A'$) has one N=N double bond, $R(N^1N^2) \sim 1.2$Å compared to $r_e[N_2(X^1\Sigma_g^+)] = 1.10$Å,[26] and two weak N–NF single bonds. The NF group, $R(N^3F) \sim 1.35$Å compared to $r_e[NF(a^1\Delta)] = 1.31$Å,[26] forms an angle ($\equiv \theta$) of ~ 105° with the plane of the ring. This structure was verified to be a minimum at all levels of theory used in this paper.

Two structures [open 4 ($^3A''$)and cyclic 5 ($^3A''$)] were also found to be local minima

on the triplet PES at the ROHF/1 and UHF/1 levels (see Figure 1). However, at the Hartree-Fock level of theory the open structure is very weakly bound and separated from dissociation products by a barrier of only 3-4 kcal/mol. At the MP2 level this structure is not stable. Therefore, this open structure was not pursued at higher levels of theory. Figure 1 and Tables 1–2 give the geometrical parameters and energies of the cyclic triplet structure 5 (^{3}A"). The triplet cyclic isomer is very high in energy, about 70-80 kcal/mol higher than the ground state singlet open isomer at MP2/1 and CASPT2/MCSCF(6,6)/1 levels of theory. Although it is stable kinetically (see below), it will decay radiatively to the ground singlet state.

2. Decomposition of cyclic isomers

The decomposition of cyclic N3F to $N_2(X^1\Sigma_g^+)$+NF($a^1\Delta$) was studied using multi-configurational wave functions with active spaces ranging from (6,6) to (14,12). The minimum active space (6,6) necessary for a correct qualitative description of the dissociation process includes three bonding orbitals (the 10a', 11a' and 4a" orbitals, corresponding to two N_2 – NF bonds and the N–N π- bond) and the three corresponding antibonding orbitals (the 5a", 6a" and 12a' orbitals). Upon dissociation these orbitals convert to two π (N-N), two π*(N-N), and two π*(N–F) orbitals. The MCSCF(6,6)/1 treatment was used to locate the transition state and analyze the IRC path connecting the transition state with the cyclic isomer and products of dissociation. The energy along the IRC path is shown in Figure 2. From this figure it is seen that the IRC is dominated by R(N_2–NF). The MCSCF natural orbitals are shown in Figure 3, and the corresponding occupation numbers are listed in Table 3. It is seen from Table 3 that the occupation number of the 4a" orbital decreases from 1.93 (essentially doubly occupied) in the cyclic isomer to 1.0 in the dissociation products. Simultaneously, the 12a' orbital increases its occupation from 0.05 to 1.0. Thus, this wave function dissociates to $N_2(X^1\Sigma_g^+)$ + NF($a^1\Delta$) with two half occupied π*(N-F) orbitals.

With the foregoing information in hand the energetics were reinvestigated using larger basis sets and more flexible wave functions. These results are collected in Table 2. The

geometry of the transition state was reoptimized at the MCSCF(10,10) level. The bigger active space was constructed by adding two bonding orbitals: $\sigma(N^1\text{-}N^2)$ and $\sigma(N^3\text{-}F)$, and the two corresponding antibonding orbitals to the (6,6) active space. The transition state at the MCSCF(10,10) level is similar to the MCSCF(6,6) level result, although $R(N^3\text{–}F)$ and $R(N^2\text{–}N^3)$ increase by 0.06Å and 0.05Å respectively, see Table 1.

The height of the barrier to dissociation was recalculated using the CASPT2 method with (6,6), (10,10) and (10,8) active spaces using BASIS-1. Unlike the (10,10) active space the (10,8) active space added two doubly occupied nitrogen lone pairs to the (6,6) active space. Upon dissociation, these lone pairs become two π(N-F) orbitals. Single point CASPT2 (10,10) calculations were also performed using BASIS-2 [6-311G(d)] and BASIS-3 [6-311G(2d)]. As seen in Table 2, there is little variation in the CASPT2 predicted barrier heights, as a function of active space or basis set. The predicted barrier is in the 13-17 kcal/mol range. The barrier height is discussed further below. The exothermicity of the dissociation from the cyclic isomer is predicted to be 11-14 kcal/mol at the CASPT2/2 and CASPT2/3 levels.

The dissociation of the triplet cyclic isomer to $N_2(X^1\Sigma_g^+)$ and $NF(X^3\Sigma^-)$ was studied at the MCSCF(6,6)/1 level. The transition state located at this level of theory has no symmetry. Its structure 6 ($^3A''$) is shown in Figure 1, and the geometrical parameters are given in Table 1. Note that the $R(N^iN^3)$, i=1,2 are considerably shorter in the cyclic triplet than in the corresponding singlet. The reaction path for the dissociation is shown in Figure 4 . The height of the barrier estimated by a single point CASPT2/MCSCF(10,10)/1 calculation at the MCSCF(6,6)/1 geometry is ~16 kcal/mol, and the exothermicity of the reaction is about 106 kcal/mol.

The triplet cyclic isomer 5 ($^3A''$) is 61 kcal/mol higher in energy than the corresponding singlet 2 ($^1A'$) at the CASPT2(10,10)/1 level. At the same level of theory, the asymptote $N_2(X^1\Sigma_g^+)$+$NF(X^3\Sigma^-)$ is 36.8(36.95) kcal/mol below the singlet asymptote,

$N_2(X^1\Sigma_g^+)$+NF($a^1\Delta$), in excellent agreement with the experimental value[26] given parenthetically. Thus the $1^1A'$ and $1^3A''$ potential energy surfaces must cross. This crossing may lead to spin-forbidden predissociation of the 2($^1A'$) moiety. Note that the energy recovered from singlet cyclic N3F would be 45, rather than 8, kcal/mol if the spin-forbidden path were followed. At the singlet transition state $E(1^1A') - E(1^3A'') \sim -1$ kcal/mol at the CASPT2(10,10)/1 level of theory, suggesting a crossing in this region. However larger singlet–triplet separations, ~37 kcal/mol, are observed using coupled cluster wave functions (see discussion below). Thus a more precise description of the surface of intersection is desirable. This point is addressed in subsection III.4 below.

3. Rearrangements between isomers on the singlet PES

Attempts to locate a transition state for the rearrangement between the open and cyclic isomers on the singlet PES were unsuccessful at all calculational levels except for GVB(1P)/1. The height of the isomerization barrier at the GVB(1P)/1 level was found to be 11.5 kcal/mol (from the cyclic isomer). This is close to the barrier height for dissociation of the cyclic isomer at this computational level (11.8 kcal/mol). At the MCSCF(6,6)/1 and MP2/1 levels of theory, the cyclic isomer dissociates to $N_2(X^1\Sigma_g^+)$+NF($a^1\Delta$) before it reaches the isomerization transition state. It is likely that the barrier for isomerization from the cyclic isomer is higher than the barrier to dissociation of this isomer, and therefore that the intramolecular rearrangement between the cyclic and open singlet isomers does not occur.

Four other transition states have been found on the singlet potential energy surface at the RHF/1 and GVB(1P)/1 levels. Partial geometries and imaginary modes for these structures are shown in Figure 5. Following the GVB(1P) IRC from transition state 7 ($^1A'$) illustrates that this species corresponds to the degenerate rearrangement between two open isomers. Similarly, transition state 8 ($^1A'$), the nonplanar bicyclic structure, corresponds to a degenerate rearrangement between two cyclic isomers, with the F atom moving from one N atom to another. The GVB(1P) barriers for these rearrangements are quite high: 58 and 78 kcal/mol

respectively. The C_{2v} structures 9 ($^1A'$) and 10 ($^1A'$) (142 and 100 kcal/mol higher, respectively, than the open isomer) are found to be transition states between two open isomers at the GVB(1P) level of theory. Since all four structures 7 - 10 are much higher in energy than the transition states for dissociation of both the open and cyclic isomers, such rearrangements are extremely unlikely and were not pursued at higher levels of theory.

4. Singlet-triplet surface of intersection

The vibrational levels of cyclic $N_3F(^1A')$ are, technically speaking, resonances since they can be predissociated to $N_2(X^1\Sigma_g^+)$+$NF(X^3\Sigma^-)$ through spin-orbit interactions with the $^3A''$ state. The lifetime of the vibrational levels is determined by the relation between the $^1A'$–$^3A''$ surface of intersection and the coordinate space on the $^1A'$ surface sampled by the vibrational wavefunction. It is important to distinguish two situations, one in which the state lives long enough (for example, microseconds) to be detected and the second in which the state lives long enough (for example, days) to be useful as an energetic species, with the latter situation requiring a more detailed analysis than the former.

From Table 1 it is seen that the principal difference between the equilibrium structure of cyclic N_3F and its transition state for decomposition to $N_2(X^1\Sigma_g^+)$+ $NF(a^1\Delta)$ is attributable to changes in $R(N^1N^3)$ [= $R(N^2N^3)$]. For this reason the $^1A'$– $^3A''$ surface of intersection was characterized as a function of $R(N^1N^3)$, which represents an approximate reaction coordinate– see Figure 2. Three points on the surface of intersection, at the MRCI/5 level, are reported in Table 4: (i) the minimum energy crossing point (MECP) a local minimum on the $^1A'$– $^3A''$ surface of intersection, for which $R(N^1N^3)$=1.869Å, and two additional points with $R(N^1N^3)$ fixed at (ii) its MRCI/5 transition state value, $R(N^1N^3)$ = 1.757Å, and (iii) an intermediate value, $R(N^1N^3)$=1.826Å. In each case the remaining geometric parameters were optimized to minimize the common energy $E(^3A'')(\mathbf{R}) = E(^1A')(\mathbf{R}) \equiv E_x(\mathbf{R})$. It is seen by comparing Tables 2 and 4 that the MECP is lower in energy than the transition state and, significantly, differs from the transition state structure principally in the value of $R(N^1N^3)$. However since

$R(N^1N^3)$ is larger at the MECP than at the transtion state, the MECP lies 'behind' the barrier to spin-allowed dissociation. Further as $R(N^1N^3)$ decreases toward its value at the transition state, the energy of the intersection point increases rapidly, so that in a qualitative sense the crossing surface is either 'behind', or well above, the barrier to spin-allowed dissociation. Since the $^1A'$ - $^3A''$ surface of intersection can only be reached by tunneling through the barrier on the $^1A'$ surface or at signficant energetic cost, spin-forbidden predissociation will not prevent observation of cyclic N_3F. The lifetime of the individual vibrational levels with respect to spin-forbidden predissociation will be the object of a future publication.

The behaviour of the $^1A'$ and $^3A''$ potential energy surfaces in the vicinity of the transition state and MECP (MRCI/5 level) is illustrated from an alternative perspective in Figure 6 which reports $E(^1A')$ and $E(^3A'')$ as a function of $R(N_2 - NF)$ at the MRCI/8 level, with the remaining coordinates fixed at their transition state(MRCI/5 level) values. From this figure it is seen that $\Delta E(^3A'', {}^1A') \equiv E(^3A'') - E(^1A')$ depends very sensitively on $R(N_2–NF)$. Thus the precise energy of a crossing point is expected to depend on the level of theory used to characterize the $^1A'$ and $^3A''$ states. To address this question the $^1A'$ and $^3A''$ states were studied in this region using CCSD(T) wavefunctions. Calculations performed with BASIS-6[6-311++G(d,p)] and BASIS-7[6-311++G(2df,2pd)] are reported Table 5 and Figure 6. Since the triplet state energies were calculated using unrestricted Hartree-Fock (UHF) wave functions as the starting point, it is important to note that the spin contamination for all calculations is small, with $\langle S^2 \rangle \leq 2.04$. At the transition state the $^1A'$ and $^3A''$ state are separated by ~39kcal/mol. However at the MECP geometry the separation is reduced to 5.7 kcal/mol [BASIS-6] and 8.5 kcal/mol [BASIS-7]. Still these are fairly large splittings. To understand their origin $R(N_2–NF)$ was varied from its MRCI/5 value ($[R(N_2–NF)] = 1.87$Å) in steps of 0.01Å, using BASIS-6. In these calculations remaining geometrical parameters were fixed. When $R(N_2–NF)$ is increased by only 0.03Å, to 1.90Å, the singlet-triplet splitting decreases to 0.1 kcal/mol! Note that both the MRCI/8 and CCSD(T)/6 data reported in Figure

6 suggest that the MRCI/5 treatment underestimates the energy at the MECP.

The CCSD(T)/6 calculations in the vicinity of the MECP also indicate (as do the MRCI/5 results from Table 1 and the MRCI/8 results in Figure 6) that at the transition state $R(N^1N^3)$ is somewhat shorter than the ~1.9 – 1.95Å suggested by the MCSCF(6,6) and MCSCF(10,10). Since analytic CCSD(T) gradients are not available to us, this last point was explored by analyzing the CCSD(T)/6 potential energy surface in the vicinity of the MRCI/5 transition state. To this end, $R(N_2\text{-}NF)$ was varied in steps of ±0.05Å to ±0.20Å, from the MRCI/5 transition state, with all other geometric parameters held fixed. Exploratory changes in $R(N^3F)$ suggest that this is a reasonable procedure. The results are presented in Table 5 and Figure 6. It was found by this procedure that the CCSD(T) transition state should have $R(N_2\text{-}NF) \approx 1.86$Å. The locus of the transition state and crossing point at the CCSD(T)/6 level are consistent with the previous assertion that the relevant portion of $^1A' - {}^3A''$ surface of intersection occurs behind (or above) the barrier to spin-allowed dissociation, see Figure 6. Thus the key conclusion of this subsection, that the surface of intersection is 'behind' or above the barrier to spin-allowed dissociation, is supported at all levels of treatment.

The previous discussion has focused on the single coordinate $R(N_2\text{–}NF)$. It is interesting to ask how effective are the remaining degress of freedom in changing $\Delta E(^3A'', {}^1A')$. Analysis of the energy difference gradient, $\frac{\partial}{\partial R_\alpha}[\Delta E(^3A'',{}^1A')]$, shows that in the immediate vicinity of the MECP the singlet-triplet separation is most sensitive to $R(N_2 - NF)$ and secondarily to $R(N^1N^2)$ [equivalently, it is sensitive to both the coordinates $R(N^1N^3)$ and $\angle N^1N^2N^3$]. It is much less sensitive to θ and $R(N^3F)$. However as $R(N^1N^3)$ decreases, the $N_2 - NF$ interaction increases so that θ and $R(N^3F)$ play a more significant role in characterizing the surface of intersection.These observations are reflected in the data in Table 4.

Table 5 reports two points near the $^1A' - {}^3A''$ surface of intersection at the CCSD(T)/6 level, denoted TS+0.15 and MECP+0.03, with similar energies ~11.5kcal/mol and ~14.5kcal/mol, respectively. The small energetic difference reflects that fact that $R(N_2\text{–}NF)$ is

virtually identical for these two points, being 1.819Å and 1.817Å respectively. Thus these results are consistent with the geometry dependence of $E_x(\mathbf{R})$ in Table 4 and the discussion in the preceding paragraph.

IV. Summary and Conclusions

The potential energy surfaces for the N_3F molecule have been studied using multi-configurational wave functions. Two new isomers were found: one on the singlet, and one on the triplet PES. Both isomers have a 3-membered cyclic structure and C_s symmetry. The singlet cyclic isomer is endoergic relative to the open fluorine azide by 15-17 kcal/mol. Its kinetic stability is close to the stability of the open isomer: the barrier separating cyclic isomer from the dissociation products $N_2(X^1\Sigma_g^+)$+NF ($a^1\Delta$) is beween 11-17 kcal/mol and is lower than the barrier to isomerization. The triplet cyclic isomer is much higher in energy (about 70 kcal/mol), with a barrier to dissociation to $N_2(X^1\Sigma_g^+)$+NF($X^3\Sigma^-$) on the order of 15 kcal/mol.

The triplet dissociation products, $N_2(X^1\Sigma_g^+)$+NF($X^3\Sigma^-$), are ~37kcal/mol lower in energy than the singlet products, $N_2(X^1\Sigma_g^+)$+NF ($a^1\Delta$), consequently crossing of the $^1A'$ and the $^3A''$ surfaces may allow the cyclic singlet isomer to predissociate to the ground state products, $N_2(X^1\Sigma_g^+)$+NF($X^3\Sigma^-$). It was found that the singlet-triplet surface of intersection lies 'behind' the barrier to singlet decomposition. Thus spin-forbidden predissociation will not preclude detection of cyclic N_3F. Additional studies are required to determine whether spin forbidden radiationless decay will affect the utility of cyclic N_3F as an energetic fuel.

Acknowledgments

This work was supported by grants from the Air Force Office of Scientific Research (F49620-95-1-0077 to MSG and grant F49620-93-1-0067 to DRY). Calculations were performed on IBM RS 6000/350 and 370 workstations, generously provided by Iowa State University and on IBM RS 6000/580 and 590 work stations at Johns Hopkins University.

Many helpful discussions with Dr. Kiet Nguyen are gratefully acknowledged.

References

1. Peters, N.J.S.; Allen, L.C.; Firestone, R.A. *Inorg. Chem.* **1988**, 27, 755.

2. Christen, D.; Mack, H.G.; Schatte, G.; Willner, H. *J. Am. Chem. Soc.* **1988**, 110, 707.

3. Benard, D. J.; Winker, B. K.; Seder, T. A.; Cohn, R.H. *J. Phys. Chem.* **1989**, 93, 4790.

4. Michels, H. H.; Montgomery, J. A. Proceedings of the High Energy Density Materials Contractors Conference.; AFOSR, Washington, DC, 1989.

5. Kestner, N.R.; Brener, N.E.; Callaway, J. Proceedings of the High Energy Density Materials Contractors Conference.; AFOSR, Washington, DC, 1990.

6. Otto, M.; Lotz, S.D.; Frenking, G. *Inorg. Chem.* **1992**, 31, 3647.

7. Pople, J. A.; Binkley, J. S.; Seeger, R. *Int. J. Quantum Chem.* **1976**, 10, 1.

8. Goddard,W. A.; Dunning, T. H.; Hunt, W. J.; Hay, P. J. *Acc. Chem. Res.* **1973**, 6, 368.

9. Lam, B.; Schmidt, M. W.; Ruedenberg, K. J. *Phys. Chem.* **1985**, 89, 2221.

10. Hehre, W.J.; Ditchfield, R.; Pople, J.A. *J. Chem. Ohys.* **1972,** 56, 2257.

11. Krishnan, R.; Frisch, M. J.; Pople, J. A. *J. Chem. Phys.* **1980**, 72, 4244.

12. Pople, J. A.; Head-Gordon, M.; Raghavachari, K. *J. Phys. Chem.* **1987**, 87,5968.

13. Anderson, K.; Malmqvist, P.-A.; Roos, B.O. *J. Chem. Phys.* **1992**, 96, 1218; Anderson, K. Malmqvist, P.-Å., Roos, B. O. *J. Phys. Chem.* **1990**, 94, 5483.

14. Werner, H.-J.; Knowles, P. J. *J. Phys. Chem.* **1988**, 89,1988; Knowles, P. J.; Werner, H.-J. *Chem. Phys. Lett.* **1988**, 145, 514.

15. Gonzalez, C.; Schlegel, H.B. *J.Chem.Phys.* **1989**, 90, 2154; *J.Phys.Chem.* **1990**, 94, 5523; *J.Chem.Phys.* **1991**, 95, 5853.

16. Hariharan, P.C.; Pople, J. A., *Theor. Chim. Acta*, **1973**, 28, 213; Krishnan, R.; Binkley, J.S.; Seeger, R.; Pople. J.A. *J. Chem. Phys.* **1980,** 72, 650; Frisch, M. J.; Pople, J. A.; Binkley, J. S. *J. Chem. Phys.* **1984**, 80, 3265;

17. Schmidt, M, W.; Baldridge, K. K.; Boatz, J. A.; Elbert, S. T.; Gordon, M. S.; Jensen, J. H.; Koseki, S.; Matsunaga, N.; Nguyen, K. A.; Su, S. Windus, T. L.; *J. Comp. Chem.*. **1993**, 14, 1347.

18. Anderson, K.; Fülscher, M. P.; Lindh, R.; Malmqvist, P.-Å.; Olsen, J.; Roos, B. O.; Sadlej, A. J.; Wilmark, P.-O. MOLCAS version 2, User's Guide; University of Lund, Sweden, 1991.

19. MOLPRO is written by Werner, H.- J.; Knowles, P. J. with contributions by Almlöf, J.; Amos, R. D.; Elbert, S.T.; Taylor, P.R.

20. Gaussian 92, revision C, Frisch, M. J.; Trucks, G. W.; Head-Gordon, M.; Gill, P.M.W.; Wong, M.W.; Foresman, J. B.; Johnson, B. G.; Schlegel, H. B.; Robb, M. A.; Replogle, E.S.; Gomperts, R.; Andres, J. L.; Raghavachari, K.; Binkley, J. S.; Gonzalez, C.; Martin, R. L.; Fox, D. J.; Defrees, D. J.; Baker, J.; Stewart, J. J. P.; and Pople, J. A. Gaussian, Inc., Pittsburgh PA, 1992.

21. Yarkony, D. R. *J. Am. Chem. Soc.* **1992**, 114, 5406; Yarkony, D. R. *J. Chem. Phys.* **1990**, 92, 2457; Yarkony, D. R. *Int. Reviews of Phys. Chem.* **1992**, *11*, 195.

22. Dunning, T. H.; Hay, P. J. *Gaussian Basis Sets for Molecular Calculations*, in *Modern Theoretical Chemistry*; edited by Schaefer, H. F.; Plenum, New York, 1976;

23. McLean, A. D.; Chandler, G. *J. Chem. Phys* **1980**, *72*, 5639; McLean, A. D.; Chandler, G. private communication. The [5s4p1d] bases used in this study can be found in Yarkony, D. R. *J. Chem. Phys.* **1986**, *85*, 7261.

24. See, for example, Bartlett, R.J. *J. Phys. Chem.* **1989**, *93*, 1697, and references cited therein.

25. 5s4p2d bases are the 5s4p bases of McLean and Chandler with 2 sets of d functions from Ahlrichs, R.; Scharf, P.; Jankowski, K. Chem. Phys **1985**, *98*, 381.

26. Huber, K. P.; Herzberg, G. *Molecular Spectra and Molecular Structure IV. Constants of Diatomic Molecules*; Van Nostrand Reinhold: New York, 1979.

Table 1. Geometrical parameters[a]

Method	$R(N^1N^2)$	$R(N^2N^3)$	$R(N^3F)$	$\angle N^1N^2N^3$	θ	$N^1N^2N^3F$
			Open isomer 1 ($^1A'$)			
MP2/1	1.154	1.282	1.432	171.6	103.8[b]	180.0
MCSCF(6,6)/1	1.127	1.255	1.377	173.2	104.9[b]	180.0
MCSCF(10,10)/1	1.134	1.278	1.469	175.1	102.1[b]	180.0
			Cyclic isomer 2 $^1A'$			
MP2/1	1.249	1.501	1.422	65.4	104.7	
MCSCF(6,6)/1	1.198	1.528	1.358	66.9	105.3	
MCSCF(10,10)/1	1.229	1.500	1.440	65.8	104.7	
MRCI/4	1.213	1.471	1.395	65.7	100.3	
MRCI/5	1.181	1.468	1.383	66.3	101.6	
			Transition state 3 ($^1A'$)[c]			
MCSCF(6,6)/1	1.139	1.904	1.322	72.6	102.5	
MCSCF(10,10)/1	1.149	1.952	1.381	72.9	100.7	
MRCI/4	1.137	1.817	1.383	71.8	100.1	
MRCI/5	1.116	1.760	1.379	71.5	100.4	
			Cyclic isomer 5 ($^3A''$)			
UMP2/1	1.514	1.328	1.388	55.3	133.2	
MCSCF(6,6)/1	1.458	1.368	1.342	57.8	122.9	
			Transition state 6 ($^3A''$)[d]			
MCSCF(6,6)/1	1.416	1.646	1.340	51.1	126.8[b]	-89.5

[a] Distances in Å, angles in degrees.

[b] Angle N^2N^3F

[c] Transition state for decomposition of 2 ($^1A'$) to N_2+NF($a^1\Delta$)

[d] Transition state for decomposition of 5 ($^3A''$) to N_2+NF($X^3\Sigma^-$)

Table 2. Energetics[a]

	2 (^{1}A')		1 (^{1}A')	3 (^{1}A')	N_2+NF($a^1\Delta$)
Method	E^{tot}	E^{rel}	E^{rel}	E^{rel}	E^{rel}
MCSCF(6,6)/1[b]	-262.69893	0.0	-1.1	10.6	-24.5
SOICCI(6,6)/1[c]	-262.75520	0.0		11.2	-14.5
MRCI(6,6)/1[c]	-263.19729	0.0		12.2	-12.0
CASPT2(6,6)/1[c]	-263.24480	0.0	-16.7	13.2	-12.4
MCSCF(10,8)/1[c]	-262.70992	0.0		6.9	-19.7
CASPT2(10,8)/1[c]	-263.24770	0.0		12.8	-11.6
MCSCF(10,10)/1[b]	-262.79117	0.0	-2.0	18.0	-11.9
SOICCI(10,10)/1[d]	-262.90489	0.0		20.1	0.1
CASPT2(10,10)/1[d]	-263.24997	0.0	-15.4	16.9	-8.4
MCSCF(14,12)/1[d]	-262.80726	0.0		10.7	-18.7
MCSCF(10,10)/2[d]	-262.85904	0.0		18.3	-14.1
CASPT2(10,10)/2[d]	-263.45332	0.0		17.6	-11.0
MCSCF(10,10)/3[d]	-262.86948	0.0		16.7	-14.2
CASPT2(10,10)/3[d]	-263.50753	0.0		13.7	-13.7
MP2/1	-263.24393	0.0	-16.5		
MP4/1[e]	-263.28286	0.0	-16.4		
QCISD(T)/1[e]	-263.27668	0.0	-15.1		
MRCI/4[b]	-263.117462	0.0		19.1	
MRCI/5[b]	-263.156100	0.0		11.3	

	5 (^{3}A")		6 (^{3}A")	N_2+NF($X^3\Sigma^-$)
Method	E^{tot}	E^{rel}	E^{rel}	E^{rel}
MCSCF(6,6)/1[b]	-262.56099	86.6	96.2	–65.7
CASPT2(6,6)/1[c]	-263.15151	57.3	74.4	–49.9
MCSCF(10,10)/1[c]	-262.65929	82.8	95.8	–54.8
CASPT2(10,10)/1[c]	-263.15276	61.0	77.3	-45.2
MP2/1[b]	-263.14024	65.1		
MP4/1[e]	-263.17209	69.5		
QCISD/1[e]	-263.17476	63.9		

[a]Total energies in hartrees, relative energies in kcal/mol.

[b]Structure optimized at indicated level.

[c]Based on the MCSCF(6,6)/1 geometry. [d]Based on the MCSCF(10,10)/1 geometry.

[e]Based on the MP2/1 geometry.

Table 3. MCSCF natural orbital occupation numbers[a]

Orbital	**10 a'**	**11 a'**	**4 a"**	**5 a"**	**6 a"**	**12 a'**
Cyclic	1.914	1.943	1.929	0.086	0.078	0.050
Transition state	1.927	1.897	1.900	0.073	0.104	0.099
Point 5	1.934	1.929	1.678	0.066	0.071	0.322
Point 10	1.935	1.934	1.314	0.065	0.066	0.686
Point 15	1.935	1.934	1.101	0.065	0.066	0.899
Point 20	1.935	1.935	1.020	0.065	0.065	0.980
Point 27	1.935	1.935	0.992	0.065	0.065	1.008

[a]The orbitals are shown in Figure 3.

Table 4. MRCI/5 Analysis of Singlet-Triplet Surface of Intersection[a]

	$R(N^1N^2)$	$R(N^2N^3)$	$R(N^3F)$	$\angle N^1N^2N^3$	θ	E_x
MECP	1.089	1.869	1.371	73.0	99.3	5.3
$X(N\text{-}N^1)$	1.058	1.826	1.381	73.2	117.7	17.5
$X(N\text{-}N^1)$	1.060	1.757	1.416	72.4	134.2	37.3

[a]E_x in kcal/mol relative to $E(^1A') = -263.156100$a.u. at MRCI/5 2 ($^1A'$) structure. $\Delta E = |E(1\,^1A') - E(^3A'')| < 1cm^{-1}$.

Table 5. CCSD(T) Analysis of Vicinity of Singlet-Triplet Surface of Intersection[a]

	$^1A'$		$^3A''$	
Structure	CCSD(T)/6	CCSD(T)/7	CCSD(T)/6	CCSD(T)/7
Eq	0.0	0.0	103.7	102.9
TS	10.7	9.9	47.0	48.8
TS+0.05	11.2		33.7	
TS+0.10	11.4		22.0	
TS+0.15	11.2		11.8	
MECP	15.0	14.1	20.7	22.6
MECP+0.01	14.9		18.4	
MECP+0.02	14.7		16.4	
MECP+0.03	14.6		14.4	

[a]Eq(equilibrium structure), TS and MECP from MRCI/5 treatment. Relative energies in kcal/mol. E(Eq) = –263.40458a.u. for CCSD(T)/6 treatment, and –263.53928a.u. for CCSD(T)/7 treatment. TS(MECP)+x= TS(MECP) structure with R(N_2 – NF) increased by x Å as discussed in text.

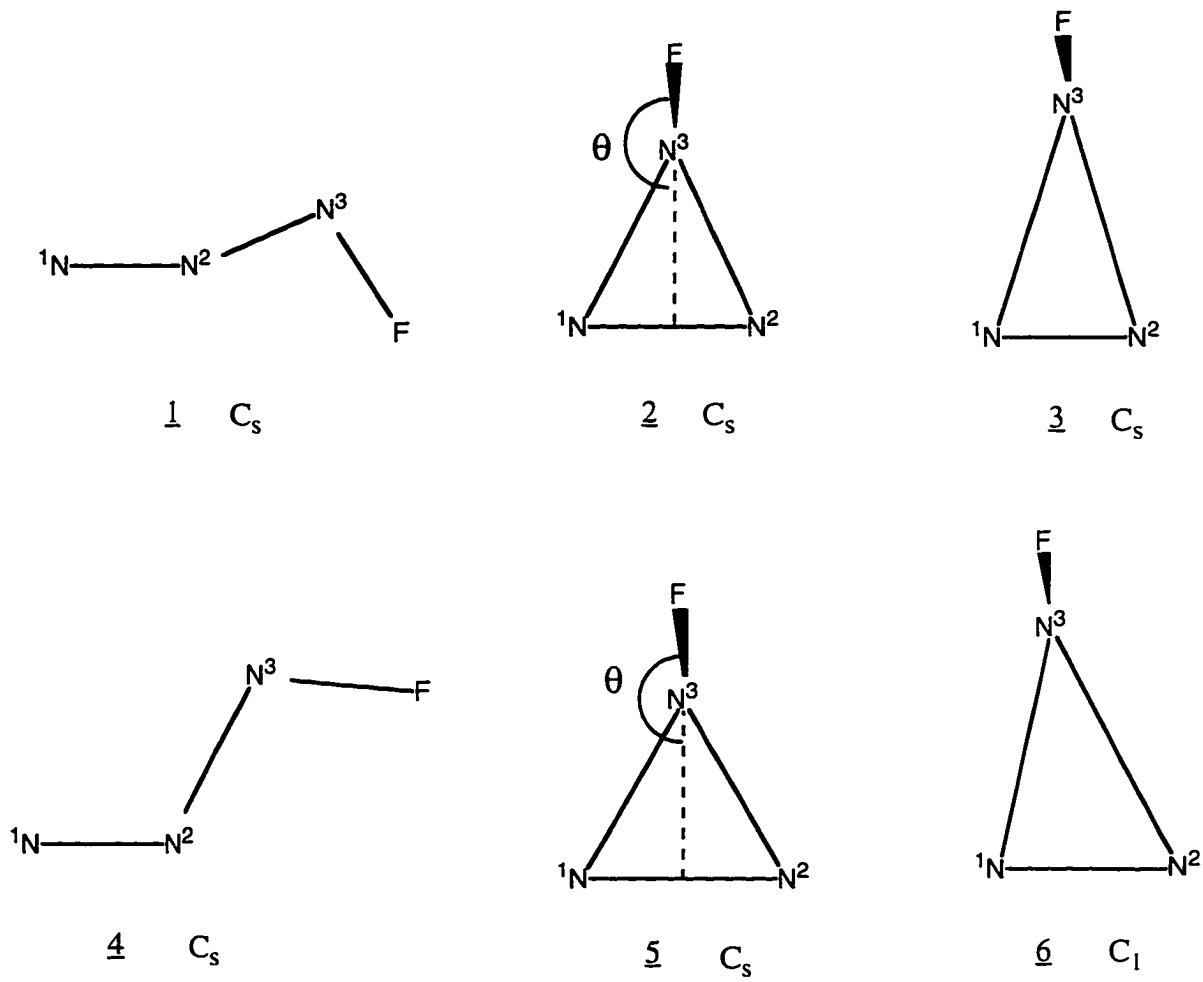

Figure 1. Structures of the stationary points on the PES's of singlet and triplet N_3F.
Singlet: 1, 2 - minima, 3 - transition state.
Triplet: 4, 5 - minima, 6 - transition state.

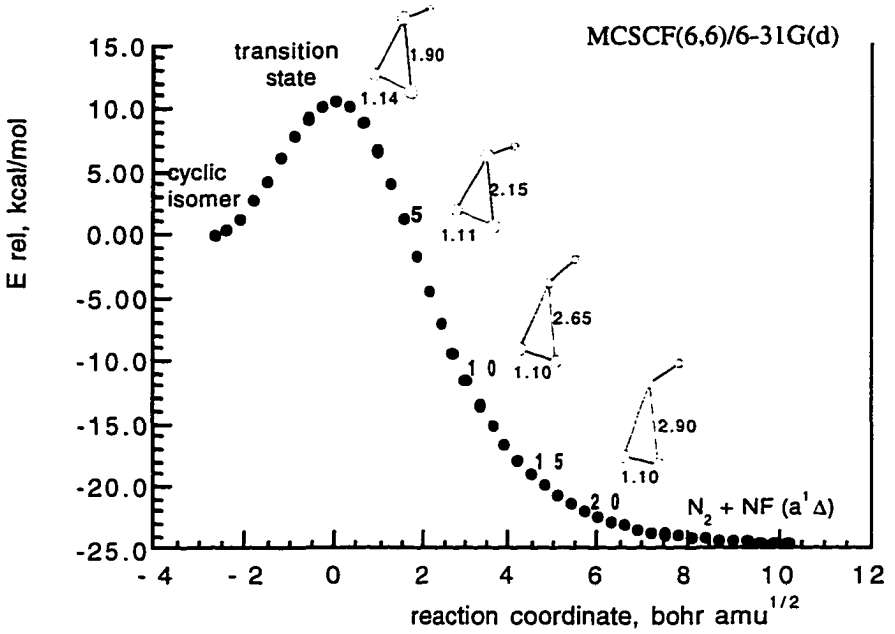

Figure 2. MCSCF(6,6)/6-31G(d) reaction path for decomposition of singlet cyclic N_3F.

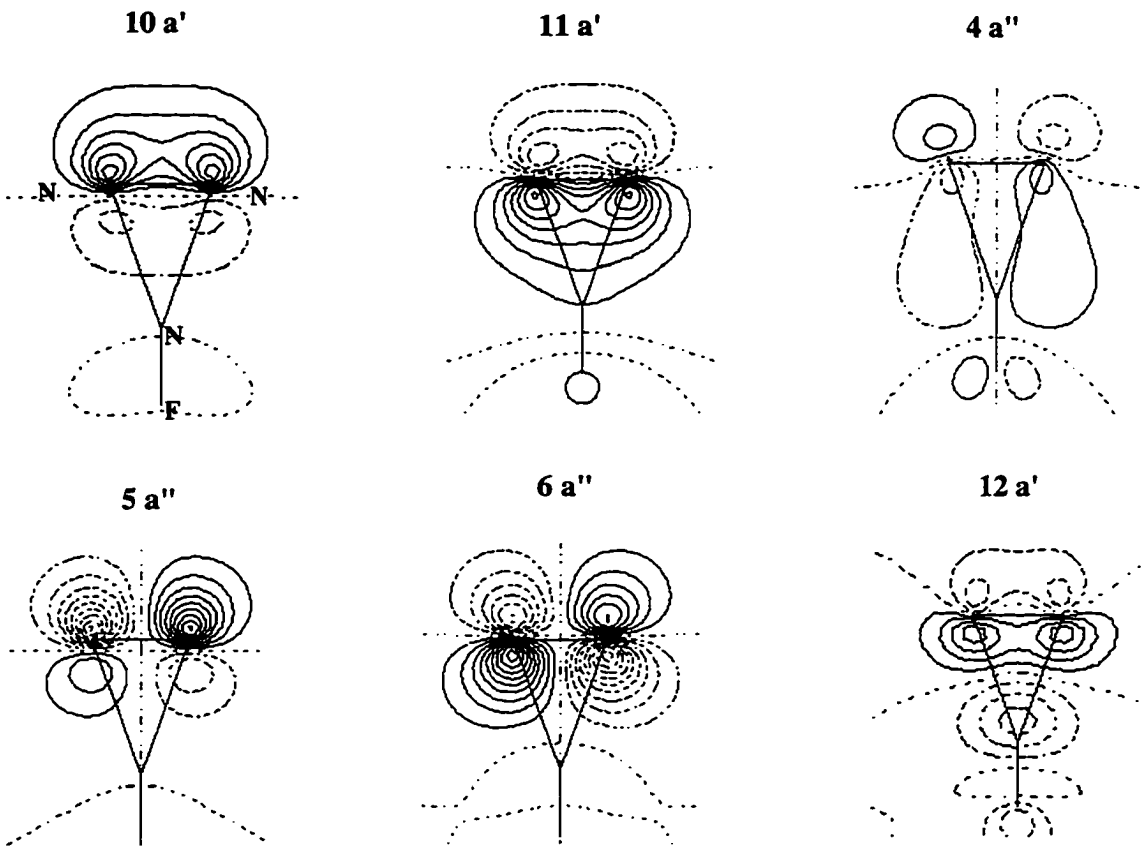

Figure 3. MCSCF/6-31G(d) natural orbitals for singlet transition state 3 in the plane of the N_3 ring.

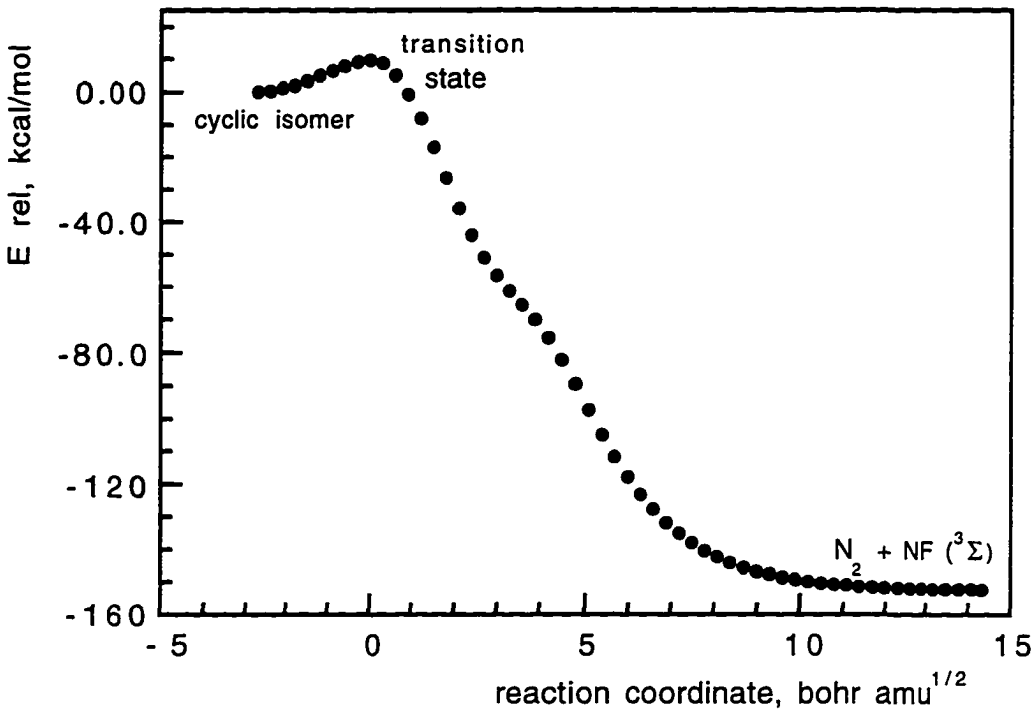

Figure 4. MCSCF(6,6)/6-31G(d) reaction path for decomposition of triplet cyclic N_3F.

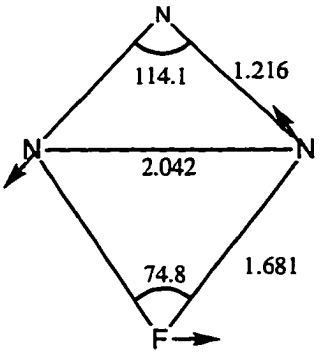

7 C_{2v}

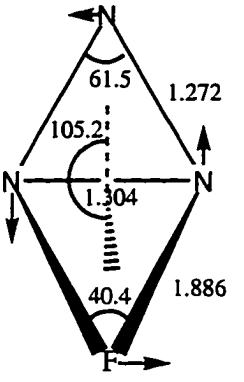

8 C_s

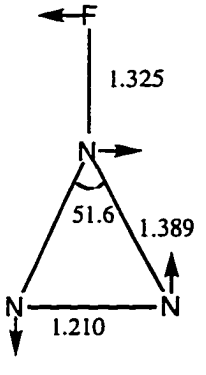

9 C_{2v}

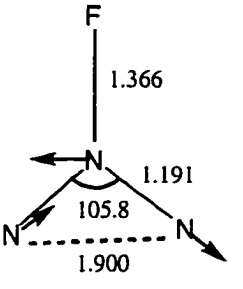

10 C_{2v}

Figure 5. RHF/6-31G(d) geometries and relative energies for transition states of rearrangements on the singlet PES of N_3F.

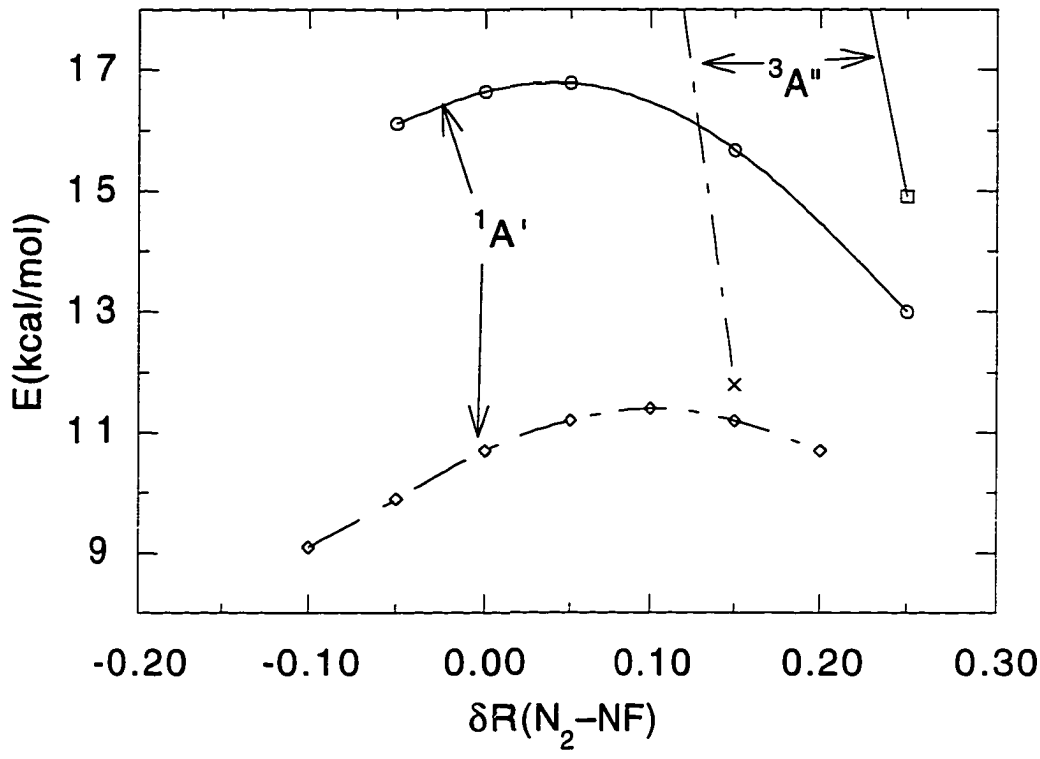

Figure 6. E(^{1}A') and E(^{3}A") as function of δR(N_2–NF) ≡ R(N_2–NF) - R(N_2–NF)(TS). R(N_2–NF)(TS) obtained at MRCI/5 level. Solid curves at MRCI/8 level; dashed curves at CCSD(T)/6 level.

CHAPTER 4. POTENTIAL ENERGY SURFACES FOR DISSOCIATION REACTIONS OF HIGH ENERGY ISOMERS OF N_2O_2

A paper accepted for publication in *Journal of Physical Chemistry*

Galina Chaban, Mark S. Gordon, and Kiet A. Nguyen

Abstract

The kinetic stability with respect to dissociation to two NO molecules was studied for several high energy isomers of N_2O_2 using multi-configurational wavefunctions. All of these isomers are 50-80 kcal/mol higher in energy than 2 NO. Three N_2O_2 isomers (a 4-membered D_{2h} isomer, a planar C_{2v} isomer, and a bicyclic C_{2v} isomer) are found to be kinetically stable: the estimated barriers to dissociation are about 40 kcal/mol for the D_{2h} isomer, and about 20 kcal/mol for each of the other two isomers. Reaction paths for their dissociation were determined using the intrinsic reaction coordinate method and multi-configurational wavefunctions.

Introduction

The possible existence of high energy isomers of NO dimer has been of considerable experimental and theoretical interest recently due to their potential role as new high energy density materials (HEDM)[1-6]. Stimulated emission pumping experiments of Wodtke and co-workers[1], and studies of photoelectron spectra of $N_2O_2^-$ by Arnold and Neumark[2] provide indirect evidence for the existence of several high energy N_2O_2 species. A number of metastable N_2O_2 isomers have also been predicted recently in theoretical papers [4-6]. Relative energies of these isomers are in the range of 40-80 kcal/mol above the energy of 2 NO fragments. However, in order to be useful as high energy compounds, these species must be

kinetically stable; that is, they must be separated from the lower energy isomers and dissociation products by relatively high barriers on the potential energy surfaces.

Besides the adiabatic kinetic stability, the possibility of surface crossings must also be considered, to ensure that there is no lower energy path to products due to non-adiabatic couplings that can decrease the stability of such compounds[7]. An example is the high energy asymmetric NNOO isomer [5,6]. This structure corresponds to a local minimum on the $^1A'$ potential energy surface and is stable to the spin-allowed decomposition a-N_2O_2 -> N_2O($X\ ^1\Sigma^+$) + O (^1D). However, the minimum energy crossing point for the singlet and triplet surfaces lies only 2 kcal/mol above the a-N_2O_2 isomer, leading to its predissociation to N_2O ($X\ ^1\Sigma^+$) + O (^3P) products [5]. Consequently, this isomer is not a viable HEDM candidate.

In this paper, we present minimum energy reaction paths for dissociation of several previously predicted[4,6] high energy N_2O_2 species to 2 NO fragments, including potential energy barriers separating them and approximate minimum energy crossing points between nearby singlet and triplet states. We predict that some of the high energy isomers may be kinetically stable with respect to the N_2O_2 -> 2 NO dissociation channel.

Theoretical approach

The N_2O_2 potential energy surfaces have been studied using *ab initio* electronic structure methods employing multi-configurational self-consistent-field (MCSCF)[8] wavefunctions. MCSCF wavefunctions are necessary for a qualitatively correct description of dissociation processes that involve bond breaking. Two kinds of wavefunctions were used. One, denoted MCSCF(10,10), included all possible configurations, consistent with the appropriate symmetry and spin, that may be obtained by distributing 10 active electrons in 10 active orbitals. Generally speaking, five NO and NN bond orbitals, and the five corresponding anti-bonding orbitals were included in the active space for various isomers. These active orbital choices will be discussed in more detail for each individual isomer. The

second active space, MCSCF (14,12), included two oxygen lone pair orbitals (one on each oxygen atom) in addition to the (10,10) space. Inclusion of oxygen lone pairs is necessary to obtain a consistent description of some reactions.

The stationary points on the N_2O_2 potential energy surface have been identified using analytic gradients of MCSCF energies. These stationary points were determined to be minima, transition states, or higher order saddle points by calculating the hessian (by finite differencing analytic gradients), and verifying that there are 0, 1 or >1 negative eigenvalues, respectively. Minimum energy paths (MEPs) were determined using the intrinsic reaction coordinate (IRC) method with the second order algorithm developed by Gonzalez and Schlegel[9] and a step size of 0.15 $amu^{1/2}$ bohr. Stationary point searches and IRC calculations were performed using MCSCF(10,10) and MCSCF(14,12) wavefunctions and the 6-31G(d)[10] basis set. These calculations were done using the GAMESS[11] electronic structure program.

The energies of stationary points, as well as selected points along the MEPs, were recalculated with the multi-configurational second order perturbation theory method (CASPT2[12]) to account for dynamic correlation. The CASPT2 wavefunctions were based on MCSCF(10,10) (denoted as CASPT2(10,10)) and MCSCF(14,12) (denoted as CASPT2(14,12)) reference wavefunctions with 6-31G(d) and 6-311+G(2d)[13] basis sets. These calculations were performed using the MOLCAS[14] program. The effect of basis set improvement on the relative energies is small, with corrections on the order of 2-4 kcal/mol. On the other hand, the addition of dynamic correlation via CASPT2 has a much larger effect, with corrections ranging from 8 to 23 kcal/mol.

Results and discussion

The four high energy singlet isomers of N_2O_2 considered in this paper are shown in Figure 1, with the structural parameters obtained at the MCSCF(10,10)/6-31G(d) level of

theory. The structure and energetics of isomers **1-3** have been studied previously [4] at several levels of theory including the MCSCF(10,10) and CASPT2(10,10) levels used in this paper. The Hartree-Fock and MP2/6-31+G(d) structures for isomer **4** have been reported by Arnold and Neumark [2]. All four isomers are relatively high in energy: planar isomers **1**, **2**, and **4** are about 50 kcal/mol higher than 2 NO, and the bicyclic isomer **3** is about 80 kcal/mol above the energy of 2 NO. Here we consider the kinetic stability for each of these isomers with respect to dissociation to two NO molecules.

1. Dissociation of D_{2h} cyclic isomer 1

Isomer **1** in Figure 1 has a planar ring structure with four equal N-O bonds (D_{2h} symmetry). This isomer was first reported by Chaban, Klimenko and Charkin[15]. The detailed electronic structure of this isomer is described in reference 4 . The smaller MCSCF(10,10) active space used to study this isomer includes four σ (N-O) bonds, four corresponding σ^* (N-O) anti-bonding orbitals, and the π (N-N) and π^*(N-N) orbitals. An expanded (14 electron, 12 orbital) active space includes additional electrons and orbitals that correspond to the lone pair on each oxygen that interacts with the π space. The MCSCF(14,12) natural orbitals and their occupation numbers are shown in Figure 2. Orbital labels are given using C_S symmetry notations in order to have the same orbital labels for the entire dissociation reaction path. There is significant configurational mixing in this isomer, with 0.366 electrons occupying orbitals that are empty at the single configuration level of theory. The D_{2h} isomer is 50 kcal/mol higher in energy than 2 NO molecules at the CASPT2(14,12)/6-311+G(2d) level of theory. This energy is overestimated at the MCSCF level by about 20 kcal/mol. The effect of the active space on the dissociation exothermicity is very small.

The transition state for decomposition of **1** to 2 NO and the associated energetics are shown in Figure 3. The transition state geometry is predicted to have C_s symmetry. Both

active spaces predict considerable asymmetry in the transition state structure, although there are significant differences in the structural details. For example, the longest N-O distance shortens by nearly 0.4 Å upon going from the MCSCF(10,10) to the MCSCF(14,12) level. MCSCF(14,12)/6-31G(d) natural orbitals for the transition state structure are shown in Figure 4. Note that the anti-bonding σ^* orbital corresponding to the partially broken N-O bond (13 a') has a significant occupation number of 0.695 electrons. Indeed, the set of virtual orbitals that would be empty in the Hartree-Fock wavefunction contain slightly more than one electron at this MCSCF(14,12) transition state structure. The effect of the expanded active space on the MCSCF barrier height is rather small (only 3 kcal/mol), but when dynamic correlation is included at the CASPT2 level, the barrier height decreases quite significantly: from 52 to 39 kcal/mol. This is probably due to significant changes in the geometry of the transition state upon going from the MCSCF(10,10) to the MCSCF(14,12) level.

Energetics along the dissociation path **1** $\rightarrow$ 2 NO are presented in Figure 5. Although the MCSCF(10,10) active space is sufficient for a description of the D_{2h} isomer structure and the net energetics of its dissociation to 2 NO, the incorporation of the two oxygen lone pairs is essential to obtain a smoothly varying wavefunction along the reaction path that connects this isomer with 2 NO. This is shown in Figure 5a, where small black circles correspond to the minimum energy path (MEP) for this reaction at the MCSCF(10,10)/6-31G(d) level of theory, and open circles correspond to single point MCSCF(14,12)/6-31G(d) energies at the MCSCF(10,10) geometries. The MCSCF(10,10) transition state connects smoothly to the D_{2h} isomer, but the part of the IRC connecting the transition state to 2 NO has a discontinuity due to a change in the active space orbitals. This discontinuity reflects the incompleteness of the (10,10) active space: the active space after the discontinuity contains 6 a' and 4 a" orbitals while the original active space has 8 a' and 2 a" orbitals. Inclusion of the two oxygen lone pairs with a" symmetry provides a complete active space (8 a' + 4 a") that can be used consistently along the entire reaction path. Although computation of such a wavefunction is

very time-consuming (it includes 85,212 configurations vs. 9996 configurations for the (10,10) space), it is necessary to obtain a correct IRC.

The resulting MCSCF(14,12) minimum energy path is shown in Figure 5b. The barrier height for this reaction is about 40 kcal/mol at the best, CASPT2(14,12)/6-311+G(2d), level used here. Changes in the MCSCF natural orbital occupation numbers along this reaction path are shown in Figure 6 for the 12 a', 13 a', 15 a', and 3 a" orbitals. 12 a' and 15 a', almost doubly occupied and empty respectively at the isomer **1** geometry, become two singly occupied π^* (N-O) orbitals at the dissociation limit. In addition to this, the almost doubly occupied 3 a" orbital becomes empty upon dissociation, while 13 a' changes its occupation from 0 to 2. Therefore, this reaction is Woodward-Hoffmann forbidden, and this leads to the high reaction barrier.

Figure 5c illustrates the CASPT2(14,12)/6-31G(d) energies for the lowest singlet (^{1}A') and triplet (^{3}A") states at selected geometries along the ground singlet state MEP. The repulsive ^{3}A" state crosses the singlet before the transition state (that is, on the reactant side), but this crossing is predicted to occur at an energy that is about 32 kcal/mol above the reactant well. So, it is likely that singlet-triplet interaction will not destroy the stability of isomer **1**.

We conclude that the D_{2h} isomer is kinetically stable with respect to dissociation to two NO molecules. Other possible dissociation channels (for example, to $N_2 + O_2$) are likely to contain even higher potential energy barriers since considerably more electronic and geometric rearrngements would be involved; therefore, this isomer should be considered to be a possible candidate for isolation and use as a source of energy.

2. Dissociation of C_{2v} planar cyclic isomer 2

MCSCF(10,10) and MCSCF(14,12) structures and energetics for planar cyclic isomer **2** and the transition state for its decomposition into 2 NO are shown in Figure 7. Isomer **2** is

also quite high in energy, about 45 kcal/mol above the two NO fragments at the highest level of theory. This isomer has an N=N double bond, two single N-O bonds, and a single O-O bond. The (10,10) active space includes these four σ and one π bond, as well as the corresponding anti-bonding orbitals. As in the case of isomer **1**, the (14,12) space includes two additional filled π orbitals, one from each oxygen atom. The transition state structure is not planar; it is twisted by about 15° (due to the broken O-O bond) and has no symmetry (although it is very close to C_2). The structural parameters obtained using the two MCSCF active spaces are quite similar.

In C_1 symmetry, the MCSCF(14,12) wavefunction includes 169,884 configurations, so IRC calculations at this level are extremely expensive. The reaction path in this case was followed only at the MCSCF(10,10) level (19,404 configuration wavefunction). This reaction path is shown in Figure 8. Also shown are CASPT2 single point energies for singlet and triplet states calculated at several points along the IRC path. The height of the barrier is estimated to be about 19 kcal/mol. There is little variation among the various levels of theory. The reaction proceeds by breaking the O-O bond first, and then breaking the N-N bond.

The lowest triplet state is higher in energy than the singlet state for all points along the reaction path at the CASPT2(10,10) level of theory (Figure 8). When the single point energies are calculated using the larger MCSCF(14,12) active space (along the same MCSCF(10,10) reaction path), the CASPT2(14,12) triplet is found to be 4 kcal/mol *lower* than the corresponding singlet, at the transition state geometry. Although the triplet state is close to the singlet in energy in the transition state region, the triplet energy is much higher in the reactant channel. Again, it is unlikely that the singlet-triplet crossing will prevent detection of isomer **2.** More careful calculations in the singlet-triplet crossing region, including determination of the non-adiabatic interactions [7] are, of course, desirable.

3. Stability of bicyclic isomer 3

Bicyclic isomer **3** (Figure 1) is one of the highest isomers on the N_2O_2 potential energy surface: its relative energy with respect to 2 NO is about 82 kcal/mol. It has a strained structure of two three-membered N-O-N rings with an O-N-N-O dihedral angle equal to 107°. The MCSCF active space (10,10) used to describe **3** included the N-N and four N-O bonding orbitals, and the five corresponding anti-bonding orbitals. This isomer, as well as the part of the potential energy surface connecting this isomer with the planar ring **1**, was studied in detail previously [6]. The two isomers were found to be separated by a barrier of 40 kcal/mol. Therefore, the stability of the bicyclic isomer with respect to isomerisation to **1** was established.

In an attempt to find a reaction path leading to the dissociation of the isomer **3**, we found that breaking one of the N-O bonds leads to a transition state connecting this isomer to another planar isomer **4**. The dissociation to two NO molecules occurs here in two steps: first, **3** isomerizes to **4** through a barrier of about 20 kcal/mol, and then, isomer **4** dissociates to 2 NO with a rather small barrier of about 7 kcal/mol.

The MCSCF(10,10)/6-31G(d) IRC path for the first (isomerisation) part of the potential energy surface is shown in Figure 9. The structures of the isomers **3** and **4**, and the structure of the isomerisation transition state, as well as their relative energies, are shown in Figure 10. When dynamic correlation (CASPT2) is included, isomer **4** is predicted to be 26 kcal/mol lower in energy than **3**, and the **3** -> **4** barrier height is 19 kcal/mol. The lowest triplet state is about 4 kcal/mol lower than singlet at the transition state geometry and is much higher in energy for both isomers (see Figure 9). Therefore, the bicyclic isomer **3** is probably kinetically stable with respect to rearrangement to isomer **4**, although the barrier for this channel is lower than for the rearrangement **3** -> **1**. Breaking one of the N-O bonds of **3** leads to rearrangement to isomer **4**, and breaking of the N-N bond leads to **1**. Since both processes involve substantial barriers, the bicyclic isomer may be a good candidate for a

metastable high energy species. Its isolation, however, may be difficult because very high energy (at least 100 kcal/mol) has to be provided to 2 NO to overcome the lowest barrier leading to this isomer.

4. Dissociation of C_s planar isomer 4

MCSCF(10,10) and MCSCF(14,12) structures of the isomer **4** are shown in Figures 10 and 11, respectively. This isomer has short (almost double) N-N (1.23 Å) and N-O (1.20 Å) bonds, one single N-O bond (1.4 Å), and one very weak N-O bond (1.7 Å). Our MCSCF structural parameters are close to those found at the MP2/6-31+G(d) level by Arnold and Neumark[2] . This isomer is about 48.5 kcal/mol higher in energy than 2 NO at the highest, CASPT2(14,12)/6-31+G(2d), level of theory (Figure 11).

The dissociation reaction **4** -> 2 NO was studied at the MCSCF(14,12)/6-31G(d) level of theory. The corresponding reaction path is shown in Figure 12, along with single point CASPT2 energies for both the lowest singlet and triplet states obtained at several selected points on the MCSCF(14,12) IRC path. The transition state for this process is shown in Figure 11. Its structure shows that the first stage of the dissociation process involves transfer of the (single bond) oxygen atom from one nitrogen atom to another. This requires only a small amount of energy, resulting in a barrier height of about 7 kcal/mol (CASPT2). The MCSCF active orbitals at the transition state structure are shown in Figure 13. During the second part of this reaction, the N-N bond breaks, with the π (N-N) and π^*(N-N) orbitals (3 a" and 4 a") rearranging into two singly occupied π^* (N-O) orbitals of the dissociation products (Figure 14).

The triplet (^{3}A") state is higher in energy than the singlet in the region of the minimum and transition state, and becomes close to the singlet state in the product (2 NO) part of the reaction (Figure 12). The small barrier for this reaction suggests that structure **4** may be stable only at low temperatures. On the other hand, this isomer has the lowest barrier

for the reverse reaction, 2 NO → isomer **4**, and may be responsible for the enhanced vibrational relaxation observed by Wodtke and coworkers[1] for excitation energies above vibrational quantum number $\upsilon \approx 12$. The barrier height is about 56 kcal/mol (2.4 eV), which is in the region where vibrational relaxation accelerates[1]. Two NO molecules at large separation, with one in its ground vibrational state and the other with the N-O bond stretched to 1.55 Å (corresponding to $\upsilon \approx 15$), have an energy that is about 4 kcal/mol above the 2NO → **4** reaction barrier height. This supports the suggestion made in reference 1 that the trajectory for collision NO($\upsilon = 0$) + NO($\upsilon \geq 12$) may pass near the transition state for formation of isomer **4** or other high energy isomers.

Conclusion

Dissociation and isomerisation reactions were studied for four high energy isomers of N_2O_2 in order to determine their kinetic stability. The isomers included the 4-membered ring D_{2h} isomer (**1**), the planar C_{2v} isomer (**2**), the bicyclic C_{2v} isomer (**3**), and the planar C_s isomer (**4**) shown in Figure 1. Minimum energy reaction paths have been determined using IRC techniques and MCSCF(10,10) and MCSCF(14,12) wavefunctions. Potential energy barriers separating the isomers from 2 NO products and approximate minimum energy crossing points between closest singlet and triplet states were determined. The energetics for these reactions were calculated using second order perturbation theory based on MCSCF wavefunctions (CASPT2).

We predict that isomers **1** and **2** may be kinetically stable with respect to dissociation to two NO molecules: the predicted barrier heights to dissociation are about 40 kcal/mol for the D_{2h} isomer, and about 20 kcal/mol for the planar C_{2v} ring. Low-lying triplet states are found to cross the singlet potential energy surfaces along the reaction paths for these two isomers, but these crossings occur in regions that are far enough from the positions of the minima that they are unlikely to destroy the stability of these isomers.

The bicyclic isomer **3** is found to isomerize to isomer **4** via a barrier of about 19 kcal/mol. In turn, the isomer **4** dissociates to 2 NO via a small barrier of about 7 kcal/mol and is probably unstable.

We suggest that isomers **1**, **2**, and **3** may be good candidates for high energy systems, and that experimental attempts should be made to synthesize them.

Acknowledgments

This work was supported by the Air Force Office of Scientific Research (grant F49620-95-1-0077). The calculations were performed in part on the IBM SP2 at the Maui Supercomputer Center, in part on a local eight node SP2 obtained with funds provided by the National Science Foundation, the Air Force Office of Scientific Research, and Iowa State University, and in part on IBM and DEC workstations provided by the same funding sources. The authors thank Professor A. Wodtke for useful suggestions regarding the manuscript.

References

1. (a) Yang, X.; Kim, E. H.; Wodtke, A. M. *J. Chem. Phys.* **1992**, *96*, 5111; (b) Yang, X.; Price, J. M.; Mack, J. A.; Morgan, C. G.; Rogaski, C. A.; McGuire, D.; Kim, E. H.; Wodtke, A. M. *J. Phys. Chem.* **1993**, *97*, 3944.
2. Arnold, D. W.; Neumark, D. M. *J. Chem. Phys.* **1995**, *102*, 7035.
3. Michels, H. H.; Montgomery, J. A. *J. Chem. Phys.* **1988**, *88*, 7248.
4. Nguyen, K. A.; Gordon, M. S.; Montgomery, J. A.; Michels, H. H. *J. Phys. Chem.* **1994**, *98*, 10072.
5. Nguyen, K. A.; Gordon, M. S.; Montgomery, J. A.; Michels, H. H.; Yarkony, D. R. *J. Chem. Phys.* **1994**, *98*, 3845.
6. Nguyen, K. A. ; Gordon, M. S.; Boatz, J. A. *J. Am. Chem. Soc.*, **1994**, *116*, 9241.

7. (a) Yarkony, D. R. *J. Am. Chem. Soc.* **1992**, 114, 5406; (b) Yarkony, D. R. *J. Chem. Phys.* **1990**, 92, 2457.

8. (a) Ruedenberg, K.; Schmidt, M. W.; Gilbert, M. M.; Elbert, S. T. *Chem. Phys.***1982**, *71*, 41; (b) Lam, B.; Schmidt, M. W.; Ruedenberg, K. *J. Chem. Phys.* **1985**, *89*, 2221.

9. (a) Gonzalez, C.; Schlegel, H. B. *J.Chem.Phys.* **1989**, 90, 2154; (b) *J.Phys.Chem.* **1990**, 94, 5523; (c) *J.Chem.Phys.* **1991**, 95, 5853.

10. Hehre, W. J.; Ditchfield, R.; Pople, J. A. *J. Chem. Phys.* **1972,** *56*, 2257.

11. Schmidt, M. W.; Baldridge, K. K.; Boatz, J. A.; Elbert, S. T.; Gordon, M. S.; Jensen, J. H.; Koseki, S.; Matsunaga, N.; Nguyen, K. A.; Su, S.; Windus, T. L.; Dupuis, M.; Montgomery, J. A. *J. Comp. Chem.* **1993**, 14, 1347.

12. (a) Anderson, K.; Malmqvist, P.-Å.; Roos, B. O. *J. Chem. Phys.* **1992**, 96, 1218; (b) Anderson, K. Malmqvist, P.-Å., Roos, B. O. *J. Phys. Chem.* **1990**, 94, 5483.

13. (a) Hariharan, P. C.; Pople, J. A., *Theor. Chim. Acta*, **1973**, 28, 213; (b) Krishnan, R.; Binkley, J. S.; Seeger, R.; Pople. J. A. *J. Chem. Phys.* **1980,** 72, 650; (c) Frisch, M. J.; Pople, J. A.; Binkley, J. S. *J. Chem. Phys.* **1984**, 80, 3265.

14. Anderson, K.; Blomberg M. R. A.; Fülscher, M. P.; Kellö, V.; Lindh, R.; Malmqvist, P.-Å.; Noga, J.; Olsen, J.; Roos, B. O.; Sadlej, A. J.; Siegbahn, P. E. M.; Urban, M.; Widmark, P.-O. MOLCAS version 3, University of Lund, Sweden, 1994.

15. Chaban G. M.; Klimenko N. M.; Charkin O. P. In *Structure and Properties of Molecules.* Transactions of Ivanovo Institute of Chemical Technology. Ivanovo, **1988**, 20-31.

1. D_{2h}

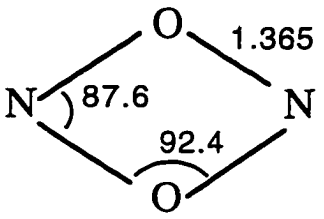

2. C_{2v}

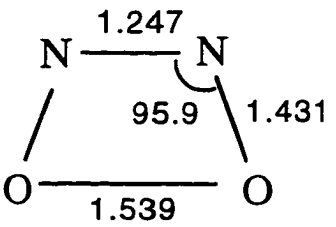

3. C_{2v}

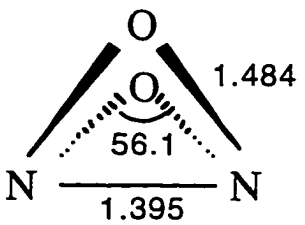

4. C_s

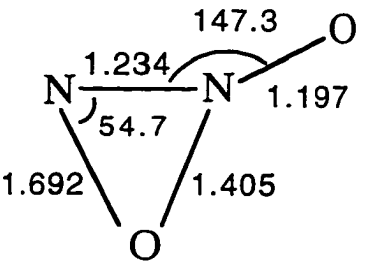

Figure 1. MCSCF(10,10)/6-31G(d) geometric parameters (bond lengths in Å, angles in degrees) for N_2O_2 high energy isomers.

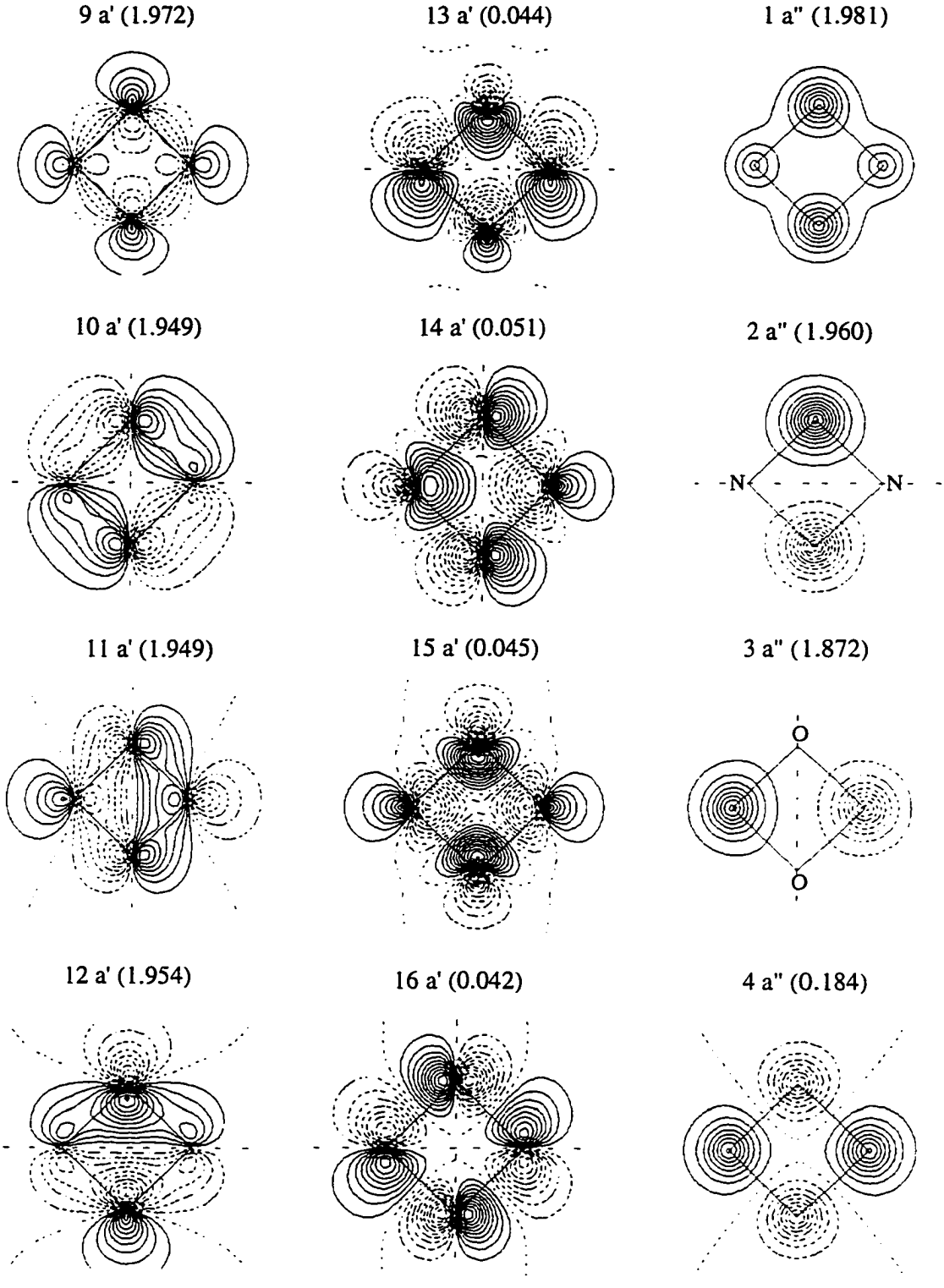

Figure 2. MCSCF(14,12)/6-31G(d) natural orbitals for isomer **1**. a' orbitals are given in the x-y plane, a" orbitals are given in the plane shifted by 0.2 Å parallel to the x-y plane.

	minimum	transition state	dissociation products
	D2h 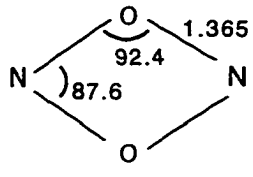	Cs 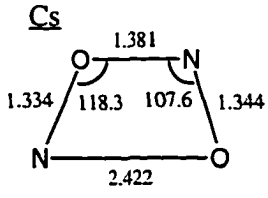	2 NO
MCSCF(10,10)/6-31G(d) geometries, Å, deg.			
Relative energies, kcal/mol			
MCSCF(10,10)/6-31G(d)	**0.0**	**50.9**	**-71.0**
CASPT2(10,10)/6-31G(d)	**0.0**	**54.3**	**-49.0**
CASPT2(10,10)/6-311+G(2d)	**0.0**	**52.2**	**-48.7**
	D2h 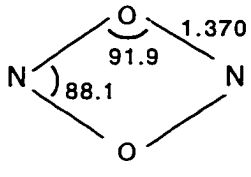	Cs 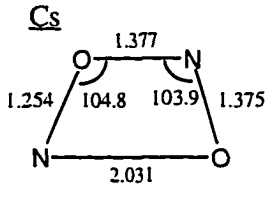	2 NO
MCSCF(14,12)/6-31G(d) geometries, Å, deg.			
Relative energies, kcal/mol			
MCSCF(14,12)/6-31G(d)	**0.0**	**47.5**	**-68.7**
CASPT2(14,12)/6-31G(d)	**0.0**	**41.5**	**-48.4**
CASPT2(14,12)/6-311+G(2d)	**0.0**	**39.4**	**-49.8**

Figure 3. Structure and energetics for the D_{2h} cyclic isomer (**1**) and the transition state for its decomposition to two NO molecules.

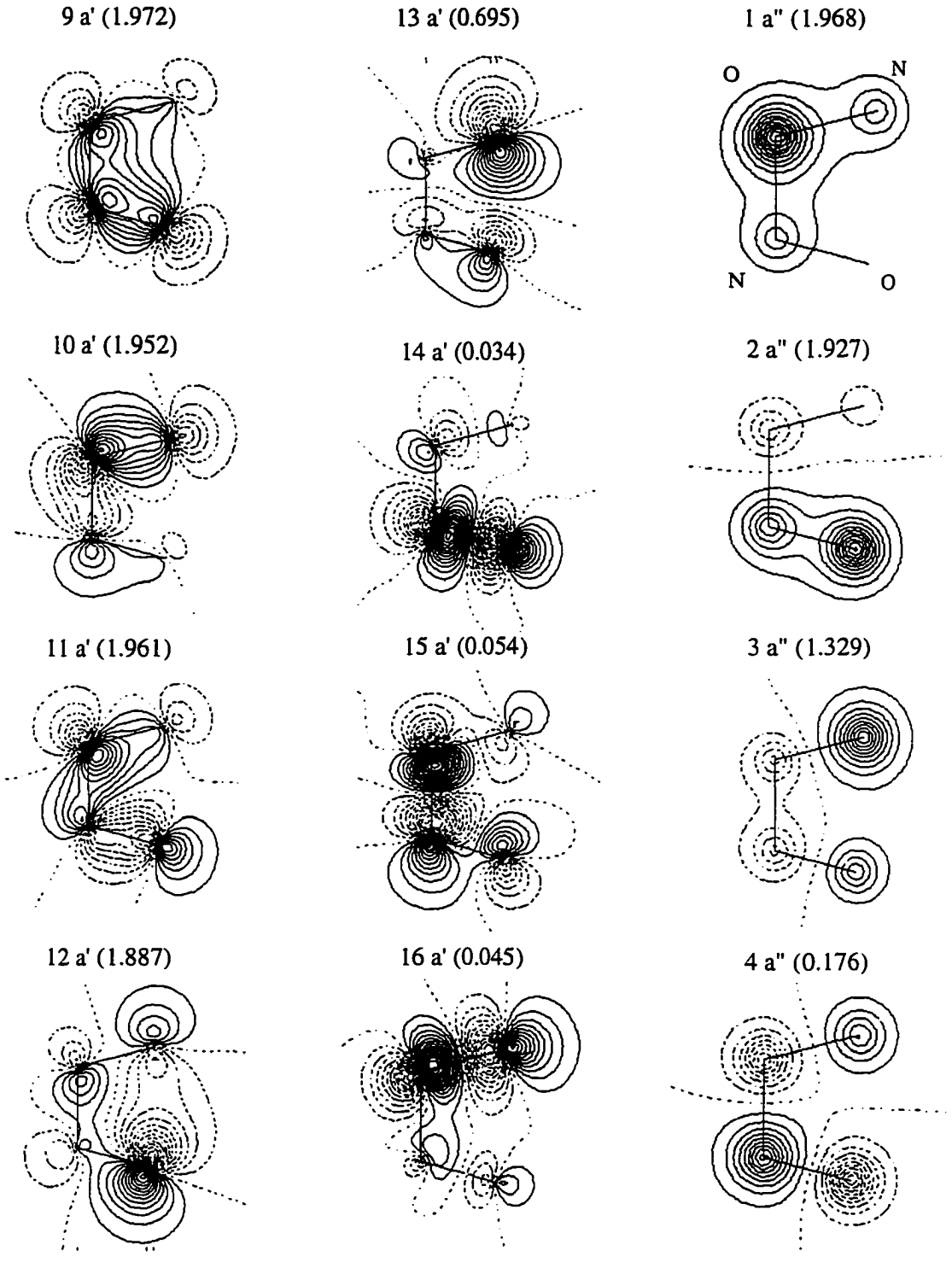

Figure 4. MCSCF(14,12)/6-31G(d) natural orbitals for the transition state for dissociation of isomer **1**. a' orbitals are given in the x-y plane, a" orbitals are given in the plane shifted by 0.2 Å parallel to the x-y plane.

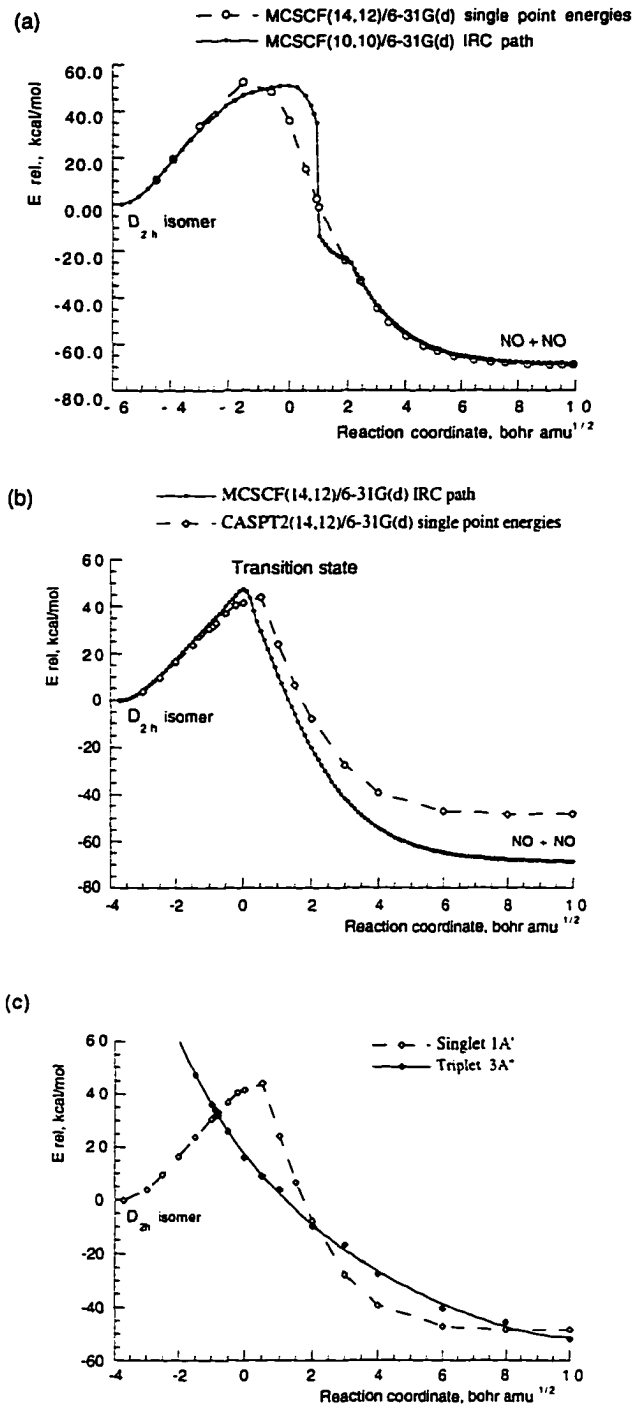

Figure 5. Reaction path for decomposition of D_{2h} isomer (**1**) to 2 NO:
a) MCSCF(10,10)/6-31G(d) IRC path and MCSCF(14,12)/6-31G(d) single point energies (open circles); b) MCSCF(14,12)/6-31G(d) reaction path and CASPT2(14,12)/6-31G(d) single point energies; c) CASPT2(14,12)/6-31G(d) energies for singlet (^{1}A') and triplet (^{3}A") states along the dissociation reaction path.

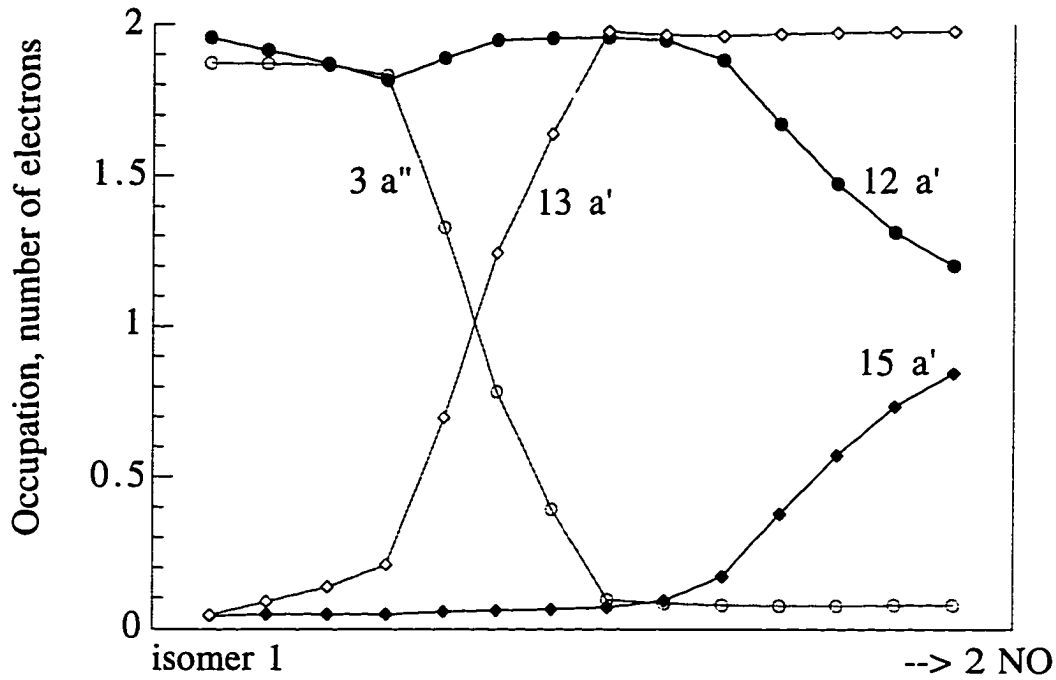

Figure 6. MCSCF(14,12) natural orbital occupation numbers along the dissociation isomer **1** $\rightarrow$ 2 NO.

	minimum	transition state	dissociation products
	C_{2v}	C_1	
MCSCF(10,10)/6-31G(d) geometries, Å, deg.	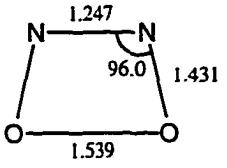	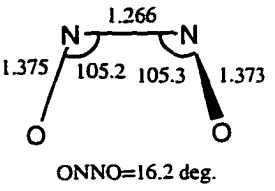 ONNO=16.2 deg.	2 NO
E rel. kcal/mol			
MCSCF(10,10)/6-31G(d)	**0.0**	**19.8**	**-41.6**
CASPT2(10,10)/6-31G(d)	**0.0**	**19.6**	**-47.7**
MCSCF(10,10)/6-311+G(2d)	**0.0**	**20.2**	**-47.0**
CASPT2(10,10)/6-311+G(2d)	**0.0**	**20.5**	**-53.1**
	C_{2v}	C_1	
MCSCF(14,12)/6-31G(d) geometries, Å, deg.	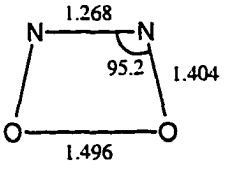	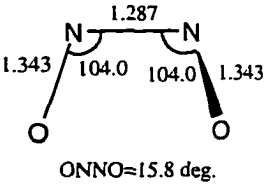 ONNO=15.8 deg.	2 NO
E rel. kcal/mol			
MCSCF(14,12)/6-31G(d)	**0.0**	**22.6**	**-62.3**
CASPT2(14,12)/6-31G(d)	**0.0**	**18.7**	**-44.2**
MCSCF(14,12)/6-311+G(2d)	**0.0**	**22.5**	**-60.6**
CASPT2(14,12)/6-311+G(2d)	**0.0**	**18.7**	**-44.9**

Figure 7. Structure and energetics for C_{2v} planar isomer (**2**) and the transition state for its decomposition to two NO molecules.

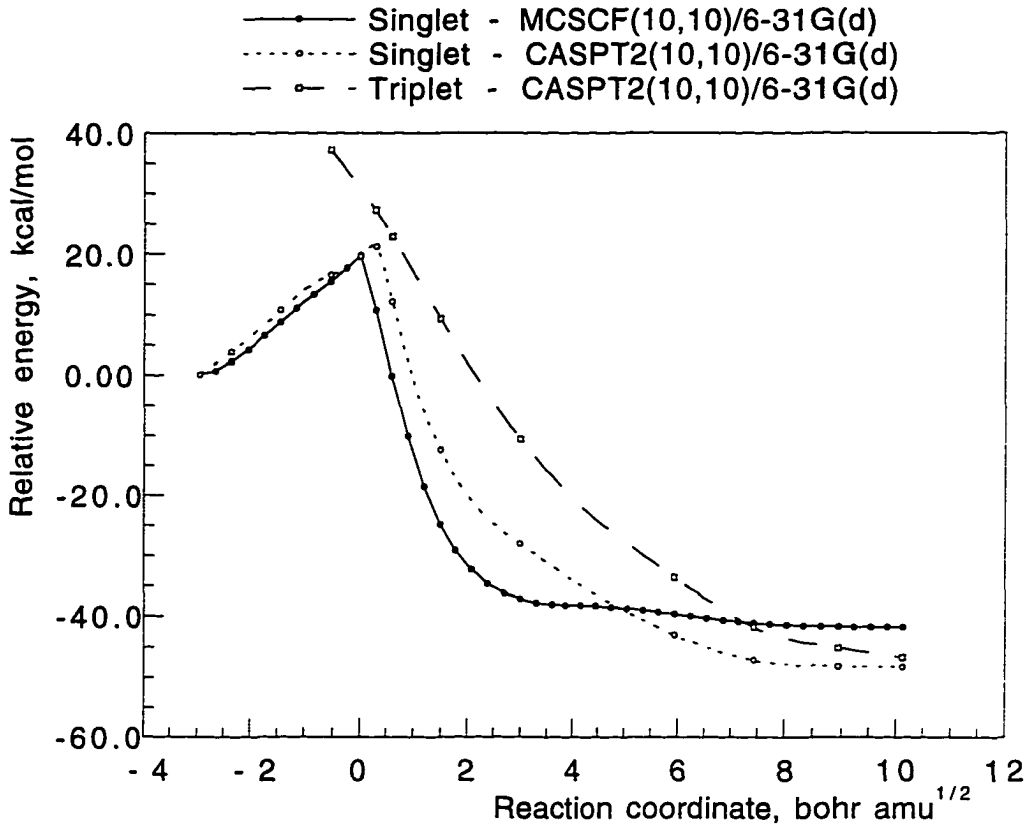

Figure 8. MCSCF(10,10)/6-31G(d) reaction path for decomposition of C_{2v} isomer (**2**) to two NO molecules.

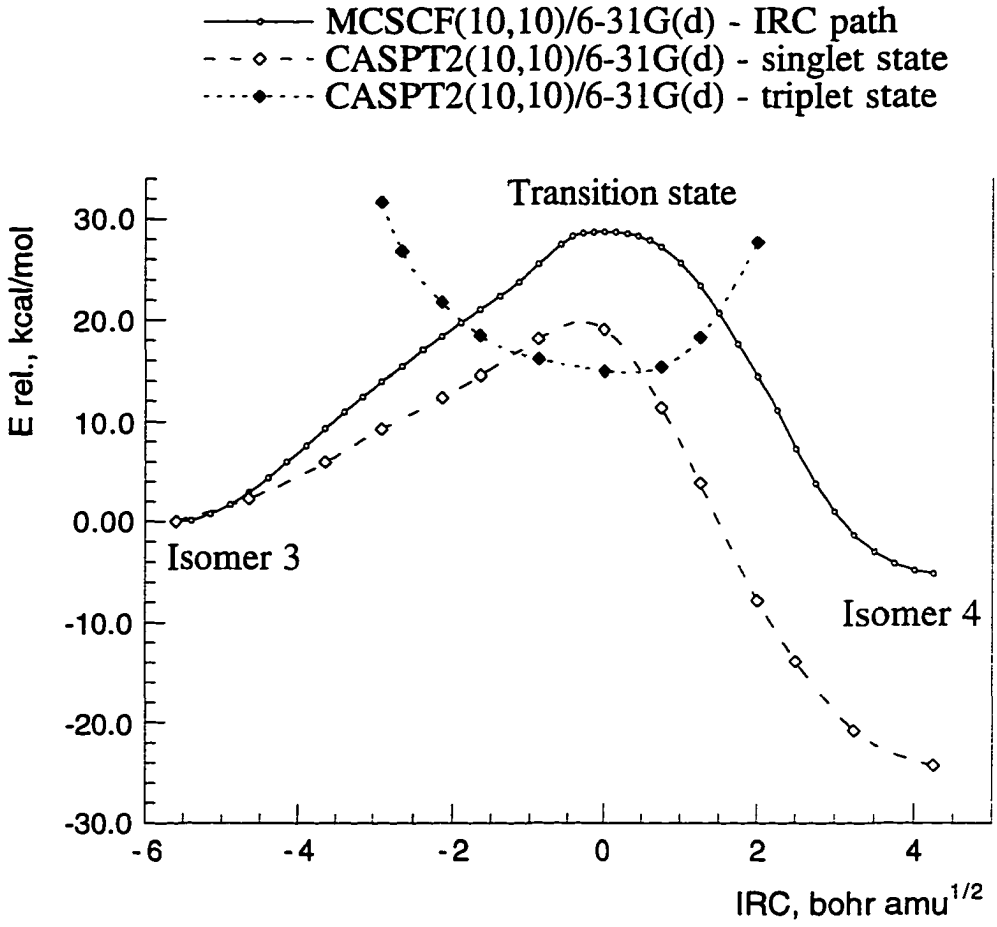

Figure 9. MCSCF(10,10)/6-31G(d) reaction path for isomerisation **3** -> **4**.

	Isomer 3	Transition state	Isomer 4
	C_{2v}	C_1	C_s
MCSCF(10,10)/6-31G(d) geometries (Å, deg)	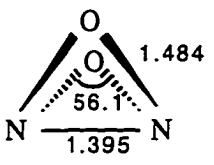 D(ONNO)=107 deg.	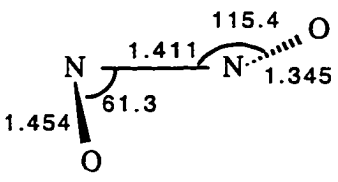	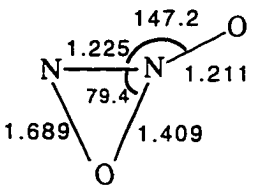
Relative energies (kcal/mol)			
MCSCF(10,10)/6-31G(d)	**0.0**	**28.7**	**-5.2**
CASPT2(10,10)/6-31G(d)	**0.0**	**19.0**	**-24.3**
MCSCF(10,10)/6-311G+(2d)	**0.0**	**31.9**	**-4.8**
CASPT2(10,10)/6-311G+(2d)	**0.0**	**19.5**	**-26.2**

Figure 10. MCSCF(10,10)/6-31G(d) geometries and relative energies for the N_2O_2 isomers **3** and **4**, and the transition state for **3** -> **4** isomerisation.

	Isomer 4	Transition state	Dissociation products
	Cs	Cs	
MCSCF(14,12)/6-31G(d) geometries (Å, deg)	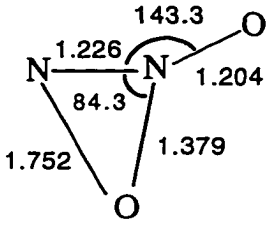	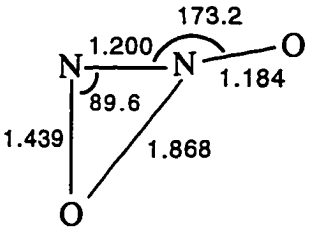	2 NO
Relative energies (kcal/mol)			
MCSCF(14,12)/6-31G(d)	**0.0**	**12.3**	**-80.7**
CASPT2(14,12)/6-31G(d)	**0.0**	**7.8**	**-51.8**
CASPT2(14,12)/6-311G+(2d)	**0.0**	**7.3**	**-48.5**

Figure 11. MCSCF(14,12)/6-31G(d) structure and relative energies for the isomer **4** and the transition state for its dissociation to 2 NO.

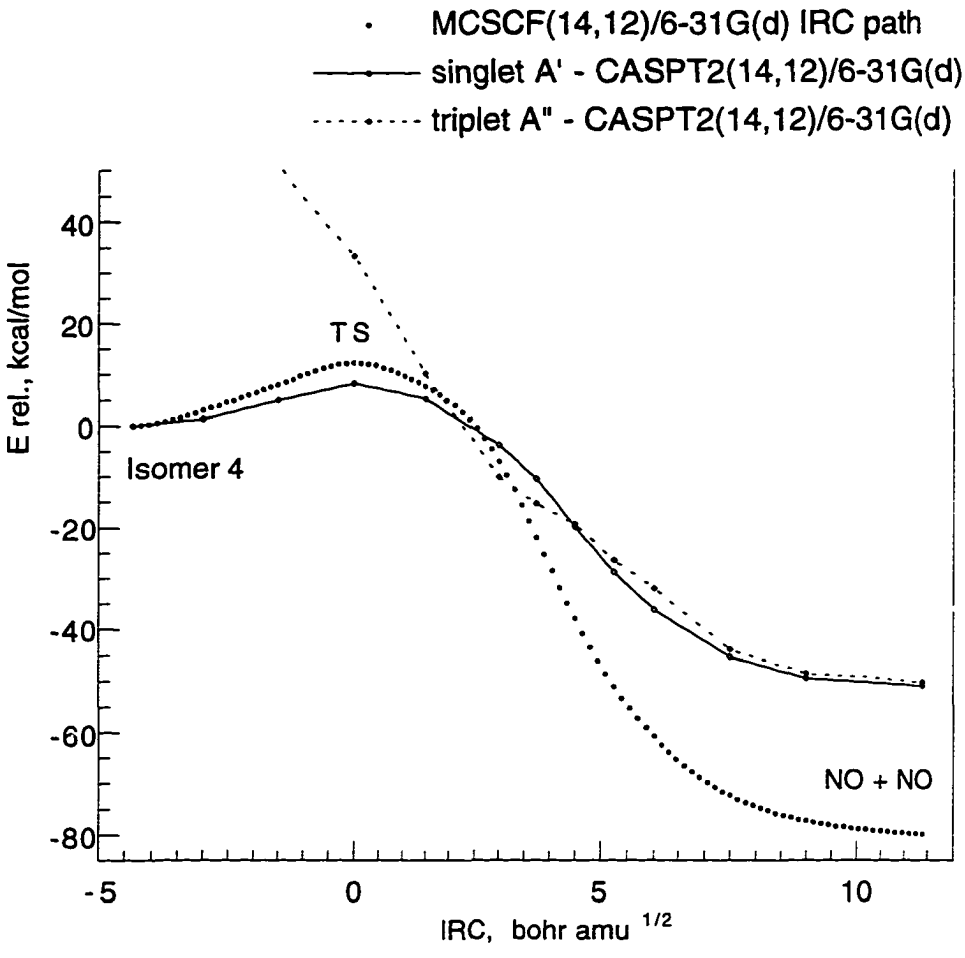

Figure 12. MCSCF(14,12)/6-31G(d) reaction path for decomposition of isomer **4** to two NO molecules.

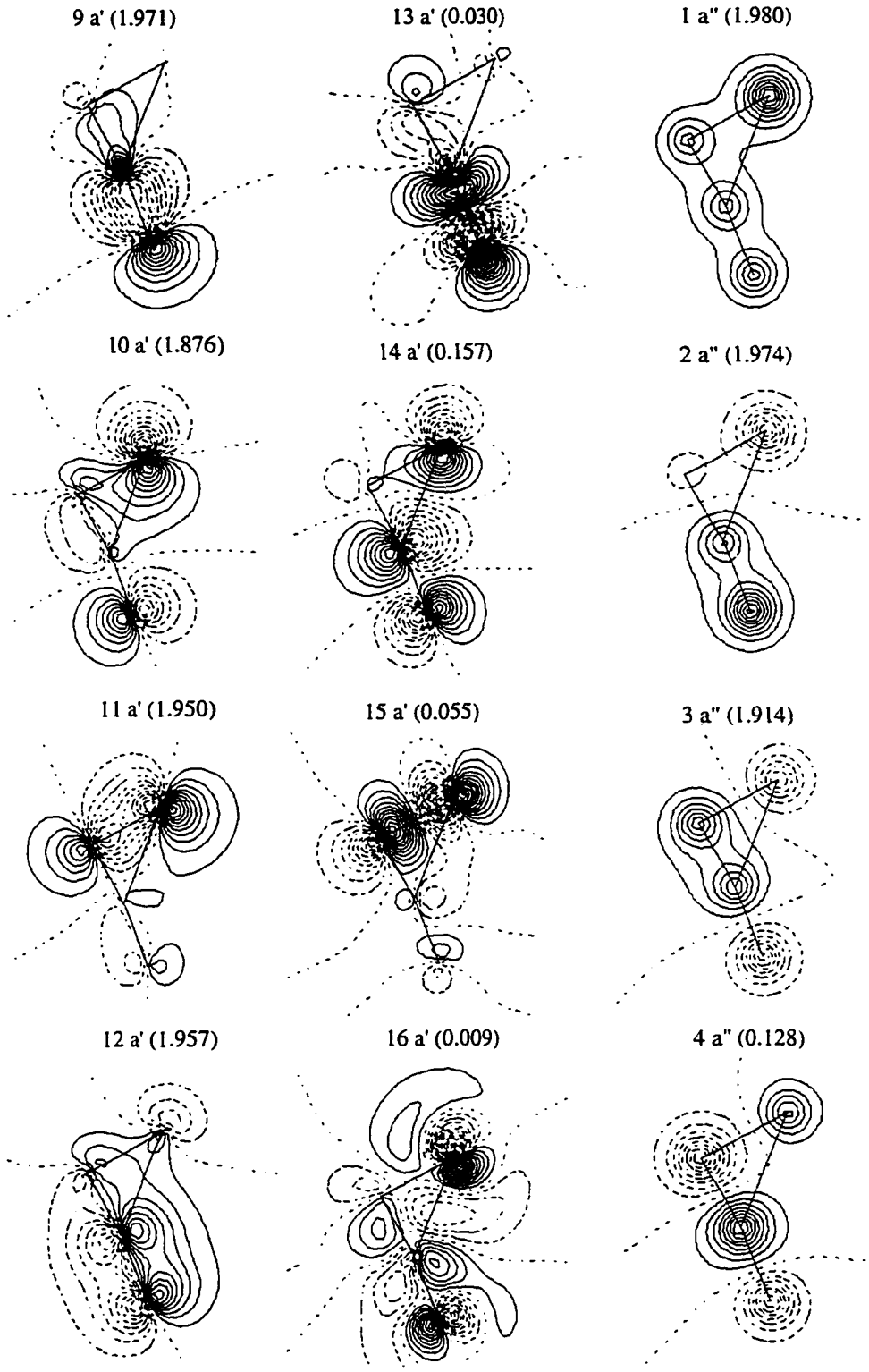

Figure 13. MCSCF(14,12)/6-31G(d) natural orbitals for the transition state for dissociation of isomer **4**. a' orbitals are given in the x-y plane; a" orbitals are given in the plane shifted by 0.2 Å parallel to the x-y plane.

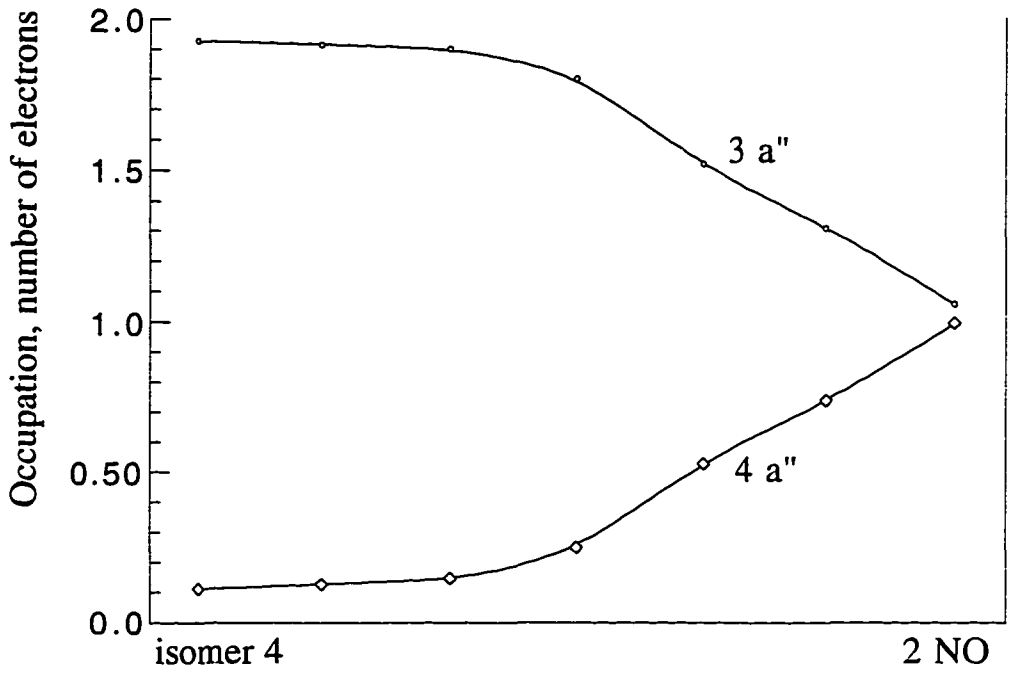

Figure 14. MCSCF(14,12) natural orbital occupation numbers along the dissociation **4** → 2 NO.

CHAPTER 5. THE STRUCTURE AND STABILITY OF M-H_2 COMPLEXES

A paper published in *Journal of Physical Chemistry*

Galina Chaban and Mark S. Gordon

Abstract

The potential stability of Van der Waals complexes M-H_2 (M = Li, Be, B, C, Na, Mg, Al, Si) is assessed using quadratic configuration interaction and large basis sets. It is found that the alkali metals and alkaline earths form very weak complexes in their ground states, but much stronger complexes in their (p) excited states. The elements B, Al, C, Si form both linear ($C_{\infty v}$) and perpendicular (C_{2v}) complexes, with greater thermodynamic stability in the latter arrangements. The complexes formed by C are likely to be kinetically unstable, and the same may be the case for Si. On the other hand, the complexes formed by B and Al are predicted to be quite stable.

Introduction

The structure and energetics of Van der Waals complexes between metal atoms and molecular hydrogen are of considerable current theoretical and practical interest. There is, for example, currently considerable interest[1] in doping solid hydrogen with a small amount (<5%) of light metal atoms, since many of the lighter metals react more exothemally with oxygen than does hydrogen. The key is to determine if these metals can form weakly bound (e.g., Van der Waals) species, so that oxidation does not have to overcome the binding energy of stronger M-H bonds (presumably, the amount of metal present would be small enough that M-M bonds would not be a consideration). This means that if a Van der Waals species exists, to be useful it must be separated from any lower energy hydride by a substantial barrier, and there must not

be an intersystem crossing that effectively lowers or even destroys the barrier.

In addition to the foregoing, it is also of interest from a purely academic perspective to understand the nature and the strength of weak metal-hydrogen interactions. Because these interactions are so weak, such predictions are challenging and require highly correlated wavefunctions with extended basis sets.

The most interesting metals M, based on the heats of formation of their corresponding oxides, appear to be Li, Be, B, C, Na, Mg, Al, Si. Therefore, in this work we have carried out a preliminary study of the potential energy surfaces that connect the separated species M + H_2, potential Van der Waals species, and the much more stable hydrides, in order to determine barrier heights on the adiabatic surfaces and to identify state crossings that might lead to unwanted nonadiabatic couplings. In addition, the binding energies for the Van der Waals complexes are estimated.

The Li-H_2 system has been of particular interest because of the low mass of Li. Both the ground and exited states have been studied previously [2-7]. Hobza and Schleyer [3] studied Li - H_2 at the MP2/6-311G (2d,2p) level of theory and found a weakly bound complex ($\sim$ 7 cm^{-1} binding energy) for the ground state linear configuration and a much stronger complex (16.4 kcal/mol) for the excited state ($^2B_2$). Konowalow found the linear Van der Waals complex to have a dissociation energy (D_e) between 13 and 18 cm^{-1} using the interacting correlated fragments (ICF) method and large basis sets [5]. Potential energy surfaces of Li-H_2 ground and lowest exited electronic states, including crossing regions, have been studied with MCSCF wavefunctions and rather small basis states (4-31G*) [6-7]. A minimum with D_e about 10 kcal/mol was found on the $^2B_2$ surface, and the transition from $^2B_2$ to $^2A_1$ was predicted to occur with high probability. Potential energy surfaces have also been studied for Na-H_2 [8-10], Be-H_2 [11-13], and Mg-H_2 [13-15] excited states. Augspurger and Dykstra found Van der Waals complexes for Mg-H_2 and Mg-HF ground states using the coupled cluster method and triple-zeta quality basis sets[16]. The B-H_2 potential surface has been studied

extensively by Alexander [17], who found the B---H_2 complex to be stable kinetically. On the contrary, a practically negligible barrier was found for the C+H_2 reaction [18-20].

In this paper we report preliminary results for M-H_2 complexes with M = Li, Be, B, C, Na, Mg, Al, and Si in their ground and some excited states, in order to determine the nature of their potential energy surfaces. This will provide some insight regarding the thermodynamic and kinetic stability of these species. The potential energy surfaces of those compounds found to be kinetically stable will be examined later in more detail.

Method of calculation

The calculations were carried out using the quadratic configuration interaction method QCISD(T) [21]. Fourth order perturbation theory (MP4SDQ) [22] was used for some large complexes that contain 4-6 H_2 molecules. The basis sets used were correlation consistent valence-triple-zeta (cc-pVTZ) [23] for Li, Be, Na, and Mg and augmented aug-cc-pVTZ [24-26] for the other metal atoms and hydrogen.

This computational method was tested for Li--H_2 and B--H_2 complexes, since these species have been calculated previously using multi-reference configuration interaction (MRCI) methods and large basis sets [5,17]. The comparison of our QCISD(T) and MP4SDQ results with those of Konowalow for LiH_2 [5] and Alexander for BH_2 [17] are presented in Table 1. For the equilibrium geometry of the B--H_2 complex, found by Alexander [17] (R_{B-H2}=3.11Å, r_{H-H}=0.742Å), the dissociation energy is 128 cm^{-1} at the QCISD(T)/ aug-cc-pVTZ level of theory as compared with 121 cm^{-1} obtained with MRCI(D)/aug-cc-pVTZ [17]. Dissociation energies for Li--H_2 complexes are also in a good agreement with Ref. 5: 15 vs 17 cm^{-1} for the linear complex and 9 vs 11 cm^{-1} for perpendicular one. (The perpendicular structure, however, is found to be a transition state on the potential energy surface of Li-H_2 at the QCISD(T) level of theory). It is also seen from Table 1, that MP4SDQ consistently reproduces QCISD(T) results, while QCISD significantly underestimates binding.

The results obtained using different basis sets from pVDZ to pVQZ are shown in Table 1 for B and Al complexes. In general, pVDZ is not an adequate basis set for such calculations, but pVTZ and pVQZ yield very similar results. We used the pVTZ-type of basis set for the rest of our calculations, assuming that it is nearly converged. It was shown previously [27-31] that the augmented correlation consistent pVTZ basis set is converged with respect to basis set superposition errors.

All of the calculations described here were performed using the Gaussian-92 program [32]. Since QCISD(T) analytic gradients are not available, the potential energy surfaces for M--H_2 Van der Waals complexes were studied by calculating grids of single-point energies at different values of M - H_2 and H-H distances. The calculations described in this paper were performed at linear ($C_{\infty v}$) and perpendicular (C_{2v}) geometries only. The structures found to be minima on the potential energy surfaces with restricted symmetry, were verified to be minima or transition states by calculating numerical hessians. The potential energy curves shown in all Figures of this paper were obtained as follows: the M-H_2 distances were fixed at different values and the H-H distances were optimized for each M-H_2 distance, that is, R (M-H_2) was used as an approximation to a reaction coordinate. Note, that the points that appear to be crossing points on these pictures do not correspond to real crossings, since the two states have the same R(M-H_2) distance, but different r (H-H) distances, optimal for each state. The curves shown should not be considered as reaction paths, since R (M-H_2) distance is not always a valid approximation to reaction coordinate.

These curves serve only as an approximate way to show part of the potential surfaces of M - H_2 systems and to give some idea about kinetic stabilities of van der Waals complexes. Positions of minimum energy crossing points between different states are discussed in the following section.

Results and discussion

The calculated geometries of van der Waals complexes and their dissociation energies are shown in Table 2.

1. Complexes of s-elements

According to our calculations, s-elements in their ground states (^2S, Li, Na and ^1S, Be, Mg) form only linear complexes with H_2. The dissociation energies are very small for these complexes. They are similar for Li and Na (about 15 cm^{-1}), and for Be and Mg (about 30 cm^{-1}). The Be and Mg complex energy wells are twice as deep as those for Li and Na and have M-H_2 distances that are shorter by about 1 Å (see Table 2). There are also local minima within C_{2v} symmetry, but they are not stable to bending (breaking C_{2v} symmetry). It is concluded that the C_{2v} complexes correspond to transition states between linear configurations at the level of theory used here. The barrier heights corresponding to these rotations are 6 and 5 cm^{-1} for Li and Na, and 13 and 12 cm^{-1} for Be and Mg complexes.

On the other hand, C_{2v} complexes correspond to minima and are very stable (Table 3) for excited states of these elements (^2P Li,Na and ^3P Be,Mg) due to interactions of occupied p-orbitals with σ^*(H-H). The dissociation energies for $^2B_2$ complexes of Li and Na are 18 and 9 kcal/mol; for $^3B_2$ complexes of Be and Mg the dissociation energies are 20 and 6 kcal/mol at the QCISD(T) level of theory and basis sets used here. However, as shown in Figures 1 and 2, these complexes may be unstable kinetically due to crossings with ground state A_1 surfaces. These crossings suggest that sufficiently strong non-adiabatic coupling between the states could result in pre-dissociation of the excited state complexes.

We have also done calculations on Be $(H_2)_n$ complexes with n=2-4 and found their dissociation energies to change almost additively with the number of H_2 molecules: 33, 65, 99, and 132 cm^{-1} for n=1, 2, 3, and 4 respectively (see Figure 3). Of course, this additivity is likely to be related to symmetry. If species having lower symmetry exist, the binding may vary somewhat for each additional H_2.

2. Complexes of B and Al

As noted above, the MRCI B-H_2 potential energy surface has been studied by Alexander [17]. He found the B--H_2 Van der Waals complex to be stable to insertion of B into H_2. The most stable complex (with D_e=121 cm^{-1}) was found for a perpendicular orientation of the H_2 molecule, with a p-orbital of B parallel to the H-H bond ($^2B_2$ state). Less stable complexes were found on the $^2B_1$ (75 cm^{-1}) and $^2\Sigma$ (68 cm^{-1}) potential energy surfaces. We have recomputed these complexes at the QCISD(T)/aug-pVTZ level to compare them with other complexes (Table 2). The agreement between QCISD(T) and MRCI is excellent for the $^2B_2$ and $^2B_1$ states, but QCISD(T) predicts a D_e of 93 cm^{-1} for the $^2\Sigma$ state, 25 cm^{-1} larger than that predicted by MRCI.

Three complexes were also found for the Al-H_2 system: linear $^2\Sigma$, and perpendicular $^2B_2$ and $^2B_1$. As in the case of the boron complexes, the most stable Al-H_2 complex is found for the $^2B_2$ state (D_e=204 cm^{-1}).

The C_{2v} parts of the B-H_2 and Al-H_2 potential energy surfaces are shown in Figures 4 and 5. The minimum energy crossing between the $^2B_2$ (complex) and $^2A_1$ (ground) states of B-H_2 and Al-H_2, respectively, occurs in a region about 15 and 30 kcal/mol above the dissociation products B + H_2 and Al + H_2 at our level of theory. The geometries of these points (not shown in figure)) are follows: B-H_2: R (B-H_2) = 1.25 Å, r (H-H) = 1.30 Å; Al-H_2: R (Al-H_2) = 1.50 Å, r (H-H) = 1.66 Å . The actual barriers for these reactions may occur in C_s symmetry. Then, they could correspond to avoided crossings and may be lower than the C_{2v} crossing points. The Al-H_2 potential energy surface, especially in the region of the crossing, will be analyzed in greater detail in the future using multiconfigurational wavefunctions. However, it is clear that the barrier to insertion of Al into H_2 is sufficient for the complex to be kinetically stable. The transition state on the $^2A_1$ surface, which separates the $^2A_1$ complex and the AlH_2 compound, is much higher in energy than the position of $^2B_2$ - $^2A_1$ crossing (about 76 kcal/mol above Al + H_2) , since the complex and the hydride have

different electronic configurations. In the case of BH_2 Alexander has found this barrier to be about 55 kcal/mol high. For both B and Al the insertion into the H-H bond is more likely to occur through the $^2B_2$ - $^2A_1$ crossing rather than via the very high $^2A_1$ transition state.

The structures and stabilization energies for several Al-(H_2)n complexes with n = 1-4 are shown in Figure 6 . Again, the addition of H_2 molecules increases the stability of the complex in an almost additive manner.

3. Complexes of C and Si

C (^3P) + H_2 potential energy surfaces were studied previously [18-20] at the CI level of theory with basis sets varying from minimal [18] to DZ[19-20]. It was found that within C_{2v} symmetry the $^3A_2$ state has a minimum corresponding to a Van der Waals complex, and that the $^3B_1$ state (corresponding to the CH_2 ground state) crosses $^3A_2$ about 2.5 kcal/mol above the dissociation to C (^3P) + H_2 . The energy of the crossing point depends very much on the basis set: it decreases from 50 kcal/mol for a minimal basis set to 2.5 kcal/mol for the largest DZ basis set used in ref.20. It was found by Harding[20] that relaxation of C_{2v} symmetry to C_s leads to a very slight decrease in energy (about 1 kcal/mol) in the region of the crossing. We recalculated the C_{2v} part of the surface using QCISD(T) with the aug-pVTZ basis set and estimate that the $^3A_2$ and $^3B_1$ minimum energy crossing point (not shown in figure) occurs at 1.5 kcal/mol above the C (^3P) + H_2 dissociation energy. The R (C-H_2) distance corresponding to the crossing point is 1.1 Å, and r(H-H) is 1.28 Å. At this level of theory, the $^3A_2$ surface has a minimum corresponding to a weak Van der Waals complex (with D_e=324 cm^{-1} , R=2.2Å, r=0.75 Å). Then, as R(C-H_2) decreases, the $^3A_2$ potential curve after a very small barrier (10 cm^{-1}) goes down again and has another minimum with R=1.2 Å, r=0.9 Å and a dissociation energy about 5.5 kcal/mol (see Figure 7). This region obviously has to be studied with multi-configurational wavefunctions, but it does not appear that there is a kinetically stable complex in the case of C.

While the C+H_2→ CH_2 reaction goes practically without a barrier, the Si (^3P) + H_2

surface seems to be more promising (Figure 8). There is a Si--H_2 Van der Waals complex on the $^3A_2$ surface which is 2 kcal/mol (720 cm^{-1}) deep, the $^3A_2$ and $^3B_1$ states crossing in a region that is 20 kcal/mol above the Si-H_2 complex. The approximate geometry of the minimum energy crossing point is R (Si-H_2) = 1.4 Å, r (H-H) = 1.67 Å. However, the $^1A_1$ state crosses $^3A_2$ at about 5 kcal above the complex (R (Si-H_2) = 1.6 Å, r (H-H) = 0.94 Å), so these regions of the Si--H_2 potential energy surfaces must be explored in greater detail using multi-reference wavefunctions in order to evaluate the non-adiabatic interactions. No complex is found on the $^1A_1$ surface for either C-H_2 or Si-H_2: the insertion of singlet C and Si to H_2 goes with no barrier at all.

We have also considered the $C_{\infty v}$ approach for both triplet and singlet C and Si. Singlet ($^1\Sigma$) and triplet ($^3\Pi$) complexes with occupied p-orbitals along the molecular axis are found for linear configurations of C-H_2 and Si-H_2. Complexes found for $^1\Delta$ and $^3\Sigma$ states with occupied p-orbitals perpendicular to the molecular axis do not correspond to minima (unstable to bending). Linear complexes are much weaker than perpendicular ones (see Table 2 for dissociation energies and geometries of different complexes).

Conclusions

QCISD(T)/cc-pVTZ calculations have been performed for a series of Van der Waals complexes M--H_2, where M=Li - C and Na - Si. We find that s-elements in their ground states form very weak linear complexes with dissociation energies of about 15 cm^{-1} (Li, Na) and 30 cm^{-1} (Be,Mg). P-elements in their ground states form much stronger complexes due to interactions of the occupied p-orbital with the H_2 molecule. P-elements form complexes with both linear and perpendicular geometries. Perpendicular complexes with the occupied p-orbital parallel to the H-H bond, however, are more stable thermodynamically, and their stability increases from B, Al to C, Si. The thermodynamic stability of perpendicular complexes increases by about a factor of two from first to second row elements, while the stability of

linear complexes remains almost the same. The equilibrium distance M-X (X-midpoint of H-H bond) of complexes decreases upon going from left to right across the periodic table, and is very similar for elements of the same group.

Kinetic stability was studied for C_{2v} complexes, since thermodynamically stable MH_2 compounds with this symmetry exist for M= B, Al, C, Si . Complexes are kinetically stable only if barriers to insertion are high enough. Van der Waals complexes and MH_2 compounds have different electronic states, and the energy of their crossing is the upper limit for the barrier of the reaction, which might occur due to an avoided crossing. B---H_2 and Al---H_2 ($^2B_2$) complexes are found to be kinetically stable. The minimum energy crossing point between $^2B_2$ and $^2A_1$ is estimated to be about 16 and 30 kcal/mol above the corresponding B and Al $^2B_2$ complexes. Complexes of C and Si are probably unstable kinetically (see Figure 7 and 8), although in the case of Si this depends on how strong is the interaction between triplet and singlet states near the crossing region. The regions of these potential surfaces close to surface crossings will be studied more carefully in a later work using multireference wave functions.

Acknowledgements

This work was supported by a grant from the Air Force Office of Scientific Research (F49620-95-1-0077). The calculations reported here were performed using IBM RS6000 workstations generously provided by Iowa State University.

References

1. (a) M.E. Fajardo. *J. Chem. Phys.* **1993**, *98*, 110 ; (b) M.E. Fajardo, S. Tam, T.L. Thompson, M.E. Cordonnier. *Chem. Phys.* **1994**, *189*, 351.
2. A. F. Wagner, A.C. Wahl, A.M. Karo, R.Krejci. *J. Chem. Phys.* **1978**, *69*, 3756.
3. P. Hobza, P.von R. Schleyer. *Chem. Phys. Letters* **1984**, *105*, 830.

4. J. García-Prieto, W. L. Feng, O. Novaro. *Chem. Phys. Letters* **1985**, *119*, 128.

5. D. Konowalow. Private communication. 1991.

6. M. Toyama , T. Uchide , T. Yasuda, T. Kasai, S. Matsumoto. *Bull. Chem. Soc. Jpn.* **1989**, *62*, 2781.

7. S. Matsumoto, K. Mizutani, A. Sekiguchi, T. Yano, M. Toyama. *Int . J. Quant. Chem.* **1986**, *XXIX*, 689.

8. P. Botschwina, W. Meyer, I. V. Hertel, W. Reiland. *J. Chem. Phys.* **1981**, *75*, 5438.

9. D. R. Yarkony. *J. Chem. Phys.* **1986**, *84*, 3206.

10. P. Halvick, D. G. Truhlar. *J. Chem. Phys.* **1992**, *96*, 2895.

11. R. A. Poirier, M. R. Peterson, M. Menzinger. *J. Chem. Phys.* **1983**, *78*, 4592.

12. V. Kellö, A. J. Sadlej. *Theor. Chim. Acta* **1992**, *81*, 417.

13. R. P. Blickensderfer, K. D. Jordan, N. Adams, W. H. Breckenridge. *J. Phys. Chem.* **1982**, *86*, 1930.

14. N. Adams, W. H. Breckenridge, J. Simons. *Chem. Phys.* **1981**, *56*, 327.

15. M. E. Rosenkrantz. *Proceedings of High Energy Density Matter Conference.* April 1992, Lancaster, CA.

16. J. D. Augspurger, C. E. Dykstra. *Chem. Phys. Letters* **1989**, *158*, 399.

17. M. H. Alexander. *J. Chem. Phys.* **1993**, *99*, 6014.

18. R. J. Blint, M.D. Newton. *Chem. Phys. Lett.* **1975**, *32*, 178.

19. M. E. Casida, M. M. L. Chen, R. D. MacGregor, H. F. Schaefer III. *Isr.J. Chem.* **1980**, *19*, 127.

20. L.B. Harding. *J. Phys. Chem.* **1983**, *87*, 441.

21. Pople, J. A.; Head-Gordon, M.; Raghavachari, K. *J. Phys. Chem.* **1987**, *87*, 5968.

22. Krishnan, R.; Frisch, M. J.; Pople, J. A. *J. Chem. Phys.* **1980**, *72*, 4244.

23. D.E.Woon and T.H.Dunning, Jr. (to be published).

24. T.H. Dunning, Jr. *J. Chem. Phys.* **1989**, *90*, 1007.

25. R.A. Kendall, T.H. Dunning, Jr., and R.J. Harrison. *J. Chem. Phys.* **1992**, *96*, 6796.

26. D.E. Woon and T.H. Dunning, Jr. *J. Chem. Phys.* **1993**, *98*, 1358.

27. D. Feller. *J. Chem. Phys.* **1994**, *100*, 4981.

28. S.S. Xantheas. *J. Chem. Phys.* **1993**, *99*, 8774.

29. J.E. Del Bene. *Int. J. Quantum Chem. Sym.* **1992**, *26*, 527.

30. D. Feller. *J. Chem. Phys.* **1992**, *96*, 6104.

31. D. E. Woon. *J. Chem. Phys.* **1994**, *100*, 2838.

32. Gaussian 92, revision C, Frisch, M. J.; Trucks, G. W.; Head-Gordon, M.; Gill, P. M. W.; Wong, M.W.; Foresman, J. B.; Johnson, B. G.; Schlegel, H. B.; Robb, M. A.; Replogle, E.S.; Gomperts, R.; Andres, J. L.; Raghavachari, K.; Binkley, J. S.; Gonzalez, C.; Martin, R. L.; Fox, D. J.; Defrees, D. J.; Baker, J.; Stewart, J. J. P.; and Pople, J. A. Gaussian, Inc., Pittsburgh PA, 1992.

Table 1. Comparison of different methods and basis sets.

M	State	R (M-X[1]), Å	D_e, cm^{-1}	Method
Li	$^2\Sigma$	5.2	13	MP4SDQ/aug-cc-pVTZ
		5.2	13	QCISD/aug-cc-pVTZ
		5.2	15	QCISD(T)/aug-cc-pVTZ
		5.1	17	ICF-CI/CASSCF[2]
B	$^2B_2$	3.1	121	MR-CI(D)/aug-cc-pVTZ[3]
			115	MP4SDQ/aug-cc-pVDZ
			98	QCISD/aug-cc-pVDZ
			119	QCISD(T)/aug-cc-pVDZ
			121	MP4SDQ/aug-cc-pVTZ
			102	QCISD/aug-cc-pVTZ
			128	QCISD(T)/aug-cc-pVTZ
			116	MP4SDQ/cc-pVTZ[4]
			100	QCISD/cc-pVTZ
			127	QCISD(T)/cc-pVTZ
			119	MP4SDQ/cc-pVQZ[4]
			101	QCISD/cc-pVQZ
			130	QCISD(T)/cc-pVQZ
Al	$^2B_2$	3.22	152	QCISD(T)/aug-cc-pVDZ
			204	QCISD(T)/aug-cc-pVTZ
			210	QCISD(T)/aug-cc-pVQZ

1) X - midpoint of H-H bond. r(H-H)=0.742Å.

2) Reference 5.

3) Reference 17.

4) augmented basis set on H atoms.

Table 2. Characteristics of QCISD(T) Van der Waals complexes of M atoms with H_2 molecule.

M	State	R (M-X[1]), Å	D_e [2], cm^{-1}	M	State	R (M-X), Å	D_e, cm^{-1}
Li	$^2\Sigma$	5.21	15	Na	$^2\Sigma$	5.50	13
	$^2A_1$ [3]	5.40	9		$^2A_1$ [3]	5.70	8
Be	$^1\Sigma$	4.21	33	Mg	$^1\Sigma$	4.66	30
	$^1A_1$ [3]	4.35	20		$^1A_1$ [3]	4.80	18
	$B^2\Sigma$	3.87	93	Al	$^2\Sigma$	4.62	89
	$^2B_2$	3.11	130		$^2B_2$	3.25	204
	$^2B_1$	3.33	78		$^2B_1$	3.60	103
C	$^1\Sigma$	3.61	120	Si	$^1\Sigma$	4.25	112
	$^3\Pi$	3.54	81		$^3\Pi$	4.15	84
	$^3A_2$	2.21 [4]	324		$^3A_2$	2.25 [4]	720

1) X - midpoint of H-H bond.

2) With respect to dissociation to M (ground state) + H_2.

3) Transition states between two linear minima.

4) Equilibrium distance r(H-H)=0.75 and 0.76Å for C-H_2 and Si-H_2 $^3A_2$ complexes, and 0.743 Å for other complexes.

Table 3. Complexes of Li, Na, Be, and Mg excited states with H_2 molecule.

M	State	R (M-X[1]), Å	R (H-H), Å	D_e [2]
Li	$^2B_2$	1.66	0.84	18.2 kcal/mol
	$^2B_1$	1.89	0.75	7.3 kcal/mol
	$^2\Sigma$	6.27	0.743	27 cm^{-1}
Na	$^2B_2$	2.14	0.79	9.2 kcal/mol
	$^2B_1$	2.36	0.75	3.8 kcal/mol
	$^2\Sigma$	7.27	0.743	19 cm^{-1}
Be	$^3B_2$	1.36	0.98	20.4 kcal/mol
	$^3B_1$	1.78	0.76	1.9 kcal/mol
	$^3\Sigma$	4.32	0.743	98 cm^{-1}
Mg	$^3B_2$	2.01	0.80	5.6 kcal/mol
	$^3B_1$	2.77	0.743	0.7 kcal/mol
	$^3\Sigma$	5.07	0.743	84 cm^{-1}

1) X - midpoint of H-H bond.

2) With respect to Li, Na (^2P) + H_2 or Be, Mg(^3P) + H_2 .

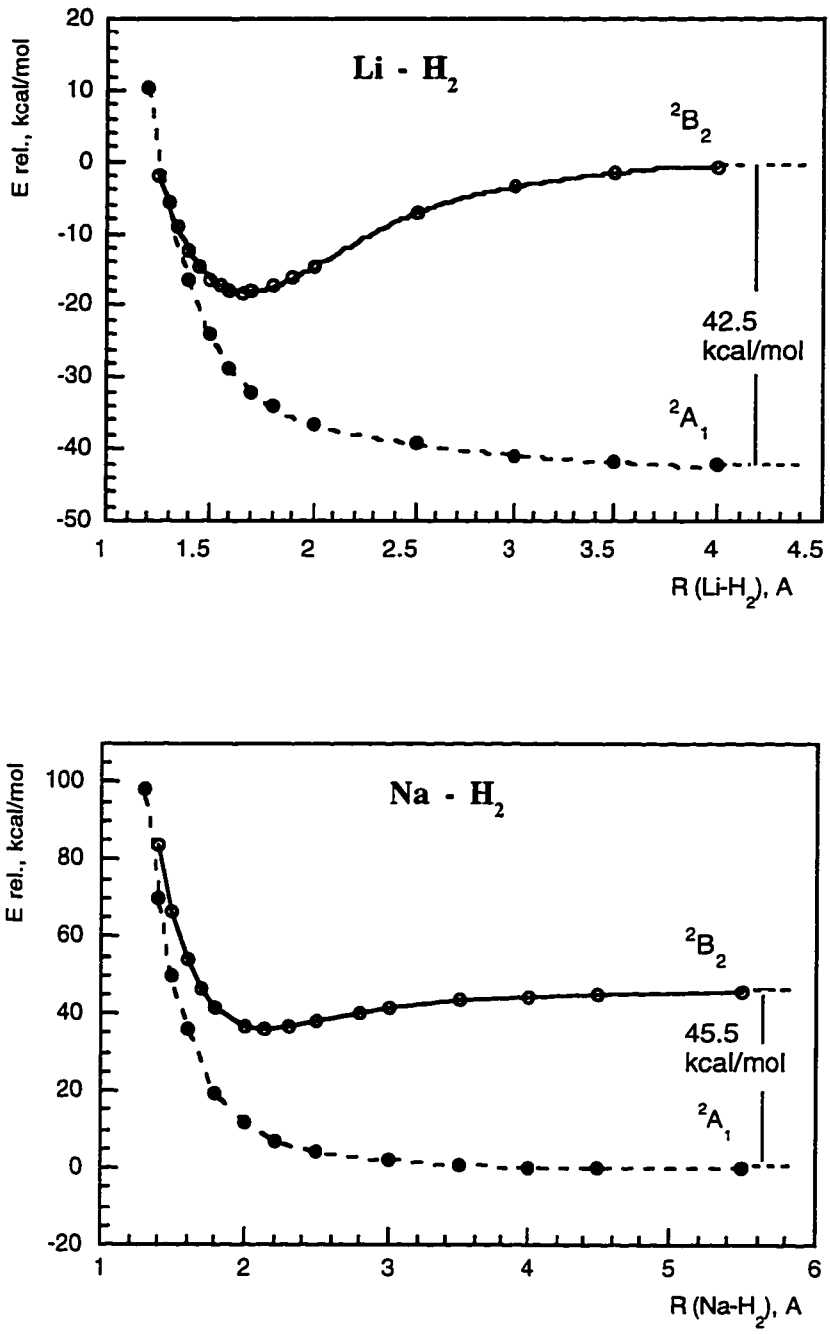

Figure 1. C_{2v} potential energy curves for Li - H_2 and Na - H_2 systems (QCISD(T) / aug-pvtz).

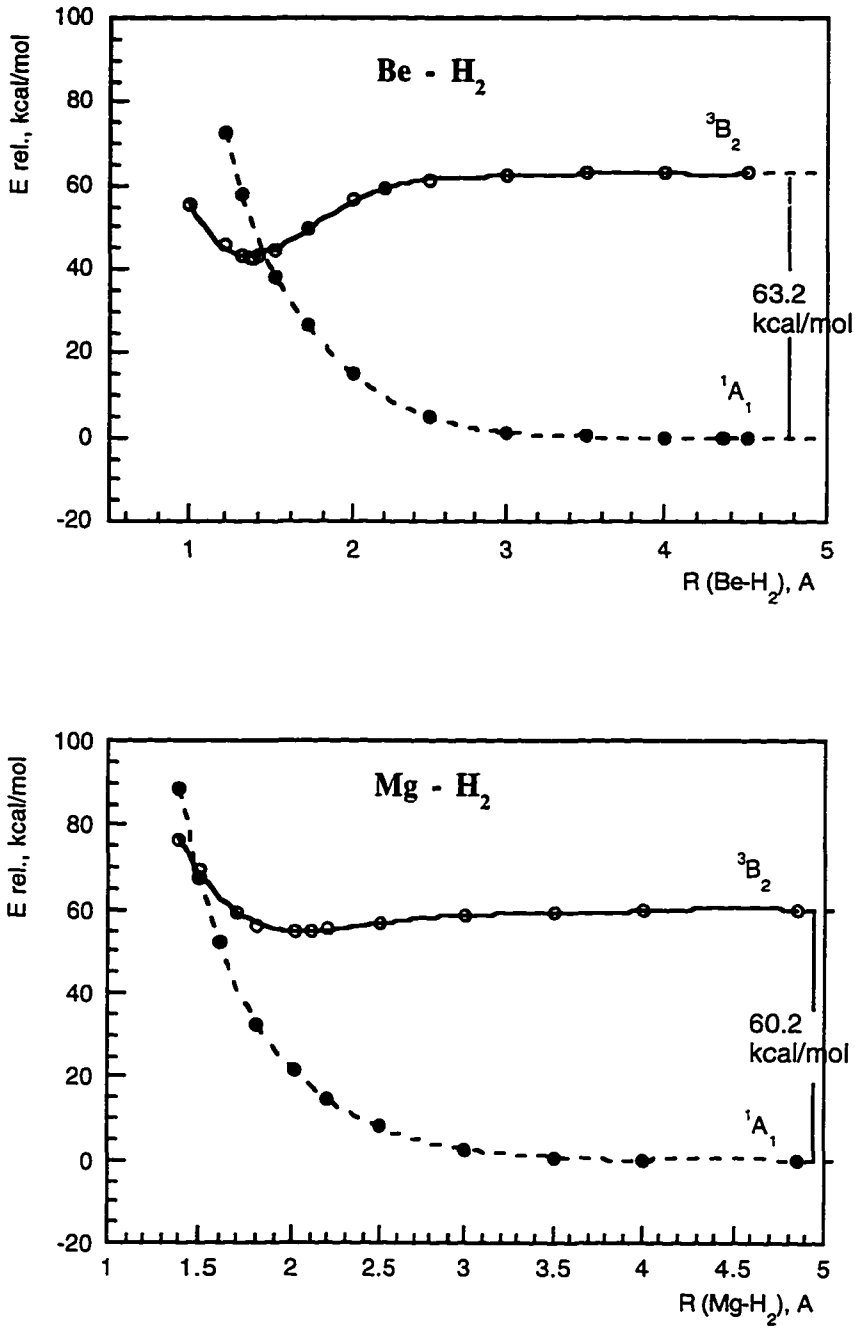

Figure 2. C_{2v} potential energy curves for Be - H_2 and Mg - H_2 systems (QCISD(T)/aug-pvtz).

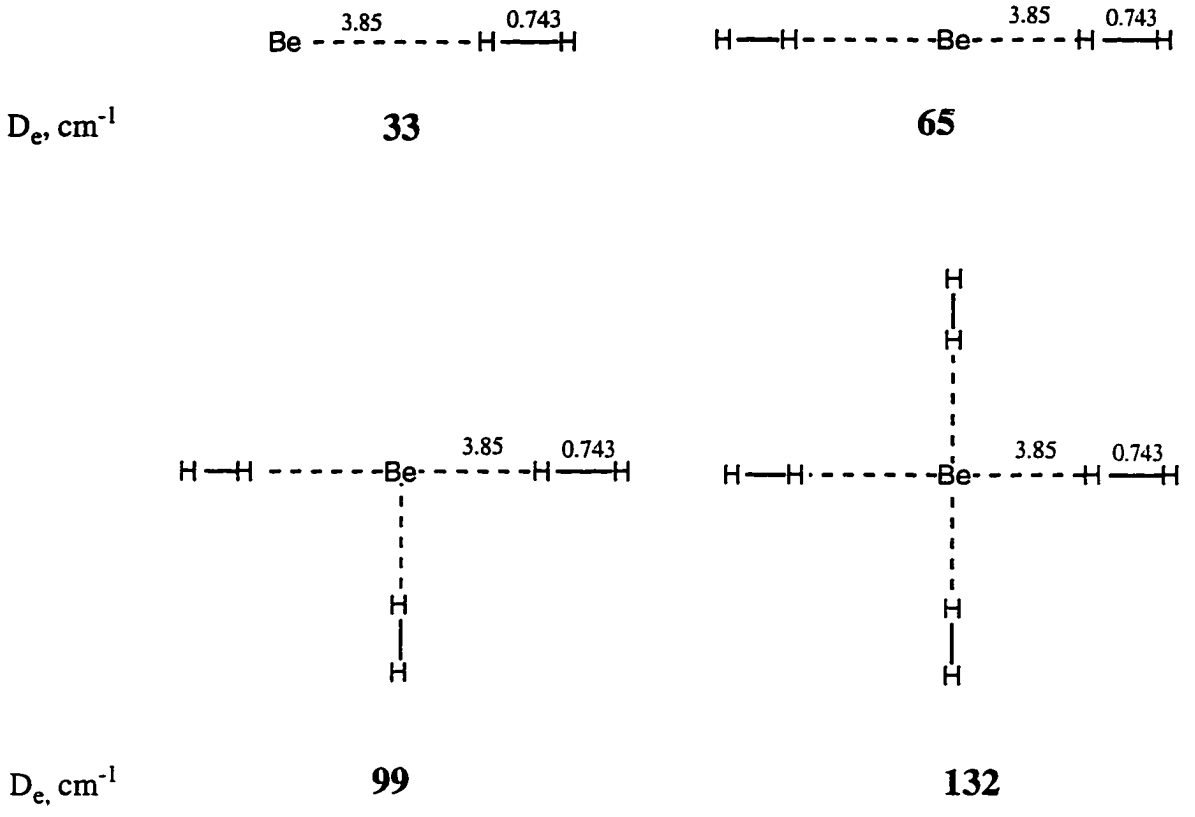

Figure 3. Van-der-Waals complexes of Be with H_2 molecules (QCISD(T)/cc-pVTZ).

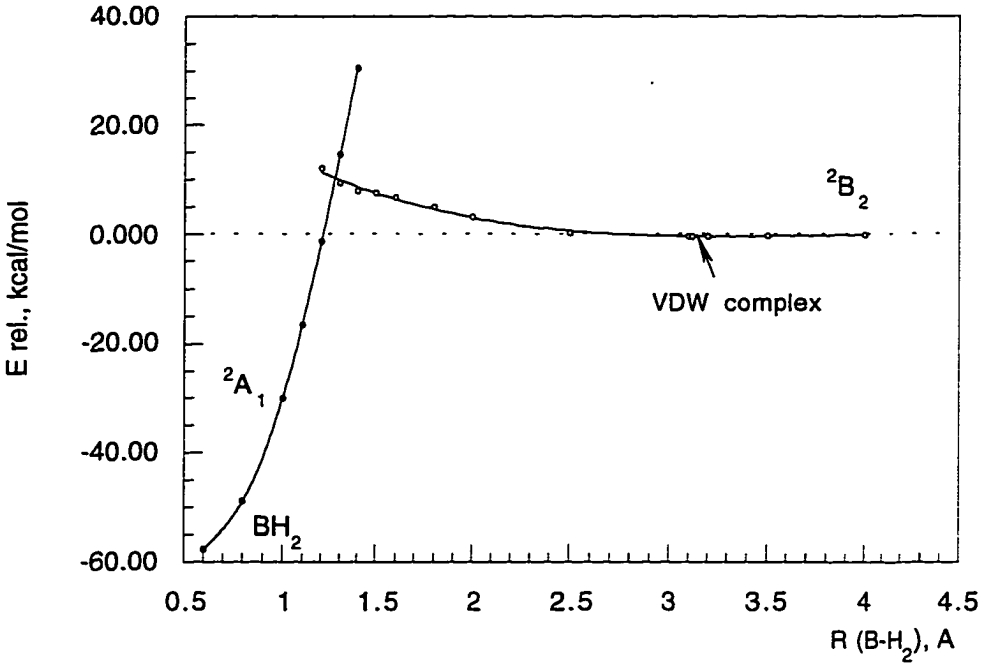

Figure 4. QCISD(T)/aug-pvtz potential energy surfaces for B-H_2 (C_{2v} symmetry).

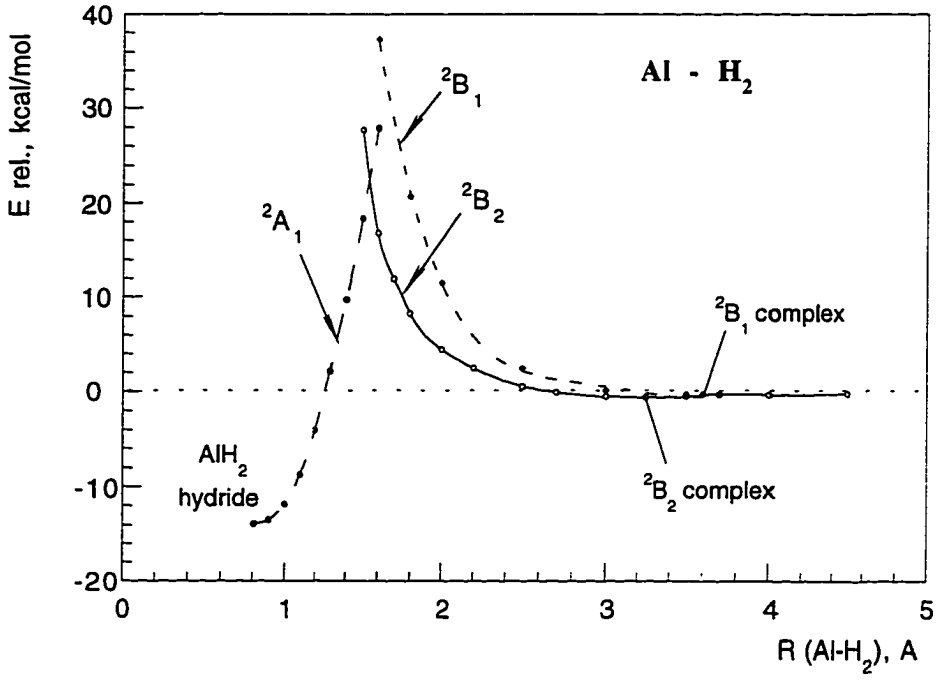

Figure 5. QCISD(T)/aug-pvtz potential energy surfaces for Al-H_2 (C_{2v} symmetry).

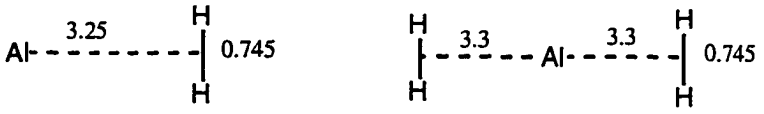

D_e, cm^{-1}			
	QCISD(T)	**204**	**398**
	MP4SDQ	**184**	**371**

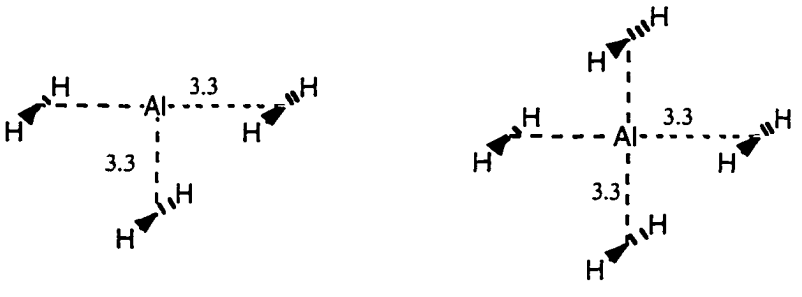

MP4SDQ	**560**	**747**

Figure 6. Van-der-Waals complexes of Al with H_2 molecules.

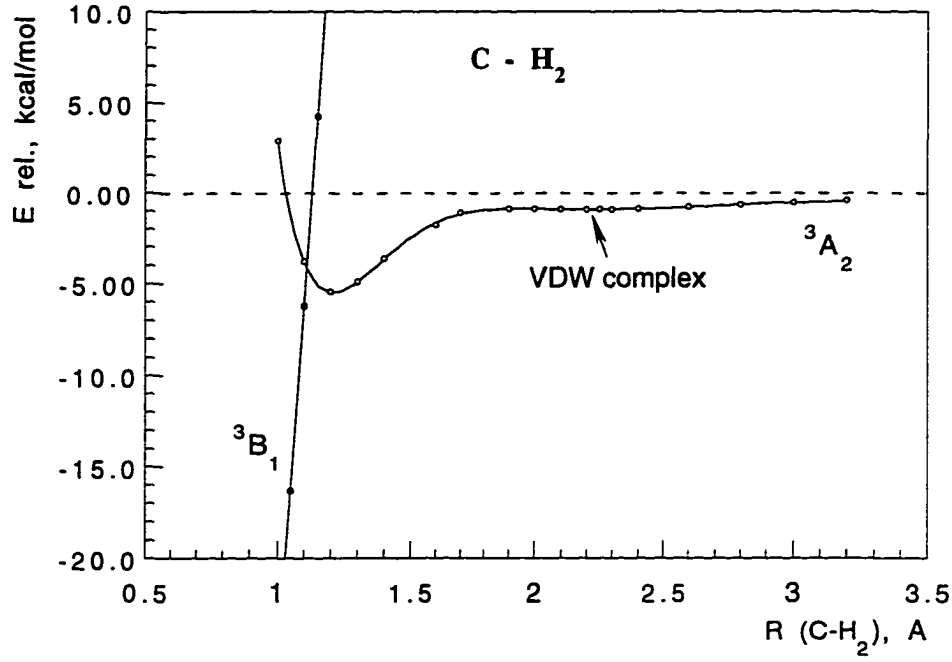

Figure 7. QCISD(T)/aug-pvtz potential energy surfaces for C-H_2 (C_{2v} symmetry).

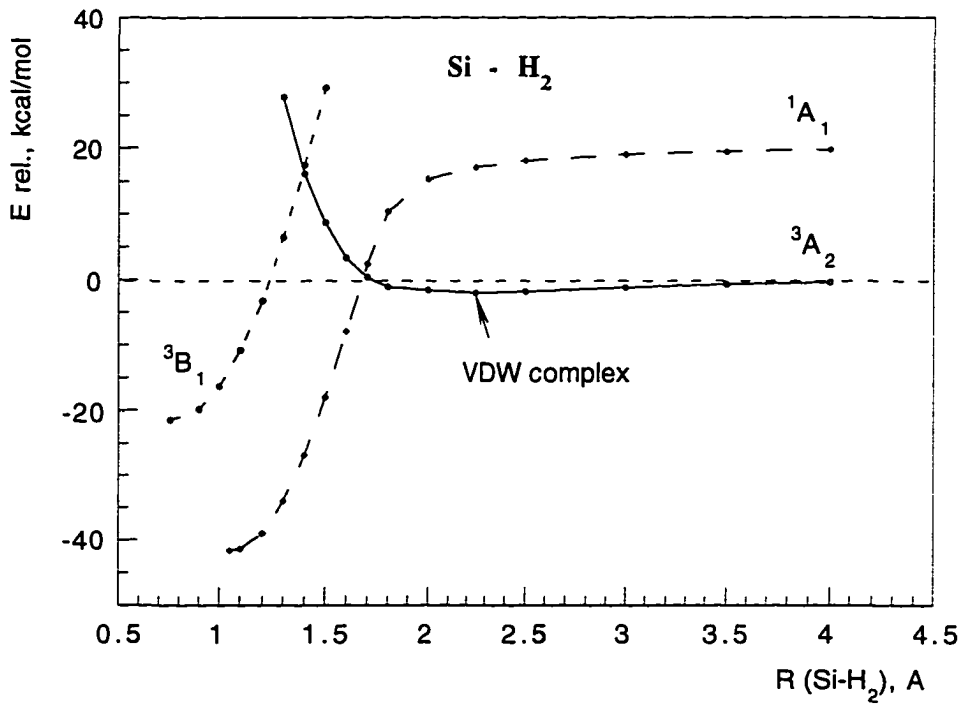

Figure 8. QCISD(T)/aug-pvtz potential energy surfaces for Si - H_2 (C_{2v} symmetry).

CHAPTER 6. THE STRUCTURE AND STABILITY OF VAN DER WAALS COMPLEXES OF Al WITH H_2

A paper accepted for publication in *Chemical Physics Letters*

Galina Chaban and Mark S. Gordon

Abstract

Fragments of the C_{2v}, $C_{\infty v}$, and C_S potential energy surfaces have been studied for the AlH_2 molecule. The kinetic stability of the most stable van der Waals complex with $^2B_2$ symmetry has been considered with respect to its rearrangement to the lower lying AlH_2 hydride found on the $^2A_1$ surface. The Al---H_2 ($^2B_2$) complex is found to be kinetically stable, with the lowest energy crossing point between the $^2B_2$ and $^2A_1$ states estimated to occur at about 30 kcal/mol above the dissociation limit Al + H_2. Calculations of the C_S potential energy surfaces showed very little change in electronic configurations of the two lowest $^2A'$ states comparing to the $^2B_2$ and $^2A_1$ states they result from when symmetry is lowered from C_{2v} to C_S. This fact, as well as the high energy location of the crossing point, suggest that the probability for the adiabatic reaction Al---H_2 ($^2B_2$) $\rightarrow$ AlH_2 ($^2A_1$) through an avoided crossing is very low.

Introduction

Weakly bound complexes between light (second and third period) atoms and molecular hydrogen have been of considerable theoretical and practical interest recently because of their possible role in improvement of energetic properties of hydrogen based rocket fuels [1-8]. Experimental work is now in progress on deposition of Li, B, and Al atoms into solid hydrogen [1]. These elements are supposed to form weak complexes with H_2 molecules in a

solid matrix and provide additional storage of chemical energy that can be released during combustion.

Recently, we have performed calculations on van der Waals complexes between atoms Li, Be, B, C, Na, Mg, Al, Si and H_2 [6], in order to estimate their thermodynamic and kinetic stabilities. We found that the alkali metals and alkaline earths form very weak complexes in their ground states (D_e = 15 - 30 cm^{-1}). The elements B, Al, C, Si form complexes that are more stable thermodynamically, with the most stable ones corresponding to a C_{2v} orientation of the H_2 molecule and a partially occupied p-orbital parallel to the H-H bond:

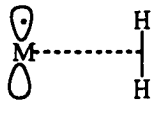

However, these elements also form stable MH_2 compounds with C_{2v} symmetry, and therefore, the kinetic stability of these complexes with respect to the reaction $M{-}{-}{-}H_2 \rightarrow MH_2$ becomes important and needs to be considered.

Previous studies of the C - H_2 potential energy surface [9-11], as well as our study of C and Si complexes [6] showed that the complexes formed by C are kinetically unstable, and the same is likely be the case for Si. On the other hand, the complexes formed by B and Al are predicted to be kinetically stable [5,6]. In view of both energetic and environmental considerations, Al seems to be a likely candidate for inclusion in hydrogen fuel and merits further investigation. An ab initio study of the potential energy surfaces for several electronic states of AlH_2 within C_{2v} symmetry has been recently published by Fang[12]. These calculations also showed that the insertion reaction of ground state Al atoms into H_2 is difficult, but that photoexcited Al atoms can react with H_2.

Our previous QCISD(T)/aug-cc-pVTZ calculations of Al-H_2 complexes [6], as well as similar CCSD(T)/aug-cc-pVTZ calculations of Partridge, Bauschlicher and Visscher [7] showed that the most stable van der Waals complex corresponds to a $^2B_2$ state and has a dissociation

energy D_e over 200 cm^{-1}. However, inclusion of zero point energies and relativistic corrections leads to an estimation of only 38 ± 26 cm^{-1} for the D_0 of the Al-H_2 complex (reference 7).

Here, we present a detailed study of the Al - H_2 system, including ground state C_{2v} and C_s potential energy surfaces in the region of surface crossing. The main purpose of this study is to examine the kinetic stability of the $^2B_2$ van der Waals complex with respect to formation of AlH_2 hydride.

Method of calculation

Some of our calculations were performed using the quadratic configuration interaction QCISD(T) method [13] and the Gaussian 92 program [14]. Several correlation consistent basis sets were tested [15] : augmented valence-double-zeta (aug-cc-pVDZ), augmented valence-triple-zeta (aug-cc-pVTZ), augmented valence-quadruple-zeta (aug-cc-pVQZ), as well as augmented core-valence-triple-zeta (aug-cc-pCVTZ and aug-cc-pACVTZ)[16]. The latter two were used with QCISD(T), including core electrons in the correlation. The results obtained using these basis sets for one of the complexes ($^2B_2$) are shown in Table 1. As can be seen from the table, the pVDZ basis set underestimates binding substantially, while pVTZ gives reasonable results compared with pVQZ. Core-valence calculations give slightly larger binding energies. The remaining points on the AlH_2 potential energy surface were done using the aug-cc-pVTZ basis set.

Table 1. Comparison of different computational levels for $^2B_2$ complex of AlH_2.

Method	D_e[a], cm^{-1}
QCISD(T, fc)/aug-cc-pVDZ	165
QCISD(T, fc)/aug-cc-pVTZ	205
QCISD(T, fc)/aug-cc-pVQZ	217
QCISD(T)/aug-cc-pCVTZ	226
QCISD(T)/aug-cc-pACVTZ	223

[a] The dissociation energies are obtained at the QCISD(T, fc)/aug-cc-pVTZ equilibrium geometry: R_e (Al-H_2) = 3.25 Å, r (H-H) = 0.745 Å.

More extensive investigations of the Al-H_2 potential energy surfaces were performed using internally contracted multi-reference configuration interaction (MRCI) calculations based on either single state or state-averaged MCSCF(5,6) wavefunctions. The MCSCF active space consisted of 5 valence electrons distributed among 6 active orbitals. In the dissociation limit these correspond to the 4 valence orbitals of Al and the σ and σ^* orbitals of H_2. Potential energy surfaces within C_{2v} symmetry were obtained using single-state MCSCF(5,6)/aug-cc-pVTZ wavefunctions. C_s potential energy surfaces were examined with state-averaged MCSCF and MRCI wavefunctions, based on a two-state reference wavefunction. The two states averaged were the lowest $^2A'$ states reduced from the $^2A_1$ and $^2B_2$ states after lowering the symmetry from C_{2v} to C_s. The MCSCF and MRCI calculations were performed with the MOLPRO program [17].

Results and discussion

Parts of the C_{2v} and $C_{\infty v}$ potential energy surfaces for several lowest electronic states are shown in Figures 1 ($^2B_2$, $^2B_1$ and $^2A_1$) and 2 ($^2\Sigma$ and $^2\Pi$). These curves were obtained by calculating QCISD(T)/aug-cc-pVTZ single-point energies at different values of the Al-H_2 distance. Local minima corresponding to weak van der Waals complexes were found for the $^2B_2$, $^2B_1$, $^2\Sigma$ and $^2\Pi$ states. Calculations of numerical hessians (energy second derivatives) at these points, however, showed that only the $^2B_2$, $^2B_1$, and $^2\Sigma$ complexes correspond to true minima. As was mentioned earlier, the most stable Al-H_2 van der Waals complex has C_{2v} symmetry and corresponds to the $^2B_2$ state, with the singly occupied p-orbital of Al parallel to the H-H bond. Its dissociation energy (D_e) is 205 cm^{-1} at the QCISD(T,fc)/aug-cc-pVTZ level, and is about 20 cm^{-1} higher when core electrons are correlated (Table 1). The $^2B_1$ and $^2\Sigma$ complexes have D_e = 103 cm^{-1} and 89 cm^{-1}, respectively, at the QCISD(T,fc) level. Inclusion

of zero point energies and spin-orbit corrections may decrease the dissociation energies substantially [7]. No van der Waals complex is found on the $^2A_1$ potential energy surface. However, the ground state of the AlH_2 hydride has $^2A_1$ symmetry (R_{Al-H} = 1.6 Å, HAlH = 118°) and is about 13.9 kcal/mol lower in energy than Al + H_2 at the QCISD(T,fc)/aug-cc-pVTZ level of theory. Formation of AlH_2 hydride is not desirable if one wants to store Al atoms in a solid hydrogen matrix. Figure 1b shows that the lowest energy path that leads from the $^2B_2$ complex to the AlH_2 hydride passes the $^2B_2$ - $^2A_1$ crossing seam. In order to study the region of this crossing in more detail, we have calculated grids of MCSCF(5,6) and MRCI single-point energies at different values of the Al - H_2 and H - H distances.

Contour plots of the energy as a function of R (Al-H_2) and r (H-H) distances for pure $^2A_1$ and $^2B_2$ states are shown in Figures 3 (MCSCF) and 4 (MRCI). R(Al-H_2) is the distance between Al and the midpoint of the H-H bond. The thick solid line on these pictures corresponds to the crossing seam between the $^2A_1$ and $^2B_2$ states. The $^2A_1$ state is lower in energy for short R (Al-H_2) and long r (H-H) distances (upper left portion of the figures) and has a minimum corresponding to the AlH_2 hydride. The AlH_2 molecule has R (Al-H_2) = 0.82 Å and r(H-H) = 2.74 Å. This structure is in the region in which the $^2A_1$ state is the ground state. The valence electron configuration corresponding to this compound is $4a_1^2 2b_2^2 5a_1^1$. In addition to the AlH_2 minimum, the $^2A_1$ potential energy surface has a stationary point corresponding to a transition state, but this point is located on the higher part of the $^2A_1$ surface (where the ground state is $^2B_2$) and is about 80 kcal/mol above the Al + H_2 dissociation limit. Its geometrical structure corresponds to R (Al-H_2) = 1.8 Å and r (H-H) = 1.0 Å.

The $^2B_2$ state is lower for longer R (Al-H_2) and shorter r (H-H) distances (lower right portion of the figures). There is only a slight minimum on the $^2B_2$ surface corresponding to a weak van der Waals complex. Its electron configuration is $4a_1^2 5a_1^2 2b_2^1$ with the singly occupied b_2 (p_y of Al) orbital parallel to the H-H bond.

The minimum energy crossing point for the $^2A_1$ and $^2B_2$ states is found to be 27 kcal/mol above the Al + H_2 dissociation limit at the MRCI level of theory (32 kcal/mol at the MCSCF level). The geometry of the minimum energy crossing point corresponds to R (Al-H_2) = 1.51 Å and r (H-H) = 1.68 Å at the MRCI level of theory, and R (Al-H_2) = 1.55 Å and r (H-H) = 1.76 Å at the MCSCF level of theory.

A steepest descent path was determined starting from the minimum energy crossing point at the MCSCF(5,6) level of theory in the direction of the negative of the gradient on both the $^2A_1$ (downhill in energy to the AlH_2 minimum) and $^2B_2$ (downhill to the van der Waals Al---H_2 complex) surfaces. These are illustrated in Figure 3 (lighter curves starting from the minimum energy crossing point). A second reaction path was determined, starting from the $^2A_1$ transition state. This path leads to AlH_2 in one direction and to Al + H_2 in the other direction. The electron configuration changes during this reaction from $4a_1^2 2b_2^2 5a_1^1$ in AlH_2 to $4a_1^2 5a_1^2 6a_1^1$ in Al + H_2. Since the lowest point on the $^2B_2$ - $^2A_1$ crossing seam is much lower than the position of the transition state on the $^2A_1$ surface, it appears that the reaction Al---H_2 ($^2B_2$) ⇒ AlH_2 ($^2A_1$) should occur more efficiently via the $^2B_2$ - $^2A_1$ crossing.

The reaction Al---H_2 ($^2B_2$) ⇒ AlH_2 ($^2A_1$) could actually proceed through an *avoided* crossing that occurs when the symmetry is reduced from C_{2v} to C_s. To consider this possibility we have calculated sections of the C_s potential energy surface, using the AlXH angle θ = 85° and 80°, where X is the midpoint of the H-H bond. Since we used state-averaged MCSCF wavefunctions for these calculations, for comparison purposes we have also recalculated the θ = 90° surface using C_s symmetry and state-averaged MCSCF wavefunctions. The contour plots for θ = 90° and 85° are shown in Figures 5 (MCSCF) and 6 (MRCI). As can be seen, the position of the barrier (or, more correctly, the minimum point on the ridge) is higher in energy for the 85° surface, than for 90°. This point is even higher for the 80° surface.

Several points with angle θ between 90° and 80° were calculated with R(Al-H_2) = 1.51Å and R(H-H) = 1.68 Å (values at the MRCI C_{2v} minimum energy crossing point). The results of these calculations are shown in Figure 7. The energy of the lower $^2A'$ state decreases very slightly (a few cm^{-1}) at 89.5° and then increases, while the upper state energy increases continuously as θ decreases from 90°. The fact that there is almost no energy lowering when distorting to C_s symmetry suggests that there is very little interaction between these two states. The minimum energy crossing point found for C_{2v} symmetry is therefore a good estimate for the barrier height for the reaction Al---H_2 ⇒ AlH_2. This is about 30 kcal/mol and is probably sufficient for the van der Waals complex to be kinetically stable. In addition, since the two lowest $^2A'$ states tend to retaine electronic configurations very close to those of C_{2v} states ($^2B_2$ and $^2A_1$), nonadiabatic recrossing is likely to occur and reduce the reaction rate. This should enhance the stability of the van der Waals complex. Additional calculations of the energetics and derivative couplings in the vicinity of the seam of the AlH_2 conical intersection will be discussed in a subsequent paper [18].

Conclusion

The thermodynamic and kinetic stability have been studied for weakly bound (van der Waals) complexes on the AlH_2 potential energy surface because of their possible role as highly energetic materials. The most stable Van der Waals complex corresponds to C_{2v} symmetry ($^2B_2$ state). The kinetic stability of this complex was considered, since the more stable AlH_2 hydride exists with this symmetry, but has a different electronic state ($^2A_1$).

Two possible reaction paths exist for the Al---H_2 (complex) → AlH_2 hydride rearrangement. One route is via the $^2A_1$ transition state, but it involves overcoming a barrier of about 80 kcal/mol and is considered unlikely. Another way for this reaction to proceed is via an avoided crossing in C_s symmetry, with both $^2A_1$ and $^2B_2$ states reduced to $^2A'$. MRCI / MCSCF(5,6) calculations in the $^2B_2$ - $^2A_1$ crossing region show that the minimum energy

crossing point corresponds to a structure with R (Al - H_2) = 1.51Å and r (H-H) = 1.68Å (28 kcal/mol above the $^2B_2$ complex). The calculations reveal very little interaction between the $^2B_2$ and $^2A_1$ states: the distortion to C_S symmetry results in an energy lowering of the lower $^2A'$ state by only a few cm^{-1} at about 89.5 degrees; then the energies of both states go up. This suggests that the energy of the crossing point can be considered to be a good approximation to the height of the barrier for this reaction. The rather high reaction barrier (28 kcal/mol), as well as the high probability of a nonadiabatic recrossing, suggest that the reaction rate should be very low. Therefore, the $^2B_2$ complex can be considered to be kinetically stable with respect to rearrangement to AlH_2 hydride.

Acknowledgments

This work was supported by the Air Force Office of Scientific Research (grant F49620-95-1-0077). The calculations were performed on IBM and DEC workstations obtained with funds provided by the Air Force Office of Scientific Research and Iowa State University.

References

1. (a) Fajardo, M. E. *J. Chem. Phys.* **1993**, *98*, 110 ; (b) Fajardo, M. E.; Tam, S.; Thompson, T. L.; Cordonnier. M. E. *Chem. Phys.* **1994**, *189*, 351.
2. Konowalow, D. *Private communication.* **1991**.
3. Rosenkrantz, M. E. *Proceedings of High Energy Density Matter Conference,* April **1992**, Lancaster, CA.
4. Augspurger, J. D.; Dykstra, C. E. *Chem. Phys. Lett.* **1989**, *158*, 399.
5. Alexander, M. *J. Chem. Phys.* **1993**, *99*, 6014.
6. Chaban G.; Gordon M. S. *J. Phys. Chem.* **1996**, *100*, 95.
7. Partridge H.; Bauschlicher, Jr., C. W.; Visscher L. *Chem. Phys. Lett.* **1995**, *246*, 33.
8. Duncan M. A. *Proceedings of High Energy Density Matter Conference,* 1995

9. Blint R. J.; Newton M. D. *Chem. Phys. Lett.* **1975**, *32*, 178.

10. Casida M. E.; Chen M. M. L.; MacGregor R. D.; Schaefer III, H. F. *Isr.J. Chem.* **1980**, *19*, 127.

11. Harding L. B. *J. Phys. Chem.* **1983**, *87*, 441.

12. Fang W.-H. *Chem. Phys. Lett.* **1996**, *260*, 565.

13. Pople, J. A.; Head-Gordon, M.; Raghavachari, K. *J. Chem.*. Phys. **1987**, *87*, 5968.

14. Gaussian 92, revision C, Frisch, M. J.; Trucks, G. W.; Head-Gordon, M.; Gill, P. M. W.; Wong, M. W.; Foresman, J. B.; Johnson, B. G.; Schlegel, H. B.; Robb, M. A.; Replogle, E. S.; Gomperts, R.; Andres, J. L.; Raghavachari, K.; Binkley, J. S.; Gonzalez, C.; Martin, R. L.; Fox, D. J.; Defrees, D. J.; Baker, J.; Stewart, J. J. P.; and Pople, J. A. Gaussian, Inc., Pittsburgh PA, 1992.

15. a) Dunning, Jr., T. H. *J. Chem. Phys.* **1989**, *90*, 1007. b) Kendall, R. A.; Dunning, Jr., T. H.; Harrison R. J. *J. Chem. Phys.* **1992**, *96*, 6796. c) Woon, D. E.; Dunning, Jr., T. H. *J. Chem. Phys.* **1993**, *98*, 1358.

16. a) Woon, D. E.; Dunning, Jr., T. H. *J. Chem. Phys.* **1995**, *103*, 4572. b) Peterson K. A.; Dunning, Jr., T. H., to be published.

17. MOLPRO is written by Werner, H.- J.; Knowles, P. J. with contributions by Almlöf, J.; Amos, R. D.; Elbert, S. T.; Taylor, P. R. Werner, H.-J.; Knowles, P. J. *J. Phys. Chem.* **1988**, *89*,1988; Knowles, P. J.; Werner, H.-J. *Chem. Phys. Lett.* **1988**, *145*, 514.

18. Chaban G.; Gordon M. S.; Yarkony D. R. *J. Phys. Chem.*, to be submitted.

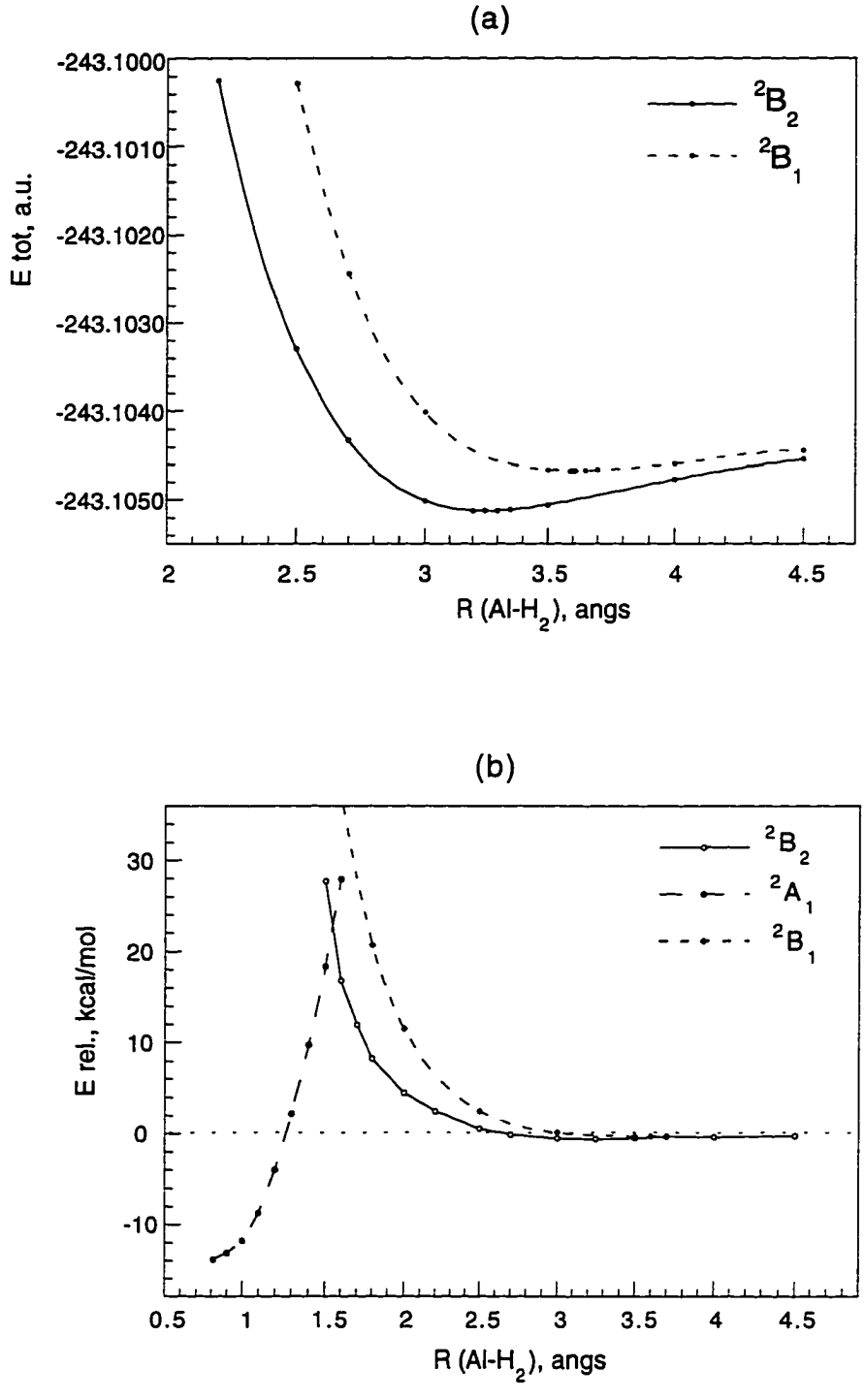

Figure 1. QCISD(T)/aug-cc-pvtz potential energy curves for C_{2v} states of Al-H_2.

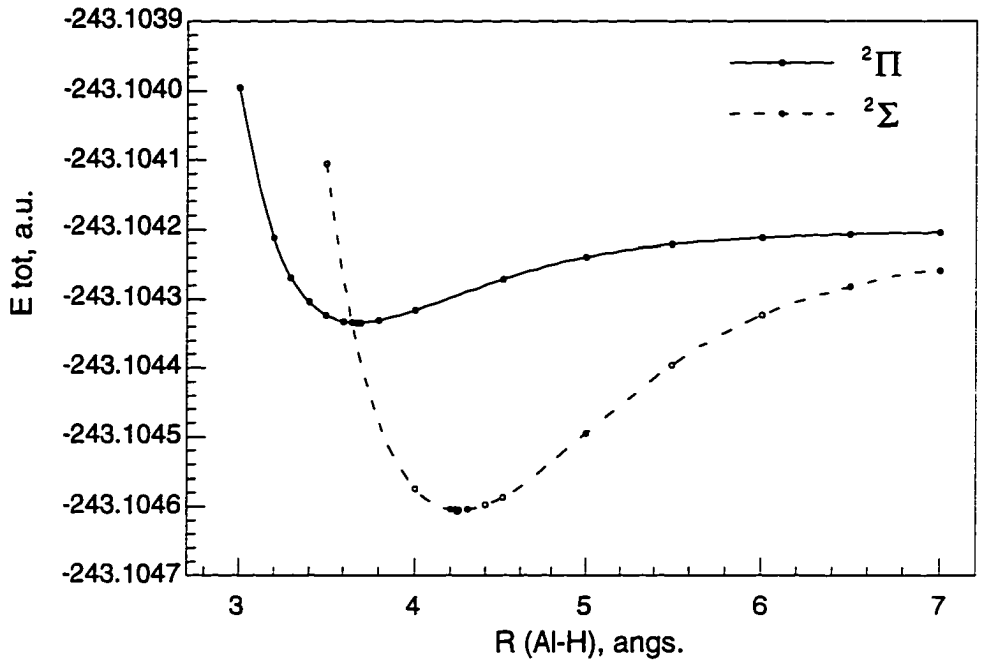

Figure 2. QCISD(T)/aug-cc-pvtz potential energy curves for $C_{\infty v}$ states of Al-H_2.

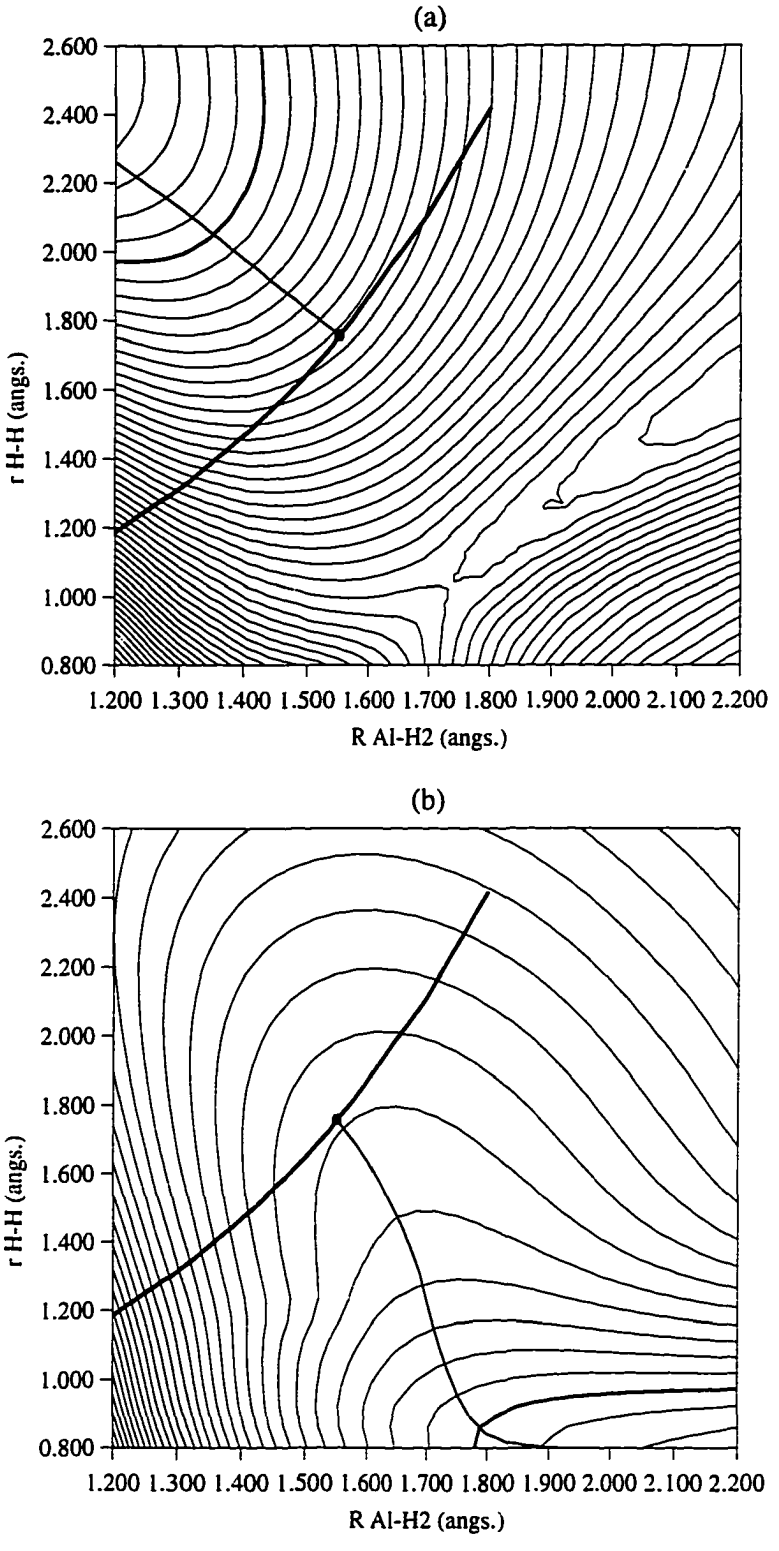

Figure 3. MCSCF(5,6)/aug-cc-pvtz potential energy surfaces of Al-H2 system in C2v symmetry: 2A1 (a) and 2B2 (b) states. Thick contour lines correspond to total energy -243.030 a.u., energy increment is 0.005 a.u.

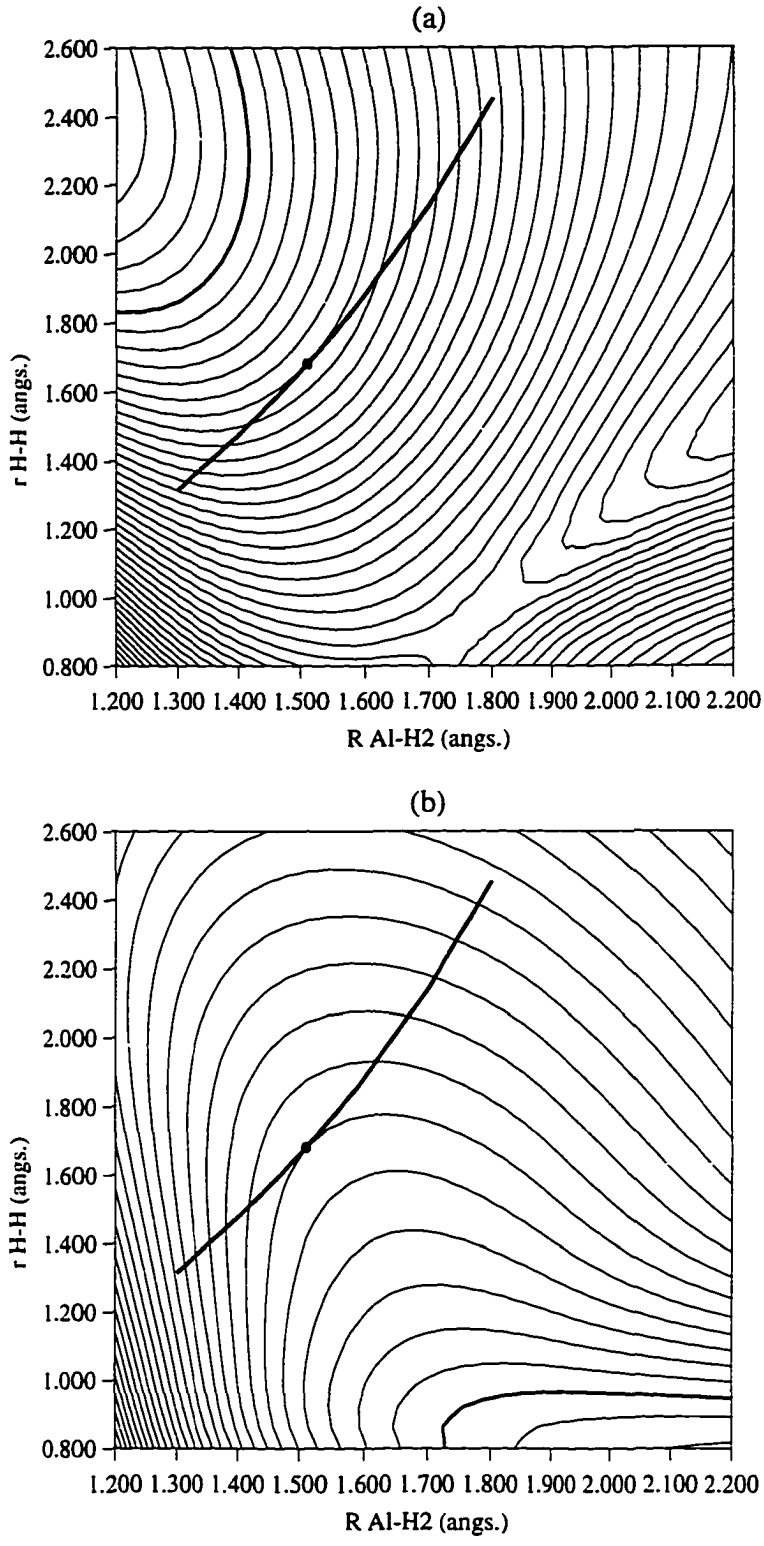

Figure 4. MRCI/MCSCF(5,6)/aug-cc-pvtz potential energy surfaces of Al-H2 system in C2v symmetry: 2A1 (a) and 2B2 (b) states. Thick contour lines correspond to -243.150 a.u. of total energy, increment=0.005 a.u.

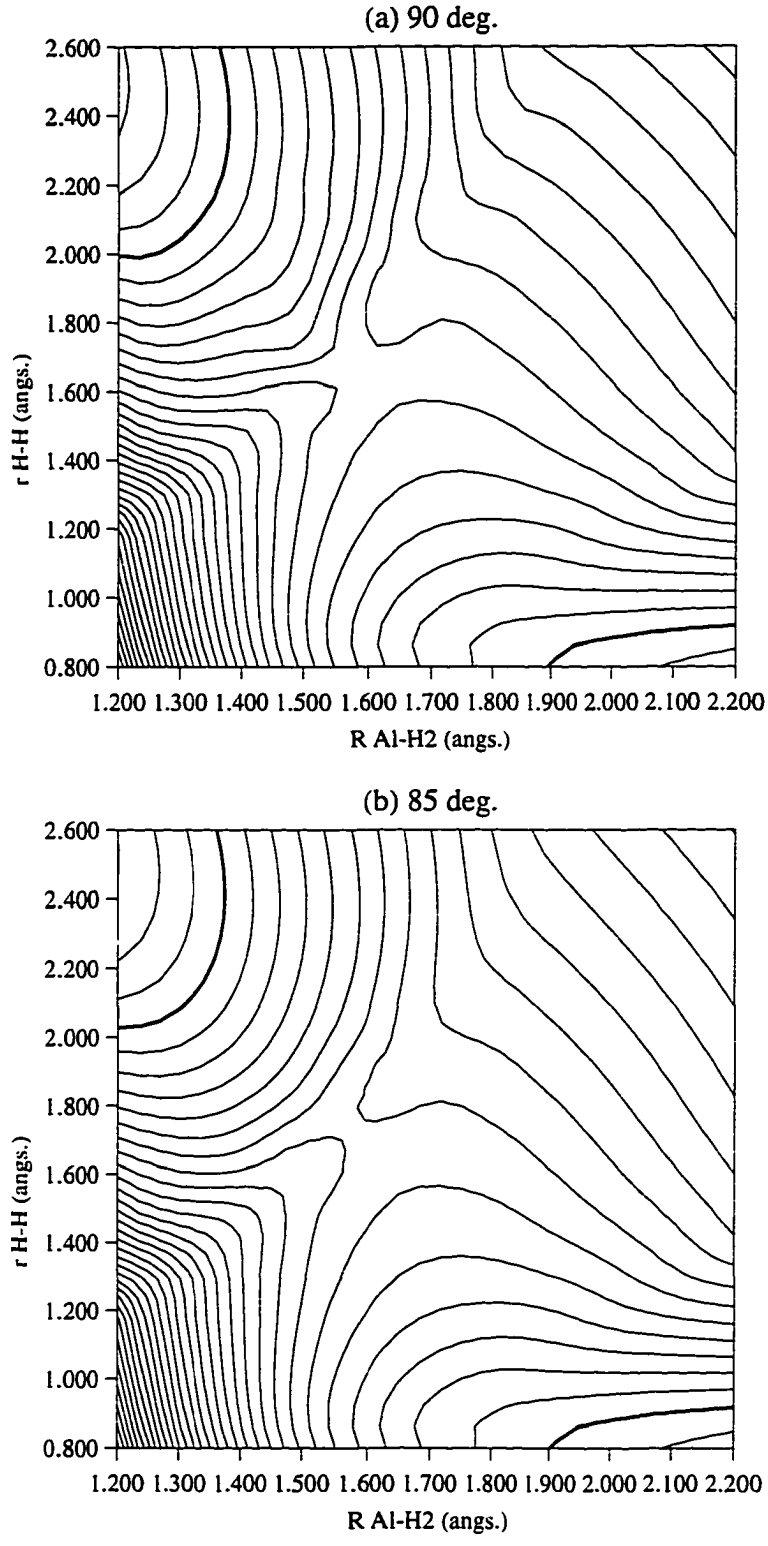

Figure 5. SA-MCSCF(5,6)/aug-cc-pvtz potential energy surfaces of Al-H2 system in Cs symmetry: angle AlXH = 90 (a) and 85 (b), X-midpoint of H-H bond. Thick contour lines correspond to -243.030 a.u., energy increment is 0.005 a.u.

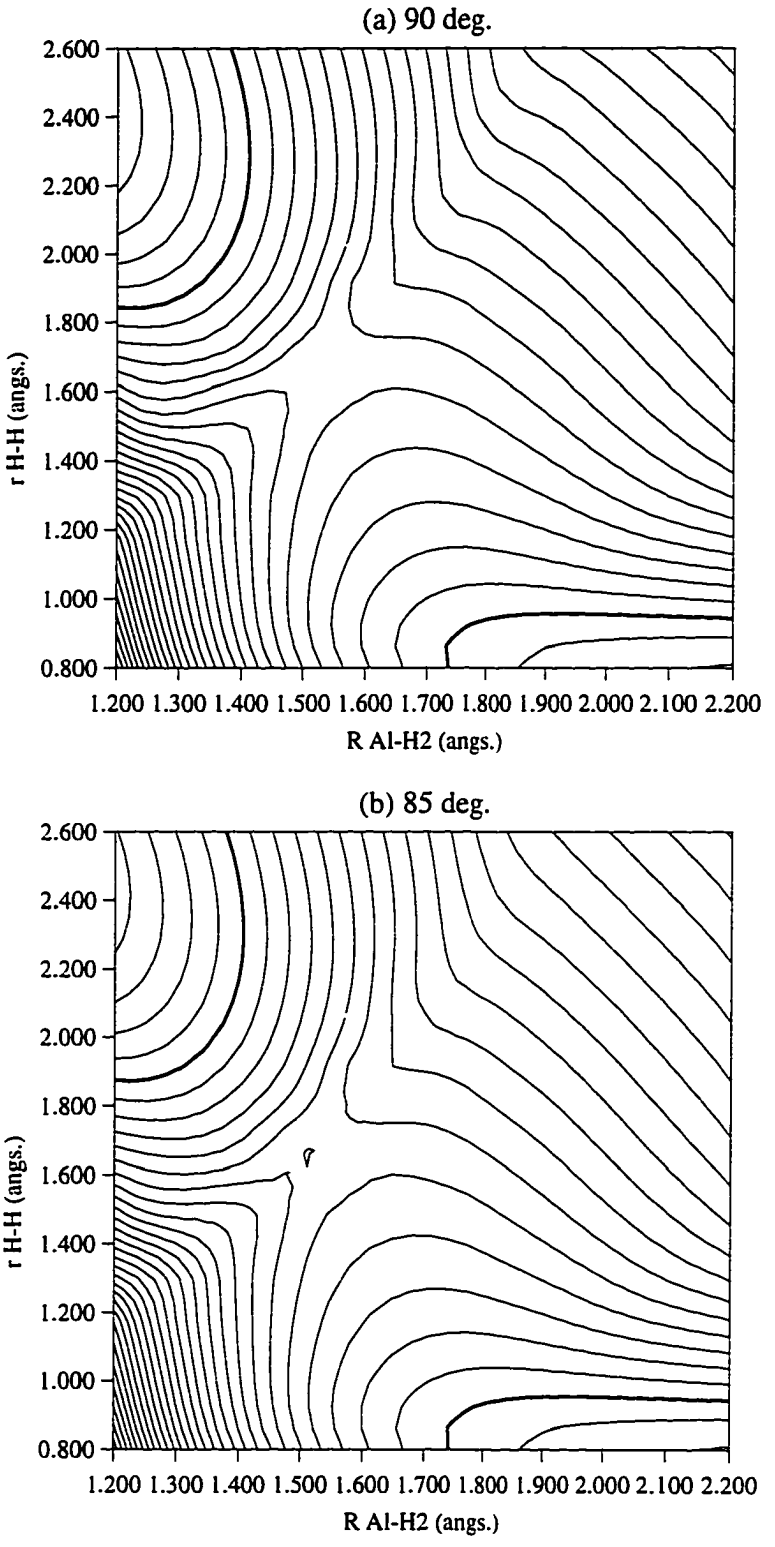

Figure 6. MRCI/SA-MCSCF(5,6)/aug-cc-pvtz potential energy surfaces of Al-H2 system in Cs symmetry: angle AlXH = 90 (a) and 85 (b), X-midpoint of H-H bond. Thick contour lines correspond to -243.150 a.u., energy increment is 0.005 a.u.

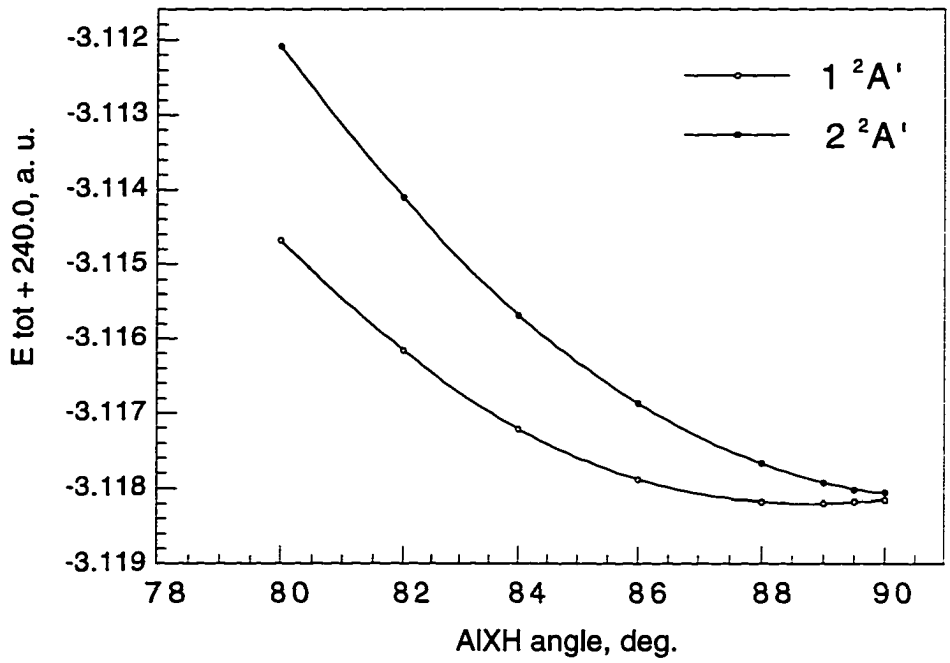

Figure 7. Energies of two lowest ^{2}A' states as function of Al XH angle (X-midpoint of H-H bond).

CHAPTER 7. GENERAL CONCLUSIONS

In this chapter, the main results presented in this dissertation are summarized, including method development and coding (chapter 1) and theoretical investigations of highly energetic chemical compounds (chapters 2-6).

Chapter 1 describes an efficient way to optimize molecular orbitals for different types of wavefunctions including RHF, ROHF, GVB, and MCSCF. Explicit formulae for the exact orbital gradient and the approximate diagonal orbital hessian are presented for each kind of wavefunction. The method is faster than the standard diagonalization techniques used for RHF and GVB. Also, it eliminates the traditional diagonalization step which is not easily parallelizable. For MCSCF, the method presented here requires more iterations than an exact second order program, but since each iteration is substantially faster, the approach leads to a more efficient overall program. In addition, the memory requirements for the approximate second order method are substantially less than those for exact second order methods. This permits MCSCF calculations for large molecules with basis sets including several hundreds of functions.

With regard to future method development work, the implementation of a state-averaged full second order MCSCF method is currently in progress. This will allow programming of nonadiabatic coupling matrix elements between the averaged electronic states in GAMESS in the future. Knowledge of nonadiabatic interactions between electronic states will help to improve characterization of highly energetic compounds and their reactions.

Thermodynamic and kinetic stabilities of high energy isomers for N_3F and N_2O_2 molecules are investigated in chapters 2 and 3 from the point of view of their possible role as sources of energy and candidates for use as fuel systems. Their energies relative to $N_2 + O_2$ and N_2 + NF products are very high (on the order of 50-100 kcal/mol). Minimum energy reaction paths of their isomerisation and decomposition are determined using IRC techniques

and MCSCF wavefunctions. In addition, the approximate minimum energy crossing points between closest singlet and triplet states are determined.

New cyclic isomers (with 3-membered nitrogen rings) are discovered on both the singlet and triplet potential energy surfaces of N_3F. They are less stable energetically than the open isomer (fluorine azide) by about 15 and 70 kcal/mol, respectively. The barriers for their dissociation to N_2+NF($^1\Delta$) and N_2+ NF($^3\Sigma$) are found to be on the order of 15 kcal/mol. Three N_2O_2 isomers (a 4-membered D_{2h} isomer, a planar C_{2v} isomer, and a bicyclic C_{2v} isomer) are predicted to be kinetically stable: the estimated barriers to dissociation are about 40 kcal/mol for the D_{2h} isomer, and about 20 kcal/mol for each of the other two isomers. Low-lying triplet states are found to cross the singlet potential energy surfaces along the reaction paths for some of the isomers, but these crossings occur in regions that are far enough from the positions of the minima that they are unlikely to destroy the stability of these isomers. The conclusion is that N_2O_2 isomers may be good candidates for high energy systems, and that experimental attempts should be made to synthesize them. As to the N_3F isomers, they will probably make good explosives rather than possible fuel materials.

As a future plan, it would be desirable to use the DRP method to perform classical trajectories calculations that start from vibrationally excited NO molecules. This could provide some insights on how N_2O_2 high energy isomers may be synthesized. Such calculations are prohibitively time-consuming at the moment, but may become possible with the progress of computer hardware and computational methods.

The potential stability of Van der Waals complexes M-H_2 (M = Li, Be, B, C, Na, Mg, Al, Si) is considered in chapters 5 and 6 because of their possible role in improvement of energetic properties of hydrogen based rocket fuels. Light elements are supposed to form weak complexes with H_2 molecules of solid matrix and provide additional storage of chemical energy that can be released during combustion. According to our calculations, alkali metals and alkaline earths form very weak linear complexes in their ground states (with dissociation

energies D_e about 15 cm^{-1} for Li and Na and 30 cm^{-1} for Be and Mg), but much stronger complexes in their (p) excited states. The elements B, Al, C, Si form both linear ($C_{\infty v}$) and perpendicular (C_{2v}) complexes. The most stable of these correspond to a perpendicular orientation of the H_2 molecule, with an occupied p-orbital parallel to the H-H bond. The thermodynamic stability of C_{2v} complexes increases from B, Al (121 and 204 cm^{-1} respectively) to C, Si (De=324 cm^{-1} and 720 cm^{-1}). Kinetic stability is considered for p element complexes since these elements form lower lying MH_2 compounds. The complexes formed by C are likely to be kinetically unstable, and the same may be the case for Si. On the other hand, the complexes formed by B and Al are predicted to be quite stable, with the barriers separating them from BH_2 and AlH_2 estimated at about 15 and 28 kcal/mol, respectively.

MRCI calculations of C_s potential surfaces for AlH_2 showed very little interaction between the two lowest $^2A'$ states resulting from the $^2B_2$ and $^2A_1$ states that cross at C_{2v} symmetry. This fact, as well as the high energy location of the crossing point (~ 28 kcal/mol) suggest that the probability of the adiabatic reaction Al---H_2 -> AlH_2 through an avoided crossing is very low. We conclude that among p-elements, Al atom is the best possible candidate for inclusion into solid hydrogen for energy storage purpose. The structures and stabilization energies for Al-(H_2)n clusters are presented with n = 2-6. It is found that the addition of H_2 molecules increases the stability of the complex in an almost additive manner.

As the next step, calculations of bigger clusters may be suggested, where two or more Al atoms are surrounded by H_2 molecules in a way they may be surrounded in the solid H_2 lattice. This can help to study the behavior of metal atoms in a hydrogen matrix, including the possibility of their migration and recombination. Classical trajectory calculations based on the dynamic reaction path method would be helpful in studying diffusion of metal atoms in hydrogen and predicting whether metal atoms will form dimers and larger clusters when the temperature is increased. This can provide useful information for experimentalists working on metal-doped solid hydrogen.

APPENDIX. DYNAMIC REACTION PATH CALCULATIONS FOR THE DISSOCIATION OF N_3F CYCLIC ISOMER

MCSCF(6,6)/6-31G(d) classical trajectory (DRP) calculations are reported here that provide additional insights on the process of dissociation of the N_3F singlet cyclic isomer to N_2 + NF singlet products. The reaction path of this dissociation is described in chapter 3. The trajectory calculations are initiated from the equilibrium structure of the cyclic isomer. The vibrational normal modes for this isomer are shown in Figure 1. An initial kinetic energy ranging from 10 to 20 kcal/mol was given in the direction of mode 4, the N_2 - NF stretching motion. Calculations were performed with step sizes of 0.2 femtoseconds. Since the barrier height for dissociation at this level of theory is 10.6 kcal/mol, 10 kcal/mol of initial kinetic energy leads only to oscillations. Dissociation also does not occur when 11 and 12 kcal/mol of initial kinetic energy is given, at least during the first 700 fs (Figure 2a). This might be due to the fact that some of the energy is consumed by other normal modes.

Changes in kinetic and potential energies with time when 12.0, 13.0, 14.0, 15.0, 15.2, and 16.0 kcal/mol of initial kinetic energy (KE) is given in positive direction of normal mode 4 are shown in Figure 2 a,b,c,d,e,f respectively. The corresponding coordinate changes in terms of the normal modes of the equilibrium structure are shown in Figure 3. Only modes with non-zero contributions (symmetric modes Q2, Q4, Q5, and Q6) are shown. It may be seen from these figures that when 13, 14 or 15 kcal/mol of kinetic energy is provided, the molecule undergoes several oscillations during the first 200 - 500 fs and then dissociates to N_2 + NF fragments. When more than 15 kcal/mol initial kinetic energy is provided (15.2 kcal/mol and higher), the molecule dissociates almost immediately. In general, the dissociation occurs sooner when more initial kinetic energy is given. However, the time required for dissociation also depends on how the energy gets distributed among the normal coordinates with time. Although initially energy is given only to Q4, part of the energy goes into other modes,

especially Q2, the bending motion of NF with respect to the NNN plane. As shown in Figure 3, dissociation occurs when Q4 and Q2 come into phase, and a resonance occurs. This explains the fact that the dissociation sometimes occurs sooner when less energy is given; for example, the molecule dissociates after about 200 fs at 14 kcal/mol kinetic energy and about 300 fs for 15 kcal/mol.

The direction in which the kinetic energy is initially provided also has a significant effect on the resulting trajectory. This is illustrated in Figures 4 and 5 a,b,c,d where the same amounts of initial kinetic energy from 13 to 16 kcal/mol are provided, but in the negative direction of normal mode 4 (the negative direction corresponds to bringing N_2 and NF closer together). This results in much faster dissociation in the case of KE = 14 and 15 kcal/mol (after about 50 and 80 fs as compared to about 300 and 200 fs in Figure 2 c and d), but the dissociation occurs later when 16.0 kcal/mol is given (see 4 d vs. 2 f). Dissociation also occurs later in the case of 13 kcal/mol initial kinetic energy (4 a). This illustrates that the resulting trajectories are very sensitive to initial phases of normal modes, and to mode-mode interactions along the trajectory (see Figure 5 for coordinate changes along the trajectories started with initial energy given in the negative direction of normal mode 4).

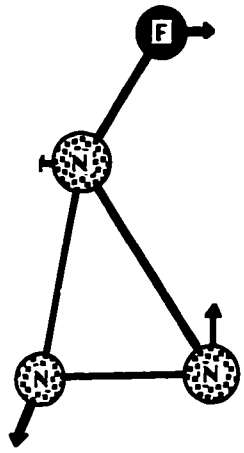

(1) 490.9 cm-1

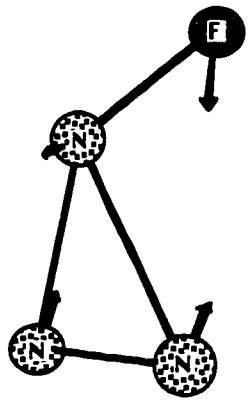

(2) 520.8 cm-1

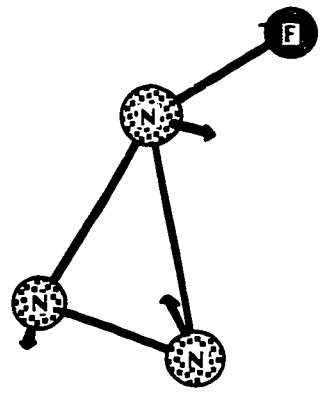

(3) 739.0 cm-1

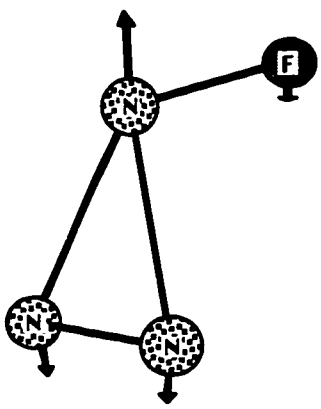

(4) 774.2 cm-1

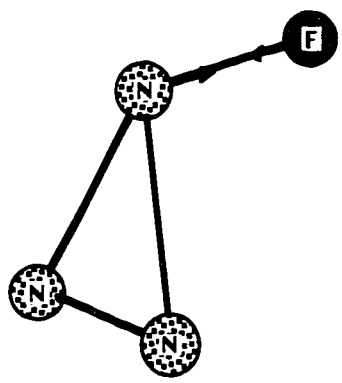

(5) 1133.2 cm-1

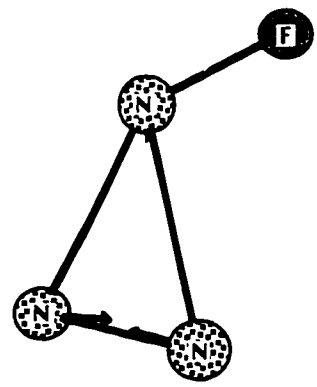

(6) 1861.8 cm-1

Figure 1. MCSCF(6,6)/6-31G(d) normal modes and frequencies of vibrations for N_3F singlet cyclic isomer.

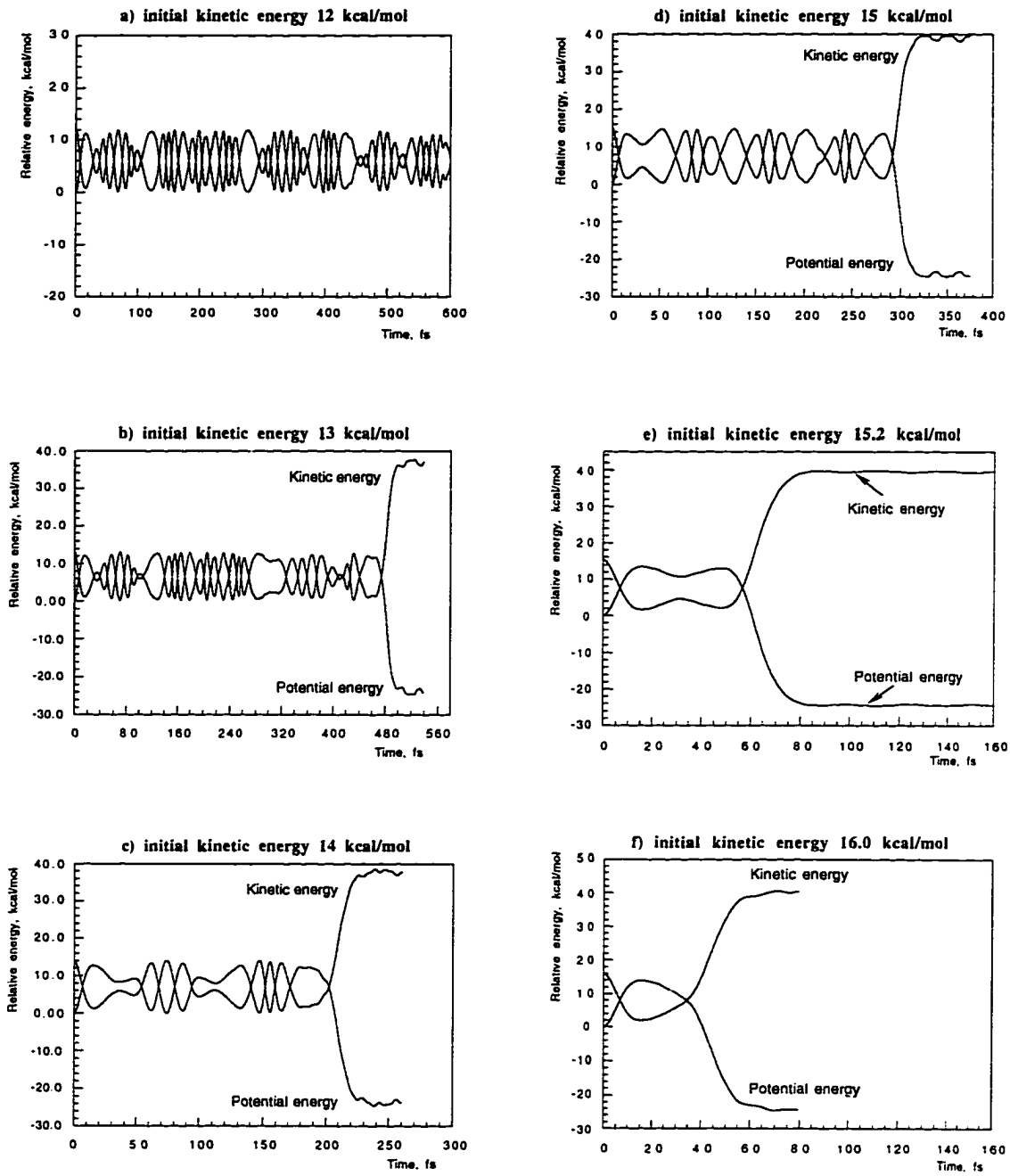

Figure 2. Kinetic and potential energy changes with time. The intial kinetic energy given in positive direction of normal mode 4 is 12.0 (a), 13.0 (b), 14.0 (c), 15.0 (d), 15.2 (e), and 16.0 (f) kcal/mol.

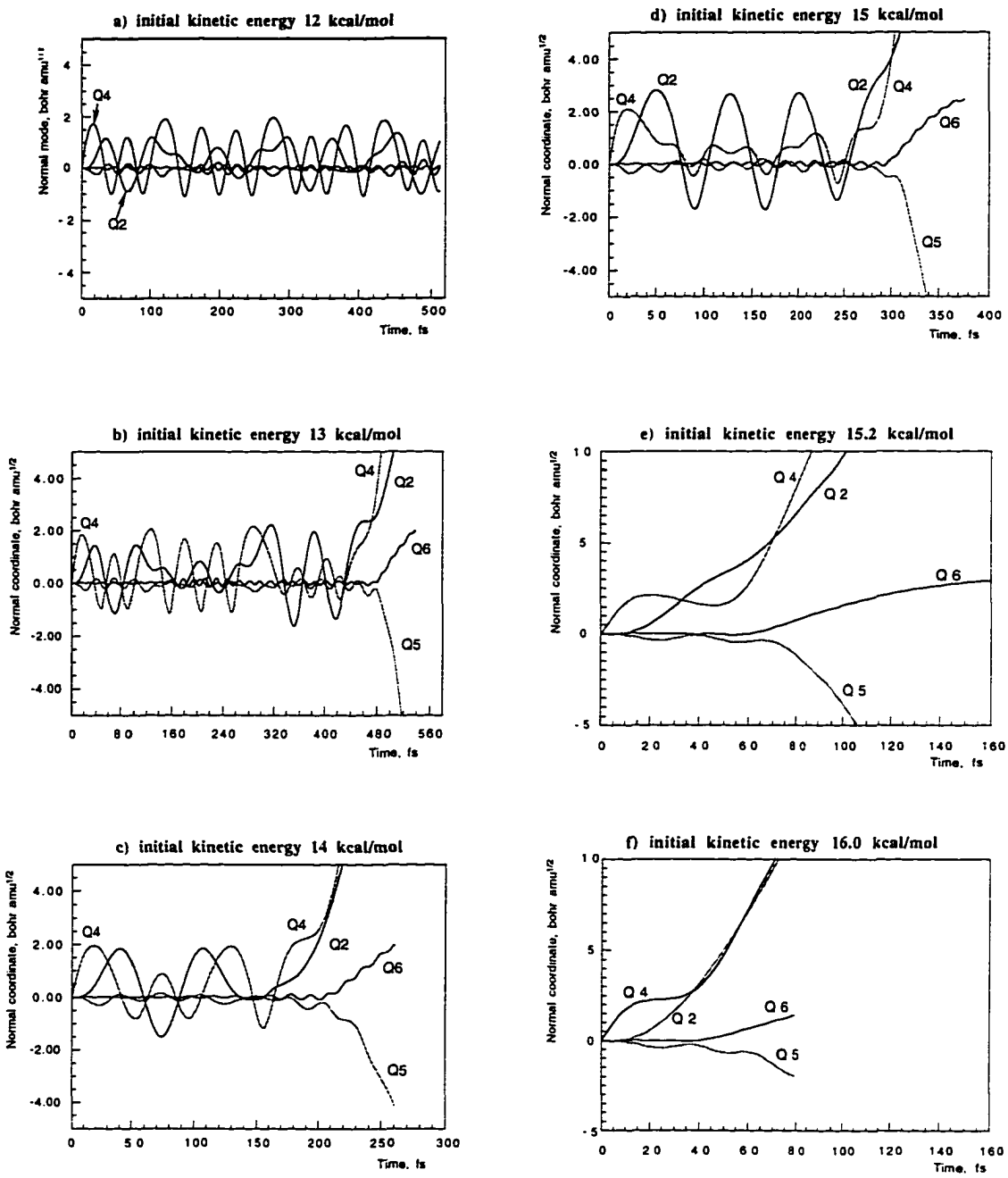

Figure 3. Changes of normal coordinates in terms of normal modes of N_3F cyclic isomer. Notations a, b, c, d, e, f correspond to those of Figure 2.

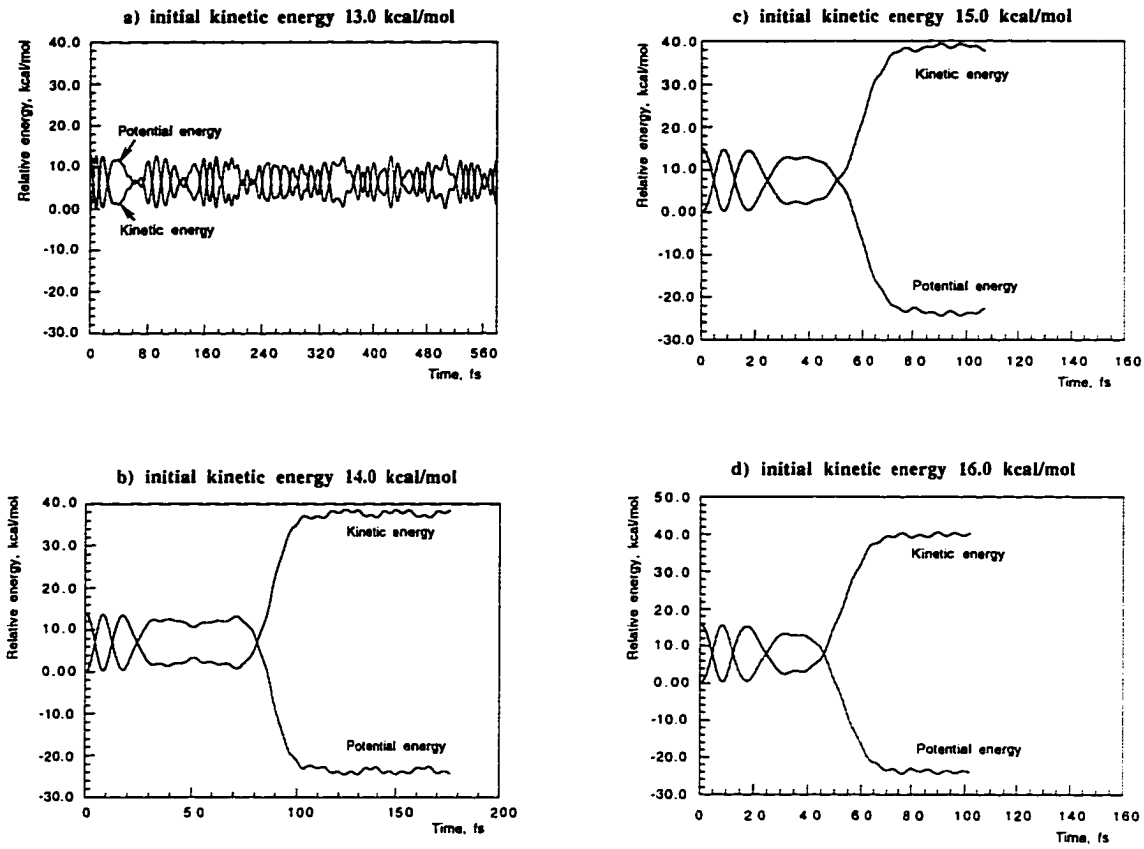

Figure 4. Kinetic and potential energy changes with time. The initial kinetic energy given in negative direction of normal mode 4 is 13.0 (a), 14.0 (b), 15.0 (c), and 16.0 (d) kcal/mol.

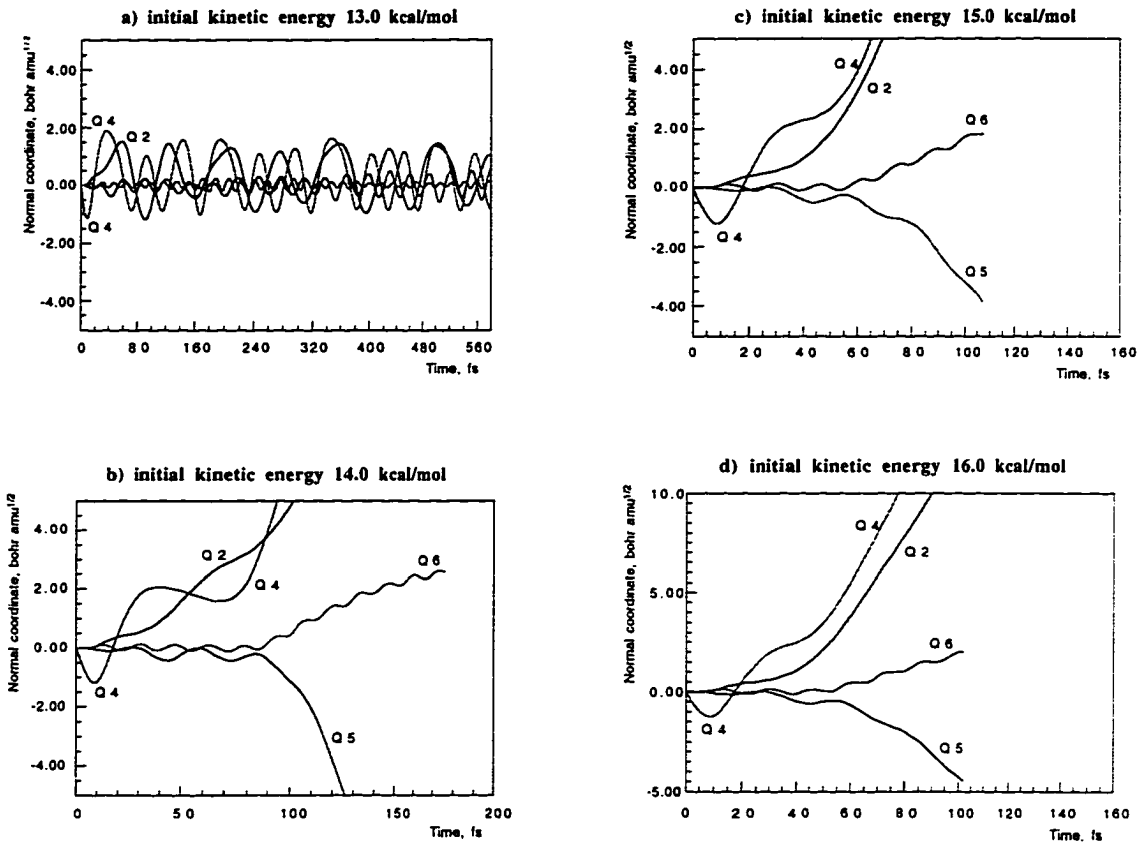

Figure 5. Changes of normal coordinates in terms of normal modes of N_3F cyclic isomer. The initial kinetic energy is given in negative direction of normal mode 4. Notations a, b, c, d correspond to those of Figure 4.